# Journal Pre-proof


Mitochondrial oxidative metabolism contributes to a cancer stem cell phenotype in cholangiocarcinoma

Chiara Raggi, Maria Letizia Taddei, Elena Sacco, Nadia Navari, Margherita Correnti, Benedetta Piombanti, Mirella Pastore, Claudia Campani, Erica Pranzini, Jessica Iorio, Giulia Lori, Tiziano Lottini, Clelia Peano, Javier Cibella, Monika Lewinska, Jesper B. Andersen, Luca di Tommaso, Luca Vigano, Giovanni Di Maira, Stefania Madiai, Matteo Ramazzotti, Ivan Orlandi, Annarosa Arcangeli, Paola Chiarugi, Fabio Marra

PII: S0168-8278(21)00024-6

DOI: https://doi.org/10.1016/j.jhep.2020.12.031

Reference: JHEPAT 8103

To appear in: *Journal of Hepatology*

Received Date: 22 March 2020

Revised Date: 18 December 2020

Accepted Date: 24 December 2020

Please cite this article as: Raggi C, Taddei ML, Sacco E, Navari N, Correnti M, Piombanti B, Pastore M, Campani C, Pranzini E, Iorio J, Lori G, Lottini T, Peano C, Cibella J, Lewinska M, Andersen JB, di Tommaso L, Vigano L, Di Maira G, Madiai S, Ramazzotti M, Orlandi I, Arcangeli A, Chiarugi P, Marra F, Mitochondrial oxidative metabolism contributes to a cancer stem cell phenotype in cholangiocarcinoma, *Journal of Hepatology* (2021), doi: https://doi.org/10.1016/j.jhep.2020.12.031.

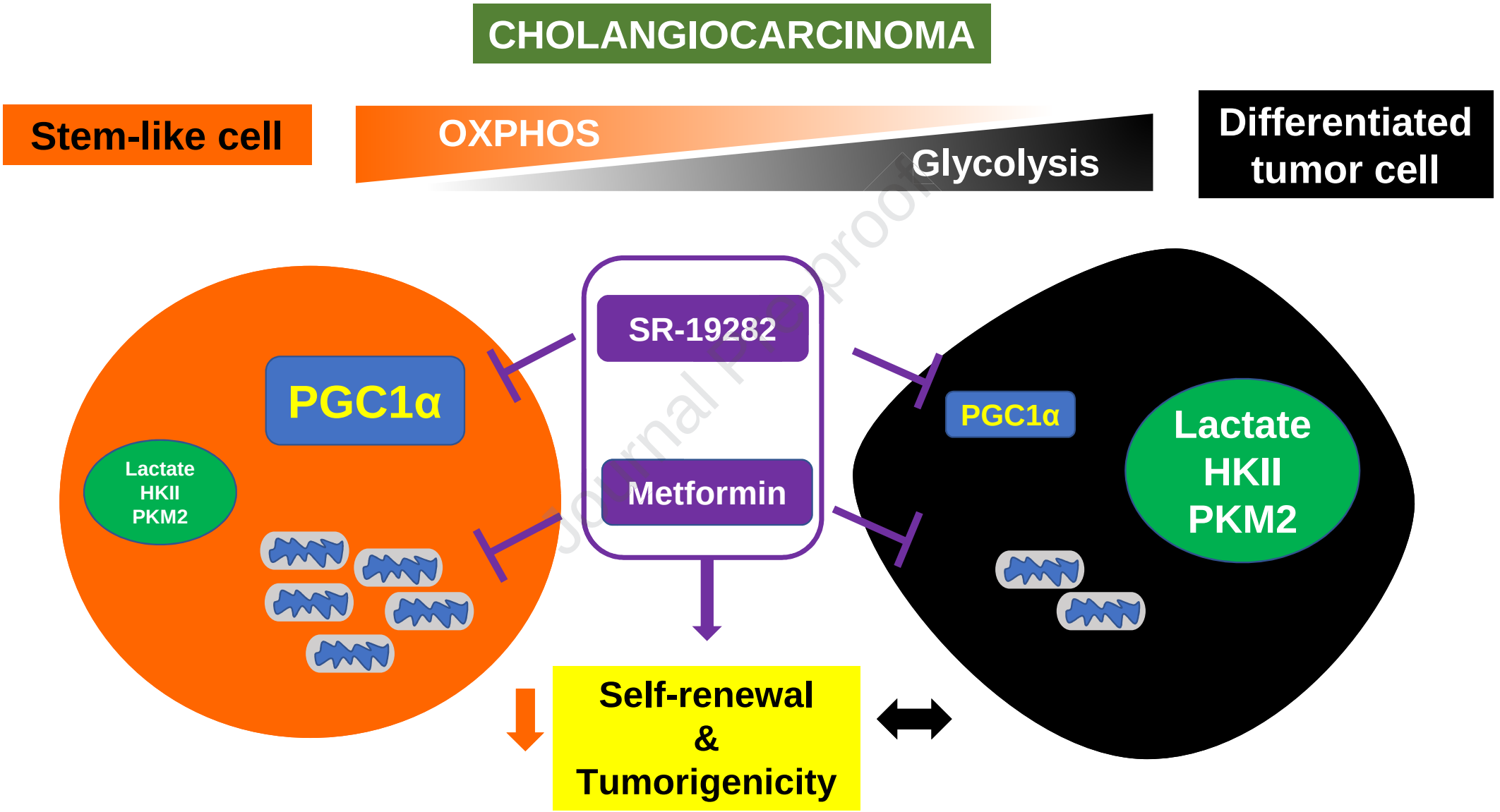

# Mitochondrial oxidative metabolism contributes to a cancer stem cell phenotype in cholangiocarcinoma

**Chiara Raggi[1], Maria Letizia Taddei[1], Elena Sacco[2,3], Nadia Navari[1], Margherita Correnti[4], Benedetta Piombanti[1], Mirella Pastore[1], Claudia Campani[1], Erica Pranzini[1], Jessica Iorio[1], Giulia Lori[1], Tiziano Lottini[1], Clelia Peano[5,6], Javier Cibella[5], Monika Lewinska[7], Jesper B Andersen[7], Luca di Tommaso[8,9], Luca Vigano[9,10], Giovanni Di Maira[1], Stefania Madiai[1], Matteo Ramazzotti[11], Ivan Orlandi[2,3], Annarosa Arcangeli[1], Paola Chiarugi[11,12], Fabio Marra[1,12,#]**

[1]Department of Experimental and Clinical Medicine, University of Florence, Florence, Italy

[2] SYSBIO, Centre of Systems Biology, Milan, Italy

[3] Department of Biotechnology and Biosciences, University of Milano-Bicocca, Milan, Italy

[4]Center for Autoimmune Liver Diseases, Humanitas Clinical and Research Center, Rozzano, Italy

[5] Genomic Unit, IRCCS, Humanitas Clinical and Research Center, Rozzano, Italy

[6] Institute of Genetic and Biomedical Research, UoS Milan, National Research Council, Rozzano, Italy

[7]Biotech Research and Innovation Centre, University of Copenhagen, Copenhagen, Denmark

[8]Department of Pathology, Humanitas Clinical and Research Center, Rozzano, Italy

[9]Department of Biomedical Sciences, Humanitas University, Rozzano, Italy

[10]Department of Hepatobiliary Surgery, Humanitas Clinical and Research Center, Rozzano, Italy

[11]Department of Experimental and Clinical Biomedical Sciences, University of Florence, Florence, Italy

[12]Excellence Center for Research, Transfer and High Education DenoTHE, Florence, Italy

**Address for correspondence:**

Fabio Marra, MD, PhD
Dipartimento di Medicina Sperimentale e Clinica
Largo Brambilla 3
I50134 Florence, Italy
Email: fabio.marra@unifi.it

And/or
Chiara Raggi, PhD
Dipartimento di Medicina Sperimentale e Clinica
Largo Brambilla 3
I50134 Florence, Italy
Email: chiara.raggi@unifi.it

**Key Words:** HUCCT1, CCLP1, OXPHOS, PGC-1α, SR-18292

**List of Abbreviations:** Cholangiocarcinoma (CCA), Cancer Stem Cells (CSCs), peroxisome proliferator activated receptor gamma coactivator 1-α (PGC-1α), oxidative phosphorylation system (OXPHOS)

**Word Count:** 6608

**Number of Figures:** 8

**Number of Tables:** 0

**Conflicts of interest:** The authors have no conflicts of interest to disclose.

**Financial support**: Funding for this work was partially provided by Associazione Italiana per la Ricerca sul Cancro (AIRC, MFGA17588, IG23117) to Dr. Raggi and (IG17786) to Prof. Marra. Dr. Lori is supported in part by a Fellowship from Fondazione Italiana per la Ricerca sul Cancro (FIRC-AIRC). Financial support from the University of Florence, Fondazione Umberto Veronesi, Italian Ministry of University and Research (MIUR) through grant "Dipartimenti di Eccellenza - 2017" to University of Milano Bicocca, Department of Biotechnology and Biosciences is also acknowledged.

**Authors' contribution:** CR, FM designed the study and wrote the manuscript. MLT, ES, NN, MC, BP, MP, CC, EP, JI, TL, GL, CP, JC, ML, JBA, LDT, LV, GDM, SM, MR, IO, AA, PC provided materials, performed the experiments, collected the data, and analyzed the results. CR, FM supervised the project and critically revised the manuscript. All authors have read and approved the final manuscript.

**Acknowledgments**

The authors thank Dr. A.J. Demetris (University of Pittsburgh, Pittsburgh, PA, USA) for cholangiocarcinoma cell lines (HUCCT1 and CCLP1). The authors thank Prof. Betti Giusti (University of Florence, Florence, Italy) for the use of ABI7900HT equipment

**Data availability statement**

The data that support the findings of this study are available from the corresponding authors [FM, CR], upon reasonable request.

**ABSTRACT**

Background and Aims: Little is known about the metabolic regulation of cancer stem cells (CSC) in cholangiocarcinoma (CCA). We analyzed whether mitochondrial-dependent metabolism and related signaling pathways contribute to stem state in CCA.

Methods: The stem-like subset was enriched by sphere culture (SPH) in human intrahepatic CCA cells (HUCCT1 and CCLP1) and compared to cells cultured in monolayer. Extracellular flux analysis was examined by Seahorse technology and high-resolution respirometry. In patients with CCA, expression of factors related to mitochondrial metabolism was analyzed for possible correlation with clinical parameters.

Results: Metabolic analyses revealed a more efficient respiratory phenotype in CCA-SPH than in monolayers, due to mitochondrial oxidative phosphorylation. CCA-SPH showed high mitochondrial membrane potential and elevated mitochondrial mass, and over-expressed peroxisome proliferator-activated receptor gamma coactivator (PGC)-1α, a master regulator of mitochondrial biogenesis. Targeting mitochondrial complex I in CCA-SPH by metformin, or PGC-1α silencing or pharmacologic inhibition (SR-18292) impaired spherogenicity and expression of markers related to the CSC phenotype, pluripotency, and epithelial-mesenchymal transition. In mice with tumor xenografts generated by injection of CCA-SPH, administration of metformin or SR-18292 significantly reduced tumor growth and determined a phenotype more similar to tumors originated from cells grown in monolayer. In CCA patients, expression of PGC-1α was correlated to expression of mitochondrial complex II and of stem-like genes. Patients with higher PGC-1α expression by immunostaining had lower overall survival (OS) and progression-free survival, higher angioinvasion and faster recurrence. In GSEA analysis, CCA patients with high levels of mitochondrial Complex II had shorter OS and time to recurrence.

Conclusions: The CCA stem-subset has a more efficient respiratory phenotype and depends on mitochondrial oxidative metabolism and PGC-1α to maintain CSC features.

**Lay summary**

The growth of many cancers is sustained by a specific type of cells with more embryonic characteristics, termed as 'cancer stem cells'. These cells have been described in cholangiocarcinoma, a type of liver cancer with poor prognosis and limited therapeutic approaches. We demonstrate that cancer stem cells in cholangiocarcinoma have different metabolic features, and use mitochondria, an organelle located within the cells, as the major source of energy. We also identify PGC-1α, a molecule which regulates the biology of mitochondria, as a possible new target to be explored for developing new treatments for cholangiocarcinoma

**Highlights**

- The metabolic characteristics of cancer stem cells in cholangiocarcinoma are not known
- Cholangiocarcinoma stem-like cells preferentially use oxidative phosphorylation as a source of energy
- PGC-1α is a key molecule regulating the metabolic features of cholangiocarcinoma stem-like cells
- Interfering with oxidative phosphorylation or PGC-1α limits the development of tumors originating from stem-like cells *in vivo*
- Expression of PGC-1α or proteins of the mitochondrial respiratory complex correlate with clinical outcomes in patients with cholangiocarcinoma

## INTRODUCTION

Cholangiocarcinoma (CCA) represents the second most common form of primary liver cancer [1-3], with limited therapeutic approaches [4, 5]. As a result, the prognosis is still dismal with a 5-year survival lower than 20% [4, 5]. These features make CCA a top priority in the field of cancer research [4, 5]. The hypothesis of the existence of a cancer stem cell population (CSCs) has been recently validated with the identification of a subpopulation of self-renewing cells that gives rise to maturational lineages with a hierarchical organization, and divide symmetrically and asymmetrically to generate the tumor mass [6-14]. CSCs, also referred to as tumor-initiating cells or tumor-propagating cells, are tumorigenic, metastatic, resistant to chemo-and radiation therapy and are responsible for tumor recurrence [8-14]. In the past years, we and others [15-17] have highlighted the biology of CSCs in CCA, identifying them as a major therapeutic target [8-14].

Recent studies have identified OXPHOS in cancer cell mitochondria as a novel approach to decrease tumor growth and chemotherapy-resistance in CCA [18, 19]. Although mitochondrial metabolism may provide new therapeutic targets, metabolic reprogramming in CCA is underestimated. In addition, the metabolic profiles of CSC may be an important factor for stemness maintenance, contributing to failure of anticancer treatments [20, 21], but little is known regarding this topic in human CCA. Here we show that mitochondrial oxidative metabolism contributes to maintain stemness features in CCA, conferring *in vivo* tumorigenic capacity and drug-resistance.

## MATERIALS AND METHODS

This section is available in the Supplementary data and in the Supplementary CTAT Table

## RESULTS

### *The CCA Stem-like subset is characterized by mitochondrial oxidative metabolism*

We recently identified a functional CSC-subset in human CCA using a 3D sphere culture model [13]. We first characterized if stemness features were associated with differences in energy metabolism, comparing spheres (SPH) generated from HUCCT1 or CCLP1 cells with the same

cells grown in monolayers (MON). Bioenergetics parameters were analyzed by Seahorse technology, which allows to simultaneously measure oxygen consumption rate (OCR) and extracellular acidification rate (ECAR), key indicators of mitochondrial respiration and glycolysis, respectively, in live cells. Seahorse mitostress, which provides respiratory parameters, showed that SPH have higher OCR than MON both in basal and in FCCP-uncoupled condition (Figure 1A; Supplementary Figure 1A-B). In addition, the response to oligomycin A, which accounts for non-phosphorylating respiration, indicated that oxygen consumption rate, even enhanced, in SPH cells is coupled to ATP production similarly, or only weakly less, to that of MON cells (see values of the coupling efficiency of oxidative phosphorylation). These data indicate that, in both HUCCT1 and CCLP1, SPH show increased mitochondrial respiration coupled to ATP production, likely related to a potentiated respiratory machinery. Seahorse analysis requires forced adhesion of SPH to perform the assay. Although no significant differences in respiratory capacity of SPH cells forced to adhere on XF plates for as long as 20 hours were observed (data not shown), we aimed to confirm the Seahorse findings with an alternative method, which may be applied to cells in suspension. To do this, we analyzed OCR of SPH maintained in suspension, using a “Clark-type” oxygen electrode. Oxygraph analysis (Figure 1B) fully confirmed Seahorse data, suggesting that the enhanced mitochondrial respiration of SPH is a property acquired during the adaptation to the three-dimensional cell growth, and not an artifact dependent on the analytical methods used.

We next used the Seahorse glycostress protocol to measure glycolytic parameters of MON and SPH of both cell lines. This test (Figure 1C, Supplementary Figure1) showed that in SPH, basal and oligomycin-accelerated ECAR are similar as in MON, indicating limited, if any, differences in glycolytic capacity and reserve. Because SPH and MON are grown in media of different composition, we aimed to rule out that these differences could modify metabolic parameters independently of the "stemness" status of the cells. When MON cells were grown in SPH culture medium for 5 days, no variations in OCR parameters or in the expression of stemness-related genes were observed, indicating that metabolic differences only depend on 3D culture as a representation of a stem-like state (Supplementary Figure 2). Taken together, these results

indicate that when HUCCT1 or CCLP1 are grown as spheres, a profound change in energy metabolic profile, with enhanced mitochondrial respiration, is observed (Figure 1D).

***The CCA stem-like subset is more sensitive to interference with mitochondrial function***

Since CCA-SPH preferentially rely on OXPHOS, we further evaluated the role of mitochondria in the stem-like compartment. In CCA-SPH a significantly higher mitochondrial membrane potential was measured with MitoTracker Red staining, together with increased mitochondrial mass (MitoTracker Green, Figure 2A). The family of peroxisome proliferator-activated receptor gamma coactivators (PGC), in particular PGC-1α [22, 23] is a master regulator of mitochondrial *de novo* synthesis, and regulates different energy-producing metabolic processes in the liver, including OXPHOS. In CCA-SPH, over-expression of PGC-1α at the protein and mRNA levels (Figure 2B-C) was observed, providing additional support for a role of mitochondria in cells of the CCA stem-like subset. In contrast, CCA-SPH cells showed reduced glucose uptake (Figure 2D), together with lower production of lactate, a metabolic product of glycolysis (Figure 2E). Down-regulation of the glycolytic pathway is also indicated by repressed gene expression of the Glut1 transporter (Figure 2F) as well as of hexokinase II (HKII) and pyruvate kinase II (PKMII) (Figure 2G). Remarkably, GSEA analysis of RNAseq data confirmed the downregulation of the glycolytic component in CCA-SPH when compared to MON (Figure 2H). In contrast, no differences in mitochondrial ROS levels was observed comparing MON and SPH, indicating that differences in glycolytic flux are not due to an impairment in mitochondrial functionality (Supplementary Figure 3A).

It is well-known that activated AMPK regulates PGC-1α expression [24]. In accordance with high levels of PGC-1α in SPH cells (Figure 2B-C), the AMP/ATP ratio was higher in SPH than in MON (Supplementary Figure 3B), together with increased activation of AMPK signaling, as demonstrated by higher levels of AMPK phosphorylation (Supplementary Figure 3C). In other tumors, AMPK activation correlates with epithelial-mesenchymal transition (EMT) [25-27]. To establish whether AMPK regulates these processes in CCA-SPH, SPH were treated with

compound C (CC), a well-established inhibitor of AMPK phosphorylation [28] (Supplementary Figure 3D). Treatment with CC markedly reduced the expression level of genes implicated in EMT, indicating a contribution of the AMPK pathway in this relevant process associated with malignancy (Supplementary Figure 3B).

To provide functional evidence for a role of mitochondria in maintaining the CCA stem-like subset, cell survival was evaluated after treatment with metformin or phenformin, two inhibitors of mitochondrial complex I. SPH were consistently more sensitive to inhibitors of mitochondrial complex I than cells grown in MON (Supplementary Figure 4A). Conversely, treatment with 2-deoxy-D-glucose, an antagonist of glucose uptake, had a greater effect on survival of glycolysis-dependent MON (Supplementary Figure 4B). Interestingly, this effect was less marked, and not statistically significant, in CCLP1 cells, which express lower levels of HKII, and have a lower ability to incorporate glucose. These results reinforce the concept that CCA stem-like cells are more reliant on mitochondrial metabolism than cells in MON, sensitive to the glycolysis pathway. Exposure to metformin dramatically reduced the expression of molecules related to stemness, self-renewal, pluripotency, drug-resistance and epithelial-mesenchymal transition, in SPH of both CCA cell lines, while virtually no effects were found in MON (Supplementary Figure 4C-D). Moreover, metformin reduced activation of the Akt pathway only in SPH. (Supplementary Figure 4C-D). These data indicate that interfering with mitochondrial respiration affects the stemness component of CCA.

***PGC-1α is required to maintain stemness features and pro-angiogenic actions of CCA***

Because PGC-1α, a critical regulator of mitochondrial function, is expressed at higher levels in SPH, we tested the effects of genetic knockdown or pharmacologic inhibition of this molecule on functional characteristics and intracellular signaling of SPH from both CCLP1 and HUCCT1. As expected, PGC-1α depletion (Figure 3A) impaired mitochondrial mass (Supplementary Figure 5A). Although PGC-1α silencing did not affect cell proliferation or apoptosis (Supplementary Figure 5B-

C), it markedly reduced CCA stem-like properties such as *in vitro* spherogenicity (Figure 3B, Supplementary Figure 5D) and expression of CSC-related genes (Figure 3C). These functional effects were accompanied by a marked downregulation of signaling pathways relevant for CCA biology in SPH silenced for PGC-1α (Figure 3D). Similarly, PGC-1α knockdown significantly reduced the ability to invade a basement-membrane-like matrix (Figure 3 E) and to migrate in a Boyden chamber assay (Supplementary Figure 5E), key features of highly malignant CCA cells. Furthermore, we found a significant correlation between expression of PGC-1α and that of many stem-like genes in a transcriptomic database of CCA patients (Figure 3F) [29].

Angiogenesis is critical to develop and sustain a microenvironment favorable to maintain the properties of CSC, and we previously demonstrated [13] that conditioned medium from CCA SPH induces a higher angiogenic response than that from MON. In SPH silenced for PGC-1α or treated with metforrmin, VEGF expression was significantly reduced in both cell lines (Supplementary Figure 6A), indicating that the action of PGC-1α is likely to be mediated by mitochondria. As a clinical counterpart, a significant correlation between VEGF and PGC-1α expression was found in a transcriptomic database of CCA patients (Supplementary Figure 6B). To confirm that PGC-1α regulates angiogenesis, we tested the effects of conditioned medium from SPH on capillary tube-like formation by human umbilical vein endothelial cells (HUVEC) in an angiogenic assay (Supplementary Figure 6C-D). As expected, depletion of PGC-1α in SPH drastically reduced the neovascular response in CCA SPH. Overall, these data show that the CSC microvascular environment is dependent on tumor metabolic activity, regulated by PGC-1α.

To obtain additional information on the potential role of PGC-1α, we employed SR-18292, a selective pharmacological inhibitor which increases PGC-1α acetylation and its inhibition [30, 31]. Treatment with SR-18292 reduced PGC-1α levels and mitochondrial mass (Figure 4A-B), cell viability, expression of Myc and STAT3, and activation of P38MAPK and AKT (Figure 4C-D). In addition, pharmacologic inhibition of PGC-1α modulated a broad range of genes implicated in

maintenance of stemness, self-renewal, and regulation of EMT (Figure 4 C-D). These data identify mitochondrial respiration and PGC-1α as relevant targets in CCA stem-like cells.

To demonstrate that interference with mitochondrial respiration may have an impact on CCA stem-compartment growth *in vivo*, we analyzed the effects of metformin and of SR-18292 on tumors obtained by subcutaneous injection of cells derived from SPH or from cells grown in MON. The growth of xenografts was monitored with a dedicated in vivo imaging system (Vevo LAZR-X photoacoustic imaging), which allows 3D-reconstruction and exact calculation of tumor volume (Figure 5). As expected, 28 days after injection, the volume of tumors derived from SPH were significantly larger than those from MON. Treatment of mice with metformin or SR-18292 did not significantly modify the volume of tumors derived from MON. In contrast, the growth of tumors derived from SPH was significantly reduced by administration of metformin or SR-18292 (Figure 5). Evaluation of tumors using a caliper and conventional volume calculation provided overlapping results (data not shown). No differences in liver/body weight ratio and lung/body weight ratio were observed (Supplementary Figure 7). These data show that interference with mitochondrial respiration or PGC-1α selectively modulates the growth of tumors derived from stem-cell enriched cultures.

Based on the results described above, we next focused on the effects of metformin and SR-18292 on the molecular characteristic of tumors derived from SPH. The weight of tumors and the number of proliferating cells, as assessed by BrdU immunostaining, were significantly reduced by treatment with both drugs (Figure 6A-B). Gene expression profiles derived from a PCR array specific for liver cancer pathways revealed common downregulated genes in tumors from mice injected with SPH and treated with metformin or SR-18292 (Figure 6C). These included markers of apoptosis (i.e. BIRC2, CFLAR, GSTP1, BID) and cell cycle (CCND1, GADD45B, EP300, PTEN) as well as genes involved in signal transduction such as the Wnt pathway, MAP kinase or Met signaling, and DNA damage and repair (i.e. MSH2, XIAP). Tumor tissues belonging to mice treated with SR-18292 showed a peculiar set of downregulated genes which contains more cell cycle-related genes,

together with genes involved in immune and inflammatory response or angiogenesis. Of note, gene cluster analysis showed that tumors from mice injected with SPH and treated with metformin or SR-18292 were more similar to those derived from MON than to those of untreated mice injected with SPH. At the protein level, suppression of PGC-1α was associated with an increase in HKII expression, suggesting a metabolic shift towards a more glycolytic-like phenotype (Figure 6D). Moreover, treatment with SR-18292 had an impact on AKT activation, EMT and angiogenesis (CD31) thus confirming the PCR array data. In aggregate, these findings indicate an OXPHOS-addicted phenotype of the CCA-stem-like component and suggest that CCA CSCs adapt to stress conditions by acquiring mitochondrial flexibility, functionally relevant for the maintenance of a stem-like phenotype.

***Genes related to the mitochondrial system predict poor prognosis in CCA patients***

To translate our *in vitro* data to the clinical setting, we exploited a published cohort of CCA patients (19), which were dichotomically stratified into 'poor' survival (<12 months, 30 patients) and 'good' survival (>12 months, 64 patients) (Figure 7A). Both groups were tested for enhanced expression of crucial mitochondrial enzymes involved in the electron transport chain (Complex I-V) as well as in the Krebs cycle, by gene set enrichment analysis (GSEA). Interestingly, expression of genes of complex II (SDHA, SDHB, SDHC, SDHD) significantly correlated with overall survival (p=0.036) whereas the other gene sets did not reach statistical significance (Figure 7B). Moreover, expression of Complex II genes predicted a shorter time-to-recurrence (TTR) (p= 0.029, Figure 7C). Accordingly, a substantial correlation between PGC-1α, Complex II and genes related to stemness was found in CCA patients (Figure 7D, Supplementary Table 1).

We next investigated PGC-1α expression at the protein level by immunohistochemistry in a different cohort, observing variable degrees of expression (Figure 8A). Notably, patients with a high PGC-1α immunostaining score had shorter OS and progression-free survival, and higher angioinvasion and recurrence compared to patients with a low PGC-1α score (Figure 8B-E). These

data further indicate that in CCA patients, PGC-1 α expression is associated with significantly worse clinical outcomes.

## DISCUSSION

CSC are endowed with self-renewal, pluripotency, plasticity and differentiation potential. Due to these characteristics, in many types of cancer they play a pivotal role in initiation, progression, and response to treatment. Recent investigation has highlighted the concept that cancer is characterized by specific metabolic features, whereby genetic and environmental variables may be accompanied by acquisition of a different metabolic state. In spite of the significance of CSC in cancer and of the limited therapeutic opportunities available in CCA, the metabolic characteristics of CSC and their potential relevance in the biology of this tumor have not been previously explored. Data reported in this study indicate that in CCA, stem-like cells undergo metabolic reprogramming, resulting in a potentiated OXPHOS system, while cells grown in MON, a condition not associated with stemness features, rely more on glycolysis to meet their energy demands. Mitochondrial respiration is far more efficient in energy production than glycolysis, generating 36 molecules of ATP per molecule of glucose, as opposed to only two molecules of ATP produced in glycolysis. In agreement with metabolic data, CCA CSC showed marked changes in the number of mitochondria, and in their membrane potential. These changes are likely to be very relevant when considering that one of the most striking characteristics of CSCs is their ability to form a specialized niche, termed the CSC microenvironment [21], to adapt to changing conditions [10, 20]. This specific milieu facilitates tumor progression by maintaining the principal properties of CSCs. Indeed, CSCs are characterized by a highly plastic metabolism, which allows them to survive under conditions of metabolic stress by readily switching between OXPHOS and glycolysis. These changes are to some extent tumor cell-specific [32]. CCA is exquisitely sensitive to a specific microenvironment, which is characterized by a thick fibrillar stroma where oxygen and nutrients may be scarce. Based on the results of this study, the acquisition of a more efficient oxidative metabolism may allow CCA stem-like cells to better survive in these conditions. Accordingly, the

machinery to build up an efficient glycolysis was more developed in MON than in SPH, compatible with the leading role of OXPHOS in this latter culture condition. These data allow to speculate that in CCA, metabolic rewiring to OXPHOS renders CSCs resistant to inhibition of glycolysis, providing the cells with a higher degree of independence from microenvironmental nutrient supply.

Mitochondria play a pivotal role in regulating respiration, and the observed changes in their number and function are clearly related to data on OXPHOS. More important, we demonstrated that these changes in metabolism had a functional role. We first analyzed the effects of metformin and phenformin, two well-established inhibitors of mitochondrial respiration complex I. SPH exposed to these drugs showed a dose-dependent reduction in cell survival, and a profound modulation of the expression of different genes implicated in the biology of CCA, an effect absent in MON, where mitochondrial respiration appears to be less essential. Specifically, genes related to stemness and to angiogenesis were significantly less expressed, while markers of epithelial differentiation, e.g. E-cadherin, increased. These effects suggest that the mitochondrial respiration pathway may support the growth and aggressiveness of CCA enriched with a stem-like component.

Although the mechanisms determining the observed OXPHOS phenotype are still unclear, we next aimed to establish a link between regulatory proteins of mitochondrial biogenesis and the stemness properties of CCA cells [33-37]. We focused on the transcription factor PGC-1*α*, a key regulator of mitochondrial biogenesis, which enhances oxidative phosphorylation in many invasive and highly malignant cancer cells [38-40]. This factor was also recently shown to regulate OXPHOS functionality and, most importantly, self-renewal and tumorigenic capacity of pancreatic $CD133^+$ CSCs [34]. In CCA cells, genetic knockdown of PGC-1α decreased CSCs markers, *in vitro* self-renewal potential and invasive capacity of stem-like cells. These results were confirmed and expanded using SR-18292, a specific inhibitor of PGC-1α. In both cell lines used in this study, exposure to SR-18292 reduced mitochondrial biogenesis and sphere formation. These effects were associated with downregulation of signaling pathways linked to malignancy and EMT, and lower expression of genes related to self-renewal, pluripotency and drug transport. These data

support the dependence of stem-like cells on mitochondrial biogenesis and activity and identify an upstream molecular mechanism.

Tumors grow in a tridimensional and multicellular environment, and cell culture is only partially representative of an *in vivo condition.* Thus, we analyzed tumor xenografts developed in mice using CCA cells from MON or SPH cultures, and the effects of treatment with metformin or SR-18292. Remarkably, the effects of these two drugs were non-significant in tumors developed after MON injection. In contrast, tumors derived from SPH were larger, and their volume was reduced inhibiting mitochondrial respiration with metformin or PGC-1α expression by SR-18292. At a molecular level, the gene signature of tumors derived from SPH was characterized by upregulation of several pathways associated with malignancy. In contrast, treatment of mice with metformin or SR-18292 made the signature of SPH-derived tumors more similar to that of tumors derived from MON. Of note, the effects of SR-18292 were not completely overlapping with those of metformin and included upregulation of genes involved in the glycolytic pathway and reduced expression of genes regulating EMT or angiogenesis. Taken together, these data provide for the first time, in CCA, a direct correlation between oxidative metabolism and PGC-1α expression, the phenotype of stem-like cells, and the development of CCA xenografts *in vivo.*

CSCs dynamically shape their microenvironment to maintain a supportive niche, and drive interactions with other tumor components, such as immune cells, cancer-associated fibroblasts, and endothelial cells, to maintain a milieu which favors their survival and growth. This is achieved via a complex crosstalk with other cells of the niche, including secretion of soluble mediators, such as VEGF, which promotes angiogenesis through paracrine signals [41-47]. In CCA SPH, PGC-1*α* silencing downregulated the ability of SPH to express VEGF, phenocopying the effects of exposure to metformin. In addition, depletion of PGC-1*α* reduced the ability of SPH-conditioned medium to induce tube formation, a functional angiogenic assay. Along these lines, acquisition of a mesenchymal phenotype, via a EMT process, is a well-established feature of highly malignant cancers [48, 49]. In SPH, PGC-1α and mitochondrial respiration significantly upregulated

molecules involved in EMT, which was also upregulated by activation of AMPK. Altogether, these data identify mitochondrial respiration as a new pathway regulated by PGC-1*α* and responsible for maintenance of a stem-like phenotype and potentially of the angiogenic niche and EMT in CCA.

The ultimate goal of translational research is to identify and validate novel pathways or targets, the interference with which could be eventually investigated in clinical trials. For this strategy to be rational and possibly successful, the targets emerging from cell culture and animal experiments must be present and modulated in biologic material collected from patients with the condition of interest. We first exploited transcriptomic data from a published cohort of CCA patients to search for possible correlations between factors implicated in mitochondrial biogenesis and respiration, expression of genes involved in the aggressive biology of CCA, and clinical outcomes of the patients. In this respect, we found several levels of interaction. Expression of PGC-1*α* in SPH significantly and directly correlated with different genes implicated in stemness and was strongly and directly correlated with expression of VEGF, supporting the relation between mitochondria biogenesis and the angiogenic niche. Remarkably, mitochondrial complex II expression correlated with a poor prognosis when patients were dichotomically divided according to their outcome, and the same factor and PGC1*α* correlated with several CSC-related genes in an oligoarray heatmap. In a different cohort of patients, high-grade staining for PGC-1α identified a subgroup of patients with shortened overall and progression-free survival.

In conclusion, we have characterized the metabolic features of CSC from CCA, highlighting the predominance of oxidative metabolism, supported by increased mitochondrial biogenesis and signals generated via PGC1*α.* These lines of information provide significant advances in the biology of CSC in CCA that could be of eventual relevance for the management of this deadly tumor.

**FIGURE LEGENDS**

**Figure 1: Metabolic characteristics of CCA cells grown as monolayers (MON) or spheres (SPH).** (A-B) Oxygen consumption rates (OCR) of HUCCT1 and CCLP1 cells, as assessed by Seahorse mitostress test (A) or oxygraph (B) analysis. Respiratory parameters include basal mitochondrial respiration, response to oligomycin A accounting for non-phosphorylating mitochondrial respiration (oligo), FCCP-uncoupled mitochondrial respiration, spare respiratory capacity and coupling efficiency, calculated as described in Materials and Methods. Data were normalized on basal respiratory parameters in MON. (C) Extracellular acidification rate (ECAR) parameters derived from Seahorse glycostress test analysis, normalized on basal glycolytic parameters of MON. Results are mean±SD of two independent experiments performed on 10 (Seahorse) and 3 (Oxygraph) replicates for each condition (*p≤0.05, ** p≤0.01, ***p≤0.001 vs. MON). (D) Energy phenotype of HUCCT1 and CCLP1 cells grown as MON (diamonds) or SPH (triangles) in basal (empty shapes) or metabolic stress (full shapes) conditions, as described in Materials and Methods.

**Figure 2: Mitochondrial mass and glycolysis are differentially regulated in CCA cells grown as MON or SPH.** (A) Mitochondrial mass and membrane potential were measured by FACS. Histograms represent the Mean Fluorescence Intensity (MFI) of the MitoTracker probes normalized to mean MFI of MON. Data are mean±SEM (n=3, *p≤0.05, **p≤0.01 vs. MON). (B) Immunoblot of PGC-1α. β-actin immunoblot was performed to ensure equal loading. (C) PGC-1α gene expression levels, presented as fold changes normalized to mean expression of MON. GAPDH was used as an internal control. Data are mean±SEM (n=3, **p≤0.01 vs. MON). (D) [$^{14}$C]-glucose uptake normalized by total proteins. Data are mean±SEM (n=3, *p≤0.05 vs. MON). (E) Extracellular lactate levels normalized by protein content. Data are mean±SEM (n=3, ***p≤0.001 vs. MON). (F) GLUT1 gene expression levels, presented as in panel C. Mean ± SEM (n=3, **p≤0.01, ***p≤0.001 vs. MON). (G) Immunoblot of HKII and PKM2, presented as in panel B. (H) Results of a GSEA Pre-ranked analysis on the Glycolysis gene set of the Hallmark MSigDB collection. ES: enrichment

score. NES: normalized enrichment score. FDR: False discovery Rate.

**Figure 3: Effects of PGC-1α silencing in CCA SPH cells.** (A) PGC-1α gene expression levels following siRNA transfection, presented as fold changes normalized to mean expression of siCTR (n=4, mean±SEM, *** p≤0.001 vs. siCTR). (B) Effects of PGC-1α silencing on CCA sphere-forming efficiency. Mean±SEM (n=3, ***p ≤0.001 vs. siCTR). Representative images of CCA SPH are shown below the barogram (original magnification 40X, scale bar 10μM). (C) Expression of different genes, expressed as fold changes normalized to mean expression of siCTR sample. Mean±SEM (n=3, *p≤0.05, **p≤0.01, ***p≤0.01 vs. siCTR). Gene groups are indicated at the bottom of the barograms. (D) Immunoblot of different proteins or phosphoproteins following PGC-1α silencing. (E) Invasion of PGC-1α-silenced CCLP1 and HUCCT1 cells was measured in modified Boyden chambers. Mean±SEM (n=5, *p≤0.05 , ***p≤0.001 vs. siCTR). Representative images of filters are shown below the barograms (original magnification 40X, scale bar 10μM. (F) Scatterplots representing correlations between expression levels of PGC-1α (x-axis) and stem-like genes (y-axis) according to a published microrarray-based study comparing CCA vs surrounding liver (GSE26566 [25]). r: Pearson's correlation coefficient, n: number of samples. All adjusted (two tails) p values were <1e-5.

**Figure 4: Effects of the PGC-1α inhibitor SR-18292 in CCA SPH cells.** (A) Sphere-forming efficiency after SR-18292 exposure. Mean±SEM (n=3, *p≤0.05, **p≤0.001 vs. control. (B) Mitochondrial mass, measured with MitoTracker Green, as described in Figure 2A, presented as fold induction normalized to mean MFI of control). Mean±SEM (n=3, *p≤0.05, **p≤0.01 vs. control). (C) Expression of different genes, expressed as fold changes normalized to mean expression of control sample) (n=3). Mean±SEM (*p≤0.05, **p≤0.01 vs. CTR). (D) Immunoblot of different proteins and phosphoproteins following SR-18292 treatment.

**Figure 5: Effects of metformin and SR-18292 on tumor xenografts.** Tumors derived from HUCCT1 cells grown as MON or SPH were obtained by subcutaneous injection in NOD/SCID mice. After 7 days, mice were treated with PBS (CTR), metformin (Metf) or SR-18292 (SR) (n=6 per group). (A) Analysis of tumor volume by Vevo LAZR-X photoacoustic imaging.
The box height represents the interquartile range (Q1–Q3), the line within the box is the median value, the lower and upper whiskers represents the lowest and the highest samples, respectively. Circles in boxplots represent outlier samples (>1.5xIQR). ***p<0.002 or less. (B) Representative high resolution ultrasound images of subcutaneous tumors from mice in each group. The cyan 3D regions represent the tumor volume obtained by tracing areas on each 2D B-mode slices from the 3D acquisition.

**Figure 6: Phenotypic characteristic of CCA-SPH xenografts following treatment with metformin or SR-18292 or in comparison to MON-derived tumors.** (A) Tumor weight, depicted as in Figure 5A. Representative dissected tumor samples are shown below the box-plot. **p≤0.002, *p=0.016. (B) BrdU incorporation by immunostaining assay. Mean±SEM (**p≤0.01). Representative stainings are shown below the barogram, BrdU-positive nuclei are in brown color. Scale bar 10µm. (C) qRT-PCR arrays focused on liver cancer pathways. Heatmap of different tumor samples based on expression of 84 genes. Gene expression levels are expressed in color code from green (low) to red (high) according to the color key scale bar. Hierarchical clustering was based on complete linkage on euclidean distances between genes (rows) or samples (columns). (D) Immunoblot of different proteins and phosphoproteins in tumor samples from different groups.

**Figure 7. Expression of respiratory Complex II is associated with poor survival and recurrence in CCA patients.** (A). Kaplan-Meyer plot showing overall survival in 94 iCCA patients stratified according to good or bad prognosis. (B) GSEA of custom gene sets representing

respiratory complex I-V and Krebs cycle. (C) Number of genes in signature, enrichment (ES) and normalized enrichment score (NES) reflect positive or negative association with a trait with FDR-corrected q-value. Enrichment plots show significantly associated respiratory complex II signature with patient outcomes. (D) Correlation between expression of Complex II (SDHA, SDHB, SDHC, SDHD) or PGC-1α genes (x-axis) and stem-like genes (y-axis) in a published microrarray-based study comparing CCA vs surrounding liver (GSE26566 [25]). r: Pearson's correlation coefficient, n: number of samples. All adjusted (two tails) p values were <1e-5.

**Figure 8: Staining for PGC-1α correlates with clinical characteristics of CCA.** (A) Immunostaining for PCG-1α in three representative CCA specimens. Homogeneous and strong staining in cancer cells (upper panel); moderate cytoplasmic immunoreactivity (middle panel); faint cytoplasmic immunoreactivity (lower panel). Original magnification 20x, scale bar 10μM. (B) Kaplan-Meier survival curves for patients grouped according to staining intensity. (C). Kaplan-Meier progression-free survival curves for the same groups as in (B). (D) Presence of angioinvasion in for patients grouped according to staining intensity (Fisher exact test, p<0.001).

**REFERENCES (Author names in bold designate shared co-first authorship)**

[1] Khan SA, Tavolari S, Brandi G. Cholangiocarcinoma: Epidemiology and risk factors. Liver Int 2019;39 Suppl 1:19-31.
[2] Bertuccio P, Malvezzi M, Carioli G, Hashim D, Boffetta P, El-Serag HB, et al. Reply to: "Global trends in mortality from intrahepatic and extrahepatic cholangiocarcinoma". J Hepatol 2019;71:1262-1263.
[3] Banales JM, Marin JJG, Lamarca A, Rodrigues PM, Khan SA, Roberts LR, et al. Cholangiocarcinoma 2020: the next horizon in mechanisms and management. Nat Rev Gastroenterol Hepatol 2020;17:557-588.
[4] Banales JM, Cardinale V, Carpino G, Marzioni M, Andersen JB, Invernizzi P, et al. Expert consensus document: Cholangiocarcinoma: current knowledge and future perspectives consensus statement from the European Network for the Study of Cholangiocarcinoma (ENS-CCA). Nat Rev Gastroenterol Hepatol 2016;13:261-280.
[5] Shaib Y, El-Serag HB. The epidemiology of cholangiocarcinoma. Semin Liver Dis 2004;24:115-125.
[6] Yamashita T, Honda M, Nakamoto Y, Baba M, Nio K, Hara Y, et al. Discrete nature of EpCAM+ and CD90+ cancer stem cells in human hepatocellular carcinoma. Hepatology 2013;57:1484-1497.
[7] Oikawa T. Cancer Stem cells and their cellular origins in primary liver and biliary tract cancers. Hepatology 2016;64:645-651.
[8] Marquardt JU, Raggi C, Andersen JB, Seo D, Avital I, Geller D, et al. Human hepatic cancer stem cells are characterized by common stemness traits and diverse oncogenic pathways. Hepatology 2011;54:1031-1042.
[9] Raggi C, Factor VM, Seo D, Holczbauer A, Gillen MC, Marquardt JU, et al. Epigenetic reprogramming modulates malignant properties of human liver cancer. Hepatology 2014;59:2251-2262.
[10] Raggi C, Mousa HS, Correnti M, Sica A, Invernizzi P. Cancer stem cells and tumor-associated macrophages: a roadmap for multitargeting strategies. Oncogene 2016;35:671-682.
[11] Raggi C, Invernizzi P, Andersen JB. Impact of microenvironment and stem-like plasticity in cholangiocarcinoma: molecular networks and biological concepts. J Hepatol 2015;62:198-207.
[12] Correnti M, Raggi C. Stem-like plasticity and heterogeneity of circulating tumor cells: current status and prospect challenges in liver cancer. Oncotarget 2017;8:7094-7115.
[13] **Raggi C, Correnti M,** Sica A, Andersen JB, Cardinale V, Alvaro D, et al. Cholangiocarcinoma stem-like subset shapes tumor-initiating niche by educating associated macrophages. J Hepatol 2017;66:102-115.
[14] **Raggi C, Gammella E,** Correnti M, Buratti P, Forti E, Andersen JB, et al. Dysregulation of Iron Metabolism in Cholangiocarcinoma Stem-like Cells. Sci Rep 2017;7:17667.
[15] Vicent S, Lieshout R, Saborowski A, Verstegen MMA, Raggi C, Recalcati S, et al. Experimental models to unravel the molecular pathogenesis, cell of origin and stem cell properties of cholangiocarcinoma. Liver Int 2019;39 Suppl 1:79-97.
[16] Nevi L, Costantini D, Safarikia S, Di Matteo S, Melandro F, Berloco PB, et al. Cholest-4,6-Dien-3-One Promote Epithelial-To-Mesenchymal Transition (EMT) in Biliary Tree Stem/Progenitor Cell Cultures In Vitro. Cells 2019;8.
[17] Carpino G, Cardinale V, Folseraas T, Overi D, Grzyb K, Costantini D, et al. Neoplastic Transformation of the Peribiliary Stem Cell Niche in Cholangiocarcinoma Arisen in Primary Sclerosing Cholangitis. Hepatology 2019;69:622-638.
[18] Pant K, Richard S, Peixoto E, Gradilone SA. Role of Glucose Metabolism Reprogramming in the Pathogenesis of Cholangiocarcinoma. Front Med (Lausanne) 2020;7:113.
[19] Dan Li, Wang C, Ma P, Yu Q, Gu M, Dong L, et al. PGC1α promotes cholangiocarcinoma metastasis by upregulating PDHA1 and MPC1 expression to reverse the Warburg effect. Cell Death Dis 2018;9:466.

[20] Ippolito L, Marini A, Cavallini L, Morandi A, Pietrovito L, Pintus G, et al. Metabolic shift toward oxidative phosphorylation in docetaxel resistant prostate cancer cells. Oncotarget 2016;7:61890-61904.
[21] Taddei ML, Cavallini L, Ramazzotti M, Comito G, Pietrovito L, Morandi A, et al. Stromal-induced downregulation of miR-1247 promotes prostate cancer malignancy. J Cell Physiol 2019;234:8274-8285.
[22] Wu Z, Puigserver P, Andersson U, Zhang C, Adelmant G, Mootha V, et al. Mechanisms controlling mitochondrial biogenesis and respiration through the thermogenic coactivator PGC-1. Cell 1999;98:115-124.
[23] Piccinin E, Peres C, Bellafante E, Ducheix S, Pinto C, Villani G, et al. Hepatic peroxisome proliferator-activated receptor γ coactivator 1β drives mitochondrial and anabolic signatures that contribute to hepatocellular carcinoma progression in mice. Hepatology 2018;67:884-898.
[24] Jäger S, Handschin C, St-Pierre J, Spiegelman BM. AMP-activated protein kinase (AMPK) action in skeletal muscle via direct phosphorylation of PGC-1alpha. Proc Natl Acad Sci U S A 2007;104:12017-12022.
[25] Wang X, Pan X, Song J. AMP-activated protein kinase is required for induction of apoptosis and epithelial-to-mesenchymal transition. Cell Signal 2010;22:1790-1797.
[26] He K, Guo X, Liu Y, Li J, Hu Y, Wang D, et al. TUFM downregulation induces epithelial-mesenchymal transition and invasion in lung cancer cells via a mechanism involving AMPK-GSK3β signaling. Cell Mol Life Sci 2016;73:2105-2121.
[27] Cantó C, Auwerx J. PGC-1alpha, SIRT1 and AMPK, an energy sensing network that controls energy expenditure. Curr Opin Lipidol 2009;20:98-105.
[28] **Liu X, Chhipa RR,** Nakano I, Dasgupta B. The AMPK inhibitor compound C is a potent AMPK-independent antiglioma agent. Mol Cancer Ther 2014;13:596-605.
[29] Andersen JB, Spee B, Blechacz BR, Avital I, Komuta M, Barbour A, et al. Genomic and genetic characterization of cholangiocarcinoma identifies therapeutic targets for tyrosine kinase inhibitors. Gastroenterology 2012;142:1021-1031.e1015.
[30] Sharabi K, Lin H, Tavares CDJ, Dominy JE, Camporez JP, Perry RJ, et al. Selective Chemical Inhibition of PGC-1α Gluconeogenic Activity Ameliorates Type 2 Diabetes. Cell 2017;169:148-160.e115.
[31] Miller KN, Clark JP, Anderson RM. Mitochondrial regulator PGC-1a-Modulating the modulator. Curr Opin Endocr Metab Res 2019;5:37-44.
[32] Vlashi E, Lagadec C, Vergnes L, Reue K, Frohnen P, Chan M, et al. Metabolic differences in breast cancer stem cells and differentiated progeny. Breast Cancer Res Treat 2014;146:525-534.
[33] **Janiszewska M, Suvà ML,** Riggi N, Houtkooper RH, Auwerx J, Clément-Schatlo V, et al. Imp2 controls oxidative phosphorylation and is crucial for preserving glioblastoma cancer stem cells. Genes Dev 2012;26:1926-1944.
[34] Sancho P, Burgos-Ramos E, Tavera A, Bou Kheir T, Jagust P, Schoenhals M, et al. MYC/PGC-1α Balance Determines the Metabolic Phenotype and Plasticity of Pancreatic Cancer Stem Cells. Cell Metab 2015;22:590-605.
[35] **De Luca A, Fiorillo M,** Peiris-Pagès M, Ozsvari B, Smith DL, Sanchez-Alvarez R, et al. Mitochondrial biogenesis is required for the anchorage-independent survival and propagation of stem-like cancer cells. Oncotarget 2015;6:14777-14795.
[36] **Pastò A, Bellio C, Pilotto G,** Ciminale V, Silic-Benussi M, Guzzo G, et al. Cancer stem cells from epithelial ovarian cancer patients privilege oxidative phosphorylation, and resist glucose deprivation. Oncotarget 2014;5:4305-4319.
[37] Lamb R, Harrison H, Hulit J, Smith DL, Lisanti MP, Sotgia F. Mitochondria as new therapeutic targets for eradicating cancer stem cells: Quantitative proteomics and functional validation via MCT1/2 inhibition. Oncotarget 2014;5:11029-11037.
[38] LeBleu VS, O'Connell JT, Gonzalez Herrera KN, Wikman H, Pantel K, Haigis MC, et al. PGC-1α mediates mitochondrial biogenesis and oxidative phosphorylation in cancer cells to promote metastasis. Nat Cell Biol 2014;16:992-1003, 1001-1015.

[39] Cheong H, Lu C, Lindsten T, Thompson CB. Therapeutic targets in cancer cell metabolism and autophagy. Nat Biotechnol 2012;30:671-678.
[40] **Li Y, Xu S,** Li J, Zheng L, Feng M, Wang X, et al. SIRT1 facilitates hepatocellular carcinoma metastasis by promoting PGC-1α-mediated mitochondrial biogenesis. Oncotarget 2016;7:29255-29274.
[41] Conley SJ, Gheordunescu E, Kakarala P, Newman B, Korkaya H, Heath AN, et al. Antiangiogenic agents increase breast cancer stem cells via the generation of tumor hypoxia. Proc Natl Acad Sci U S A 2012;109:2784-2789.
[42] **Hasmim M, Noman MZ,** Messai Y, Bordereaux D, Gros G, Baud V, et al. Cutting edge: Hypoxia-induced Nanog favors the intratumoral infiltration of regulatory T cells and macrophages via direct regulation of TGF-β1. J Immunol 2013;191:5802-5806.
[43] Maxwell PH, Dachs GU, Gleadle JM, Nicholls LG, Harris AL, Stratford IJ, et al. Hypoxia-inducible factor-1 modulates gene expression in solid tumors and influences both angiogenesis and tumor growth. Proc Natl Acad Sci U S A 1997;94:8104-8109.
[44] Bao S, Wu Q, Sathornsumetee S, Hao Y, Li Z, Hjelmeland AB, et al. Stem cell-like glioma cells promote tumor angiogenesis through vascular endothelial growth factor. Cancer Res 2006;66:7843-7848.
[45] Flavahan WA, Wu Q, Hitomi M, Rahim N, Kim Y, Sloan AE, et al. Brain tumor initiating cells adapt to restricted nutrition through preferential glucose uptake. Nat Neurosci 2013;16:1373-1382.
[46] Carcereri de Prati A, Butturini E, Rigo A, Oppici E, Rossin M, Boriero D, et al. Metastatic Breast Cancer Cells Enter Into Dormant State and Express Cancer Stem Cells Phenotype Under Chronic Hypoxia. J Cell Biochem 2017;118:3237-3248.
[47] Siebzehnrubl FA, Silver DJ, Tugertimur B, Deleyrolle LP, Siebzehnrubl D, Sarkisian MR, et al. The ZEB1 pathway links glioblastoma initiation, invasion and chemoresistance. EMBO Mol Med 2013;5:1196-1212.
[48] Gooding AJ, Schiemann WP. Epithelial-Mesenchymal Transition Programs and Cancer Stem Cell Phenotypes: Mediators of Breast Cancer Therapy Resistance. Mol Cancer Res 2020;18:1257-1270.
[49] Yang J, Antin P, Berx G, Blanpain C, Brabletz T, Bronner M, et al. Guidelines and definitions for research on epithelial-mesenchymal transition. Nat Rev Mol Cell Biol 2020;21:341-352.

**Figure 1**

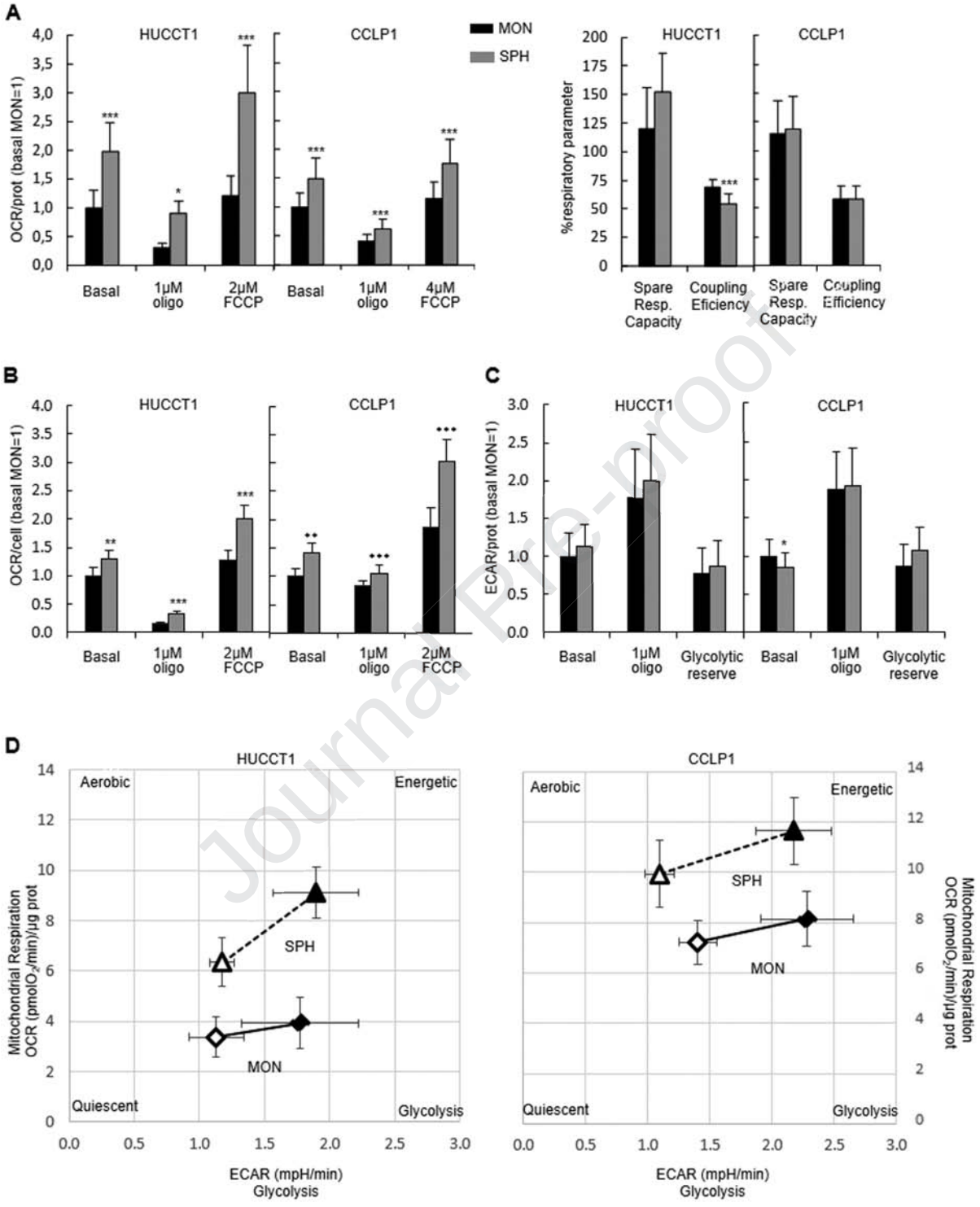

**Figure 2**

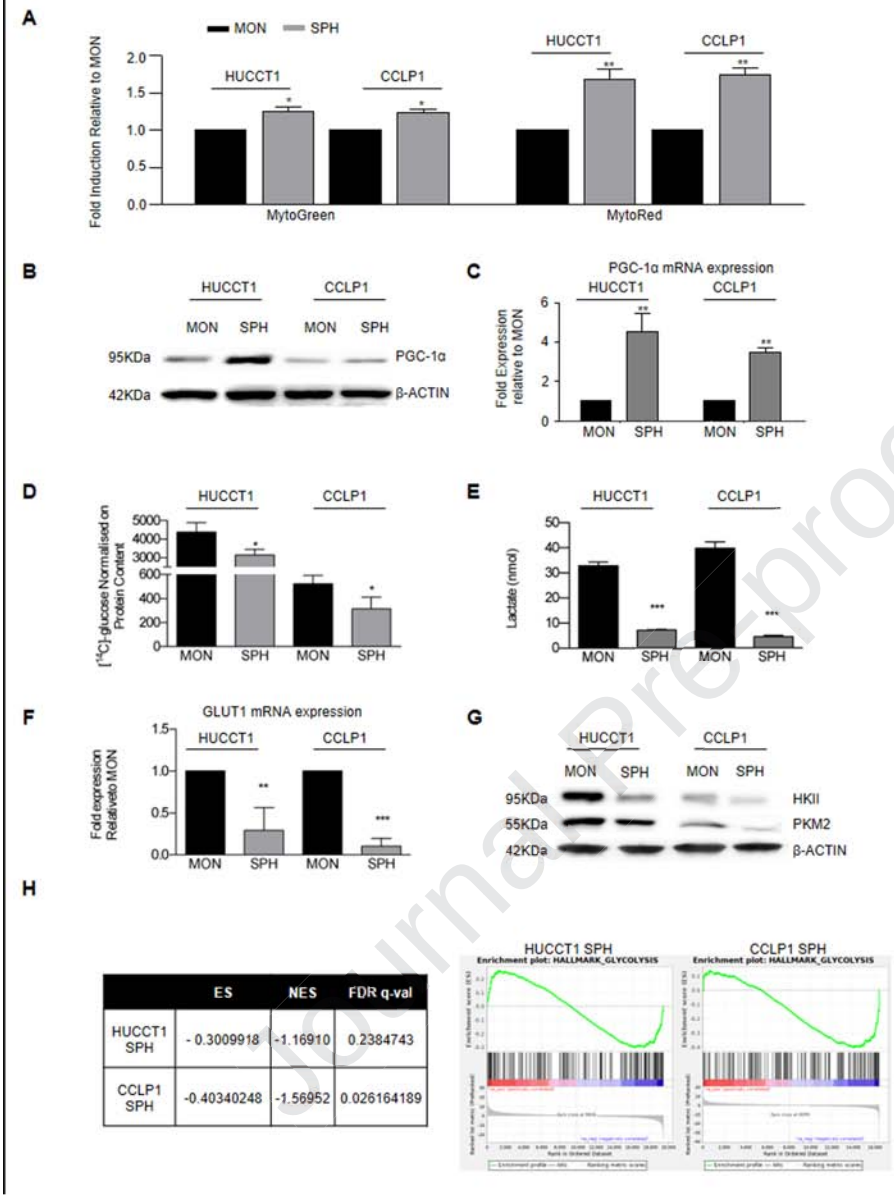


| | ES | NES | FDR q-val |
|---|---|---|---|
| HUCCT1 SPH | - 0.3009918 | -1.16910 | 0.2384743 |
| CCLP1 SPH | -0.40340248 | -1.56952 | 0.026164189 |

**Figure 3**

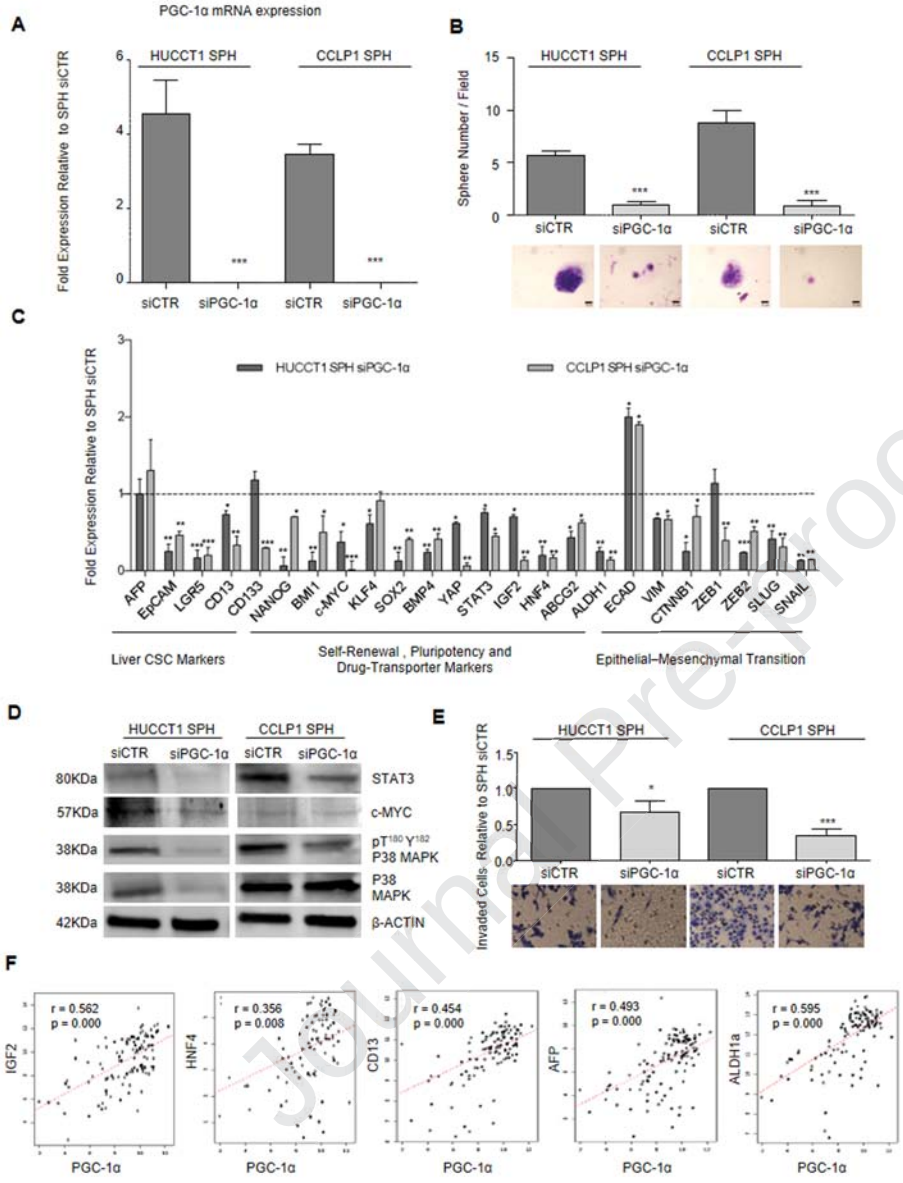

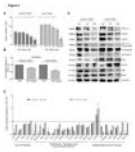

**Figure 5**

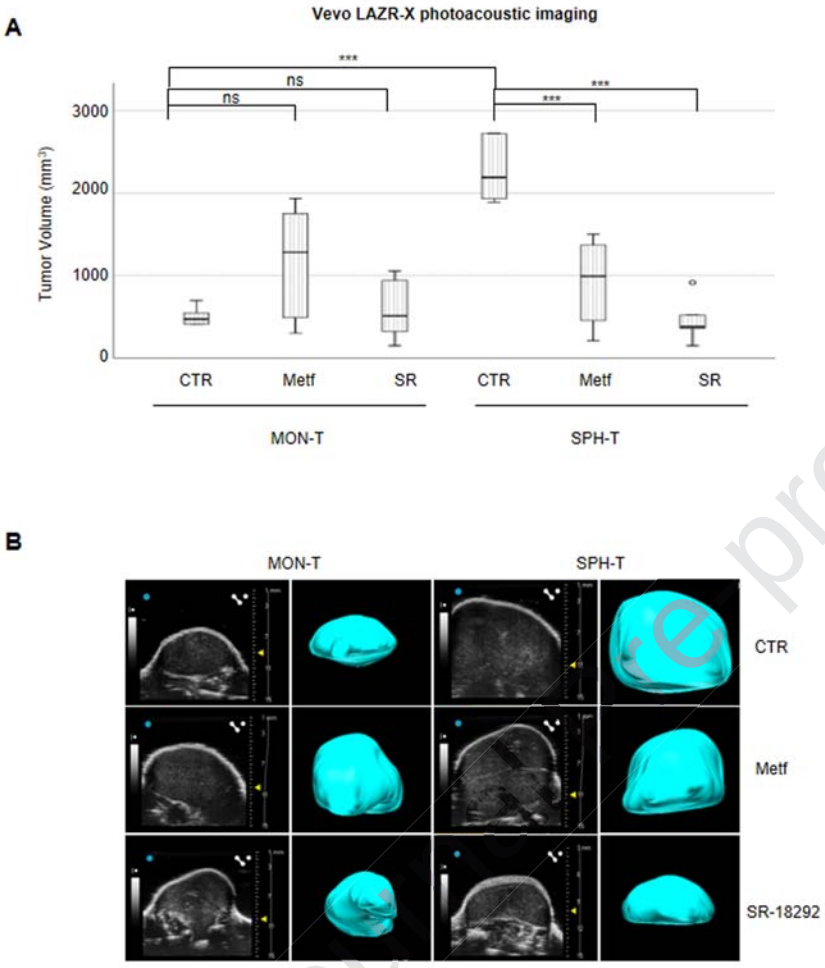

**Figure 6**

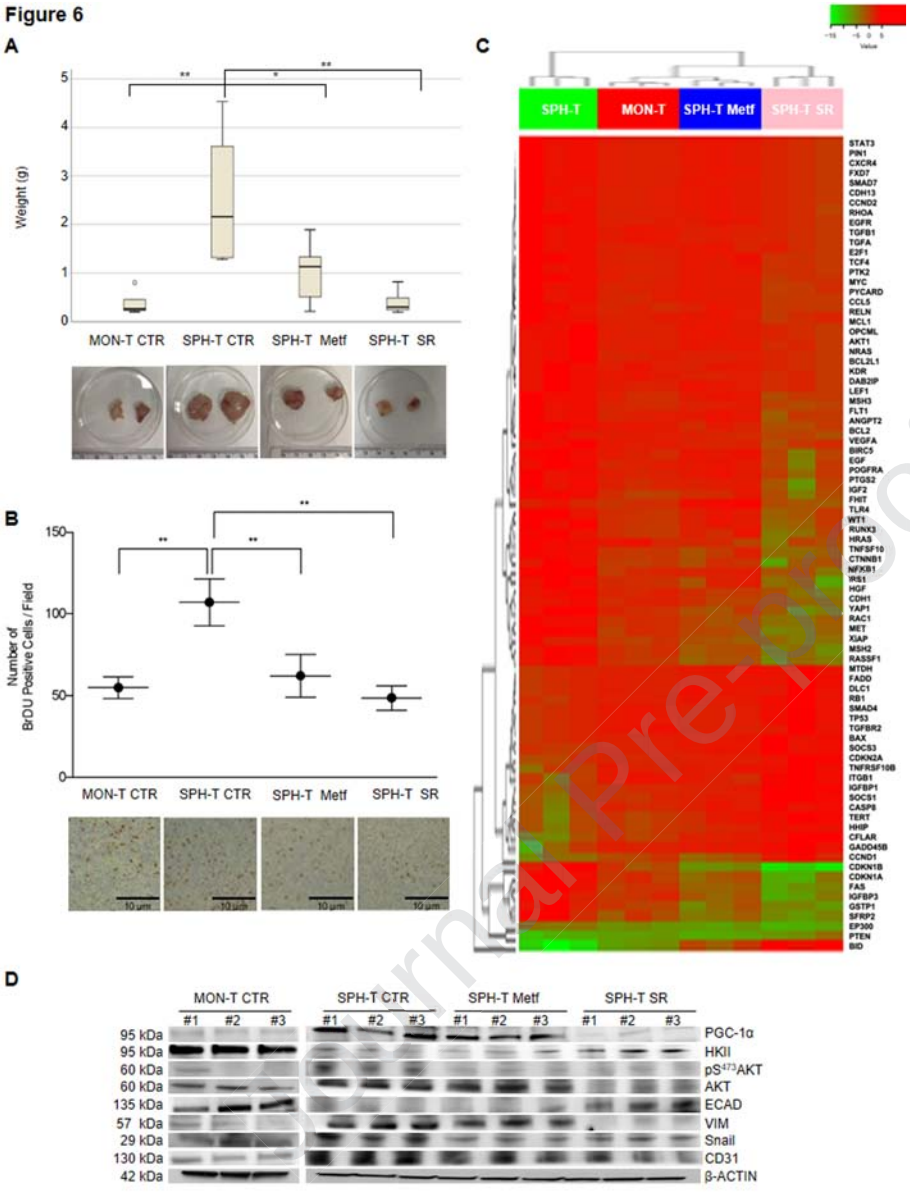

**Figure 7**

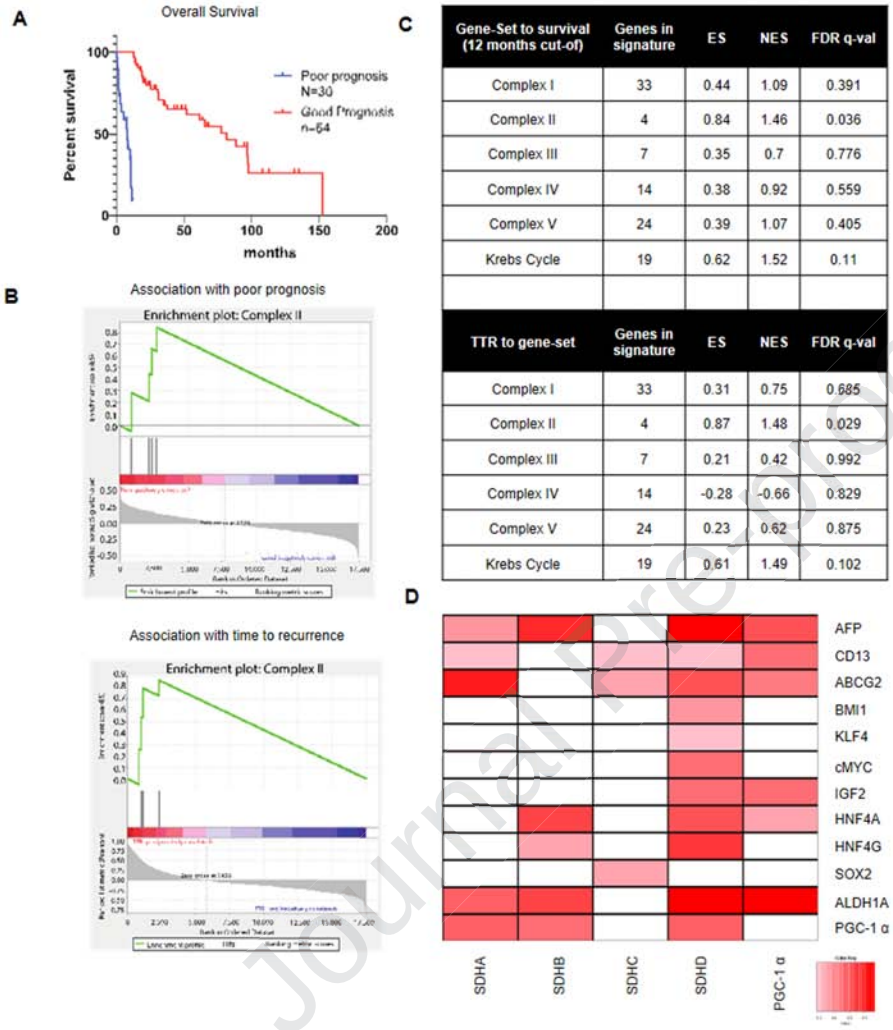


| Gene-Set to survival (12 months cut-of) | Genes in signature | ES | NES | FDR q-val |
|---|---|---|---|---|
| Complex I | 33 | 0.44 | 1.09 | 0.391 |
| Complex II | 4 | 0.84 | 1.46 | 0.036 |
| Complex III | 7 | 0.35 | 0.7 | 0.776 |
| Complex IV | 14 | 0.38 | 0.92 | 0.559 |
| Complex V | 24 | 0.39 | 1.07 | 0.405 |
| Krebs Cycle | 19 | 0.62 | 1.52 | 0.11 |
| | | | | |
| **TTR to gene-set** | **Genes in signature** | **ES** | **NES** | **FDR q-val** |
| Complex I | 33 | 0.31 | 0.75 | 0.685 |
| Complex II | 4 | 0.87 | 1.48 | 0.029 |
| Complex III | 7 | 0.21 | 0.42 | 0.992 |
| Complex IV | 14 | -0.28 | -0.66 | 0.829 |
| Complex V | 24 | 0.23 | 0.62 | 0.875 |
| Krebs Cycle | 19 | 0.61 | 1.49 | 0.102 |

**Figure 8**

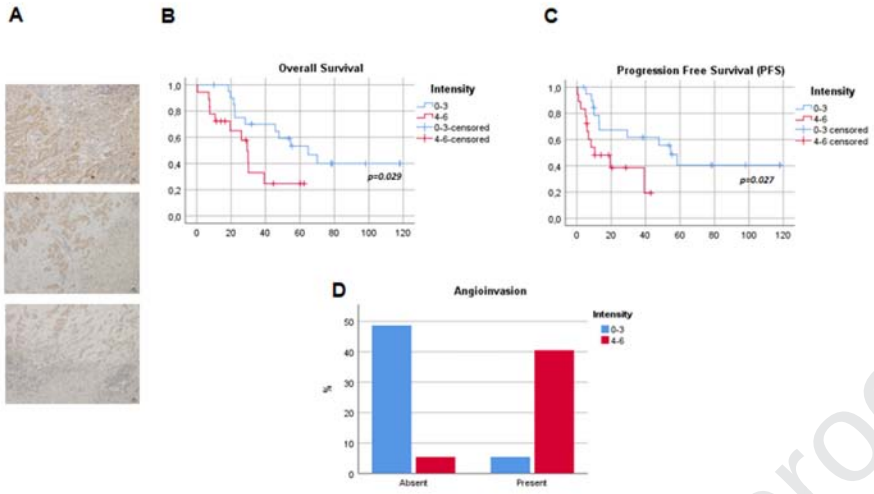

# Mitochondrial oxidative metabolism contributes to maintain a cancer stem cell phenotype in cholangiocarcinoma

**Chiara Raggi[1], Maria Letizia Taddei[1], Elena Sacco[2,3], Nadia Navari[1], Margherita Correnti[4], Benedetta Piombanti[1], Mirella Pastore[1], Claudia Campani[1], Erica Pranzini[1], Jessica Iorio[1], Giulia Lori[1], Tiziano Lottini[1], Clelia Peano[5,6], Javier Cibella[5], Monika Lewinska[7], Jesper B Andersen[7], Luca di Tommaso[8,9], Luca Vigano[9,10], Giovanni Di Maira[1], Stefania Madiai[1], Matteo Ramazzotti[8], Ivan Orlandi[2,3], Annarosa Arcangeli[1], Paola Chiarugi[8,9], Fabio Marra[1,9,#]**

**Table of Contents**

**Supplementary Materials and Methods**

**Cell cultures and reagents**

HUCCT1 and CCLP1 cells, from intrahepatic bile duct cancer tissues, were a kind gift from Dr. A.J. Demetris. Cell lines were cultured as described [1-3]. SR-18292 was purchased by MedChemExpress.

**Sphere formation assay**

The cells were grown in anchoring-independent conditions into poly 2-hydroxyethyl methacrylate (poly-HEMA)-coated dishes (Sigma Aldrich) with selective serum-free DMEM/F12 medium supplemented with 1X B27 supplement without vitamin A (Life Technologies), 20 ng/mL EGF, and 20 ng/mL bFGF (R&D Systems). To prevent cell aggregation, 1% methylcellulose (R&D System) was added to the culture medium [4, 5].

To calculate sphere-forming efficiency, 500 CCA cells were grown in anchoring-independent conditions with selective serum-free medium. After 7 days, pictures were taken to measure the number and size of CCA-SPH using a Leica DMi1microscope (Leica). Average number of formed spheres  microscopic field (20x) over five fields. CCA-SPH  volume was calculated after measuring length 1 (L1) and the length 2 (L2) using the following formula: V = (L1*L2*L2)/2 .

**Bioenergetic profiling**

Bioenergetic parameters of HUCCT1 and CCLP1 cells grown for 10 days as monolayer or spheres were analyzed using Agilent Seahorse XF24 analyzer and a “Clark-type” oxygen electrode.

Bioenergetic parameters of HUCCT1 and CCLP1 cells grown for 10 days as monolayer or spheres were analyzed using Agilent Seahorse XF24 analyzer and a “Clark-type” oxygen electrode (Oxygraph System, Hansatech Instruments, Nortfolk, UK). Before the analysis, cells were collected by trypsinization and counted: (a) 4-5x$10^6$ cells were suspended in 2ml unbuffered medium (D5030

Sigma Aldrich w/o sodium bicarbonate, containing 142mM NaCl, 10mM glucose, 2 mM glutamine, pH 7.4), and promptly analyzed by Oxygraph at 37°C. Respiratory rates were determined from the slope of a plot of $O_2$ concentration against time, divided by the cellular concentration. (b) the remaining cells were suspended in exhaust medium at the concentration $5x10^5$ cells/ml, seeded in Seahorse XF24-well plates (100µl/well), and incubated for 5h or 20h at 37°C in a humidified atmosphere of 5% CO2- 95% air. Before XF analysis culture medium was replaced with unbuffered medium (w/o glucose for measurements of glycolytic parameters) and cell cultures were let equilibrate for 1h at 37°C in a no-$CO_2$ incubator. Seahorse XF analysis was performed at 37°C simultaneously measuring Oxygen consumption rate (OCR =pmoles$O_2$/min) and Extracellular acidification rate (ECAR = mpH/min) in all the 24 wells of the XF plate, 10 devoted to each condition, MON and SPH, per cell line, and 4 as no cells-wells control. At the end of XF analysis, medium was removed, cells were gently washed with PBS, suspended in JS lysis buffer and scraped after two freeze and thaw cycles. Protein content of cell lysates was measured by Bradford assay and used for normalizing respiratory and glycolytic parameters. Oxygen consumption rate was analyzed by both Seahorse XF analyzer and Oxygraph under basal condition and under treatments with an ATP synthase inhibitor (0,5-2 µM oligomycin A), a ETC accelerator ionophore (0,25-5 µM carbonilcyanide p-triflouromethoxyphenylhydrazone or FCCP) and a ETC inhibitors mixture (1µM rotenone and 1µM antimycin A). The addition of the minimum dose of oligomycin A, and FCCP which generates the maximal effect accounted for non-phosphorylating respiration, and uncoupled respiration, respectively. The addiction of the rotenone and antimycin A mixture accounted for non-mitochondrial oxygen consumption. XF analysis of respiratory parameters was performed according to seahorse mitostress test protocol, consisting of three sequential measurements in basal condition and after the injection of the optimal doses of oligomycin A, FCCP, and rotenone/antimycin A. Respiratory parameters were elaborated using the following formulas: basal mitochondrial respiration (Basal-MR) = OCRbasal-OCRrot/ant, non phosphorylating mitochondrial

respiration (oligo-NPMR) = OCRoligo-OCRrot/ant, FCCP-uncoupled mitochondrial respiration (FCCP-MR) = OCRFCCP-OCRrot/ant, spare respiratory capacity = [OCR(FCCP)-OCR(rot/ant)/OCR(basal)-OCR(rot/ant)]x100, coupling efficiency = [1-(OCR(oligo)-OCR(rot/ant)/OCR(basal)-OCR(rot/ant)]x100. XF analysis of glycolytic parameters was performed according to seahorse glycostress test protocol, consisting of three sequential measurements in no-glucose condition and after the injection of 10mM glucose, the optimal dose of oligomycin A, and 50mM 2-Deoxy-D-glucose(2-DG) a glycolysis inhibitor (Sigma). The addition of the minimum dose of oligomycin A, which generates the maximal effect accounted for glycolytic capacity. The addiction of 2-DG accounted for non-glycolytic extracellular acidification. Data were elaborated using the following formulas: Basal glycolysis = ECARglc-ECAR2-DG, Glycolytic capacity = ECARoligo-ECAR2-DG, Glycolytic reserve = ECARoligo-ECARglc.

**Western blot analysis**

Cells were lysed at 4°C with lysis buffer (1% Triton X-100, 50 mmol/L Tris–HCl, pH 7.4, 150 mmol/L NaCl, 1 mmol/L EDTA, 1 mmol/L sodium orthovanadate, 2 mmol/L PMSF, and 1 mmol/L each of leupeptin and pepstatin). After 30 minutes of lysis, cellular extracts were centrifuged for 10 min at 12000g, and the supernatant was used for Western blot experiments as detailed elsewhere [6]. Antibodies were used for Western blot analysis according to the manufacturer's recommendations. Immunoblots were incubated overnight at 4°C with primary antibody in 1% BSA in DPBS. Mouse CD31 mAb (#3528, Cell Signaling Technology), Rabbit PKM2 mAb (#4053, Cell Signaling Technology), Rabbit Hexokinase II mAb (#2867, Cell Signaling Technology), Rabbit PGC1α Antibody (ab54481, Abcam), Rabbit E-Cadherin mAb (#3195, Cell Signaling Technology), Rabbit Vimentin mAb (#5741, Cell Signaling Technology), Rabbit Snail mAb (#3879, Cell Signaling Technology), Rabbit Phospho-Akt (Ser473) Antibody (#9271, Cell Signaling Technology), Rabbit Akt Antibody (#9272, Cell Signaling Technology), Rabbit Bax mAb

(#5023, Cell Signaling Technology), Rabbit Bcl-2 mAb (#4223, Cell Signaling Technology), Rabbit Cleaved Caspase-3 Antibody (#9661, Cell Signaling Technology), Rabbit Caspase-3 Antibody (#sc-7148 Santa Cruz Biotechnology) Rabbit Phospho- AMPKα (Thr172) mAb (#2535 Cell Signaling Technology), Rabbit AMPKα Antibody (#2532, Cell Signaling Technology) antibodies were used. Immunoblots were then incubated with secondary antibody α-rabbit/mouse (1:4000) in 1% BSA in 1x DPBS for 1hour. Monoclonal anti-β-actin antibodies produced in mouse (A5441, Sigma) or monoclonal anti-vinculin antibodies produced in mouse (V9131, Sigma) were used as internal control (1:1000) in 1% BSA in 1x DPBS. Quantification of the signal was obtained by chemiluminescence detection on an Image Quant Las4000 (GE Healthcare Life Sciences) and subsequent analysis conducted with ImageJ software.

**Quantitative real-time polymerase chain reaction (RT-PCR)**

Total RNA was extracted with the RNeasy kit (Qiagen) according to the manufacturer's instructions. The RNA concentration and quality were measured using an optical NanoDrop ND1000 spectrophotometer (Thermo Fisher Scientific). Total RNA (500 ng) was transcribed with a High-Capacity cDNA Reverse Transcription Kit (Applied Biosystems). Changes in the mRNA expression level of target genes were detected using FAST SYBR-Green PCR Master Mix and the 7900HT Fast Real Time PCR System (Applied Biosystems). All amplifications were run on a 7500 Fast RealTime PCR System (Applied Biosystems). The primers for GLUT1 were 5'-CGGGCCAAGAGTGTGCTAAA-3' (forward), 5'-TGACGATACCGGAGCCAATG-3' (reverse). Data were normalized on β2 microglobulin. Data were reported as relative quantification with respect to the calibrator sample (MON) using the $2^{-\Delta\Delta Ct}$ method. The primers for stem-like genes, pluripotency and EMT were as described in [5]. The mRNA levels of glyceraldehyde 3-phosphate dehydrogenase (GAPDH) were used for normalization. Data are reported as relative quantification

with respect to the calibrator sample (SPH NT) using the $2^{-\Delta\Delta Ct}$ method. Results shown are the mean of three different experiments ± SD.

**List of Primers**

| Gene | Sequence |
|---|---|
| AFP-FW | AAGGCCAGGAACAGGAAGTC |
| AFP-REV | CACACCGAATGAAAGACTCG |
| EpCAM-FW | TGTGGTGATAGCAGTTGTTGC |
| EpCAM-REV | CTATGCATCTCACCCATCTCC |
| LGR5-FW | CTTCCAACCTCAGCGTCTTC |
| LGR5-REV | TTTCCCGCAAGACGTAACTC |
| CD13-FW | CAGTGACACGACGATTCTCC |
| CD13-REV | CCTGTTTCCTCGTTGTCCTT |
| CD133-FW | GCTTCAGGAGTTTCATGTTGG |
| CD133-REV | GGGGAATGCCTACATCTGG |
| NANOG-FW | GTCTCGTATTTGCTGCATCG |
| NANOG-REV | GAAACACTCGGTGAAATCAGG |
| BMI1-FW | TTGCTTTGGTCGAACTTGG |
| BMI1-REV | GTGCTTCTTTTGCAGACTGG |
| CMYC-FW | CGGAACTCTTGTGCGTAAGG |
| CMYC-REV | ACTCAGCCAAGGTTGTGAGG |
| KLF4-FW | AGACAGTCTGTTATGCACTGTGG |
| KLF4-REV | TGTTCTGCTTAAGGCATACTTGG |
| SOX-2-FW | ATGGGTTCGGTGGTCAAGT |
| SOX-2-REV | GGAGGAAGAGGTAACCACAGG |
| BMP4-FW | AGCGTAGCCCTAAGCATCAC |
| BMP4-REV | AGTCATTCCAGCCCACATCG |
| YAP-FW | ACCCTCGTTTTGCCATGAAC |
| YAP-REV | TTGTTTCAACCGCAGTCTCTC |

| | |
|---|---|
| STAT3-FW | GGCATTCGGGAAGTATTGTCG |
| STAT3-REV | GGTAGGCGCCTCAGTCGTATC |
| IGF2-FW | ACACCCTCCAGTTCGTCTGT |
| IGF2-REV | GGGGTATCTTGGGGAAGTTGT |
| HNF4-FW | CTCGTCGACATGGACATGGCCGACTAC |
| HNF4-REV | GGCTTGCTAGATAACTTCCTGCTTGGT |
| ABCG2 -FW | GGCTTTCTACCTGCACGAAAACCAGTTGAG |
| ABCG2 -REV | ATGGCGTTGAGACCAG |
| ALDH1a-FW | GCACGCCAGACTTACCTGTC |
| ALDH1a-REV | CCACTCACTGAATCATGCCA |
| ECAD-FW | AGGCCAAGCAGCAGTACATT |
| ECAD-REV | ATTCACATCCAGCACATCCA |
| VIM-FW | ACACCCTGCAATCTTTCAGACA |
| VIM-REV | GATTCCACTTTGCGTTCAAGGT |
| CTNNB1-FW | GCTGGGACCTTGCATAACCTT |
| CTNNB1-REV | ATTTTCACCAGGGCAGGAATG |
| ZEB1-FW | AAGAAAGTGTTACAGATGCAGCTG |
| ZEB1-REV | CCCTGGTAACACTGTCTGGTC |
| Zeb2-FW | AGGGACAGATCAGCACCAAA |
| Zeb2-REV | GTGCGAACTGTAGGAACCAG |
| SNAIL-FW | CCTCCCTGTCAGATGAGGAC |
| SNAIL-REV | CAAGGAATACCTCAGCCTGG |
| SLUG-FW | ACAGCGAACTGGACACACAT |
| SLUG-REV | GATGGGGCTGTATGCTCCT |
| VEGFa-FW | CACTGAGGAGTCCAACATCAC |
| VEGFa-REV | AGGAAGCTCATCTCTCCTATGT |
| PGC-1α-FW | TGCATGAGTGTGTGCTCTGT |
| PGC-1α-REV | GCACACTCGATGTCACTCCA |

| | |
|---|---|
| Glut1-FW | CGGGCCAAGAGTGTGCTAAA |
| Glut1-REV | TGACGATACCGGAGCCAATG |
| GAPDH-FW | GATCATCAGCAATGCCTCCT |
| GAPDH-REV | TGTGGTCATGAGTCCTCCCA |

**RT-PCR array**

Five µg of total RNA of in vivo tumors were reverse transcribed using the QuantiNova Reverse Transcription kit (Qiagen). qRT-PCR reaction was performed using the QuantiNova LNA PCR Focus Panels 384-well plates (#SBHS-133ZE, Qiagen). In each 384-well plates, 4 different tumor samples were tested for 84 genes specifically associated with liver cancer pathways. The expression values were calculated with the ΔCt method, using ACTB, GAPDH, RPLP0 and HPRT1 as housekeeping genes as reference. A cutoff of at least 1.5-fold increases and 0.5-fold decreases were considered significant.

**Glucose uptake**

Uptake of radioactive glucose was evaluated by treating $7x10^4$ CCLP1 or HUCCT1 cells seeded in 24-well plates with a buffered solution (140 mmol/L NaCl, 20 mmol/L Hepes/Na, 2.5 mmol/L MgSO4, 1 mmol/L CaCl2, and 5 mmol/L KCl, pH 7.4) containing 0.5 µCi/mL [U-$^{14}$C] glucose for 15 min at 37°C. Cells were subsequently washed with cold PBS and lysed with 0.1 mol/L NaOH. Incorporated radioactivity was assayed by liquid scintillation counting and normalized to protein content.

**Measurement of mitochondrial mass and mitochondrial membrane potential (ΔΨm)**

SPH and MON cells were harvested by trypsinization and washed. For measurement of mitochondrial mass and ΔΨm, cells were stained with 50 nM MitoTracker Green and 50nM MitoTracker Red (ThermoFisher Scientific), respectively. Cells were incubated at 37°C for 25 min,

washed twice and analyzed by flow cytometry with FACSCanto II (BD Biosciences). Dead cells were excluded using the Zombie Aqua™ Fixable Viability Kit (Biolegend). A fluorescence minus one (FMO) sample, containing all antibodies except the one of interest, was used as a negative control. Data analysis was performed with the FlowJo software (FlowJo, LLC) [7, 8].

**Lactate assay**

Lactate was measured in the cultured media with Lactate Assay kit (Biovision) according to the manufacturer's instruction.

**Quantification of AMP/ATP ratio**

AMP/ATP ratio was calculated after the absolute quantification of ATP and AMP measured in MON and SPH cells by using the ATP Colorimetric/Fluorometric Assay Kit (BioVision) and the AMP Colorimetric Assay Kit (BioVision) respectively according to the manufacturer's instruction.

**Determination of mitochondrial ROS**

Mitochondrial ROS was measured in SPH and MON cells with MitoSOX™ Red Mitochondrial Superoxide Indicator (Thermofisher) according to the manufacturer's instruction.

**Evaluation of spheres and Giemsa staining**

CCLP1 and HUCCT1 cells (750 cells/well) were seeded in poly-HEMA-coated 96-well plates and cultured for 96 hours. Cells silenced for PGC-1α, were harvested and cytospinned onto glass slides, fixed with methanol, stained with Giemsa, and photographed with an Olympus BX51 microscope with a 40x objective.

**Tube formation assay**

This assay was carried out as previously described [5], with slight modifications. In brief, 96-well plates were coated with 70µl of pre-thawed growth factor-reduced Matrigel (BD Biosciences). The plate was then kept at 37 °C for 1 hour to allow the matrix solution to gel. $1.8x10^4$ HUVEC cells were resuspended in the respective conditioned media, added to each well and incubated at 37°C for 6h. Images were acquired under an inverted microscope. Pro-angiogenic activity was quantified by measuring the number of tube structures formed between discrete endothelial cells in each well. Each experiment was performed in triplicate. Analysis of endothelial tube formation for total tube length and branching points was performed by Wimasis (2017) image analysis tool (WimTube: Tube Formation Assay Image Analysis Solution, Release 4.0; Onimagin Technologies, Cordoba, Spain). At least 3 images from each group were analyzed for endothelial tube formation assay.

**Cell transfection**

Control siRNA and siPGC-1α SiRNA (sc-38884) were from Santa Cruz. Cells were transfected as previously described using the Amaxa nucleofection technology (Amaxa) according to manufacturer's instructions.

**Cell proliferation assay**

Proliferation was evaluated by BrdU incorporation using a colorimetric immunoassay. SPH were dissociated and 7,5 $x10^3$ cells were seeded in a 96-well plate and allowed to grow overnight in SPH medium. The Cell Proliferation ELISA-BrdU (colorimetric) Kit (Roche) was used to detect the cell proliferation according to the manufacturer's protocols.

**Survival test by crystal violet staining**

CCA cells previously cultured as monolayer or sphere were seeded in 96-multiwell plates for 24 h before receiving Metformin or Phenformin or 2-deoxy-D-glucose or SR-12898 (at different doses as

indicated in the main text) for 48 h or 72h. Cellular growth was stopped by removing the medium and by the addition of a 0.5% crystal violet solution in 20% methanol. After 5 min of staining, the fixed cells were washed with phosphate-buffered saline (PBS) and solubilized with 200 µl/well of 0.1 M sodium citrate, pH 4.2. The absorbance at 595 nm was evaluated using a microplate reader.

**Chemoinvasion and migration assays**

48 hours after transfection, CCLP1 and HUCCT1 SPH cells were washed, trypsinized, and re-suspended in serum-free medium at a concentration of 1.5 x $10^5$ cells/ml. Chemoinvasion was measured in modified Boyden chamber equipped with 8 µm pore filters (Millipore Corp,) coated with Matrigel (150 µg/ml) (BD Biosciences) as described in detail elsewhere [9]. After incubation at 37 °C (24 h), the cells invaded to the underside of the filters were fixed, stained with Giemsa, mounted and counted at 40X magnification. Migration was measured in Boyden chamber equipped with 8 µm pore filters (Millipore Corp) coated with rat tail collagen (20 µg/ml) (Collaborative Biomedical Products, Bedford, UK), as described in detail elsewhere [6]. Cells were seeded in the upper chamber, while the (FBS 20%) was placed in the lower compartment. After six hours incubation at 37 °C, cells migrated to the underside of the filters were fixed, stained with Giemsa, mounted and counted at 40X magnification.

The values for both invasion and migration were expressed as the average number of invading cells per microscopic field (40X) over five fields. Each experiment was performed in triplicate.

***In vivo* experiments**

Animal experiments were performed in accordance with national guidelines and approved by the ethical committee of the Animal Welfare Office of Italian Health Ministry. All procedures conformed to the legal mandates and the Italian guidelines for the care and maintenance of laboratory animals. All animals received human care and study protocols comply with the

institution's guidelines. Studies involving animal experiments conform to the Animal Research: Reporting of In Vivo Experiments (ARRIVE) guidelines (http://www.nc3rs.org.uk/arrive-guidelines), developed by the National Centre for the Replacement, Refinement and Reduction of Animals in Research (NC3Rs) to improve standards and reporting of animal research.

Male NOD/SCID mice of six weeks (Charles River Laboratories International) were s.c. injected with $10^6$ HUCCT1 SPH cells. . After a week, mice were randomly allocated to receive repeated courses of intra-peritoneal vehicle solution (control mice) or 200 mg/kg of metformin or 45mg/kg SR-18292, five times a week. Animals (6 per group) were monitored daily.

**Ultrasound and photoacoustic imaging**

Tumor volumes were determined in vivo imaging system (Vevo LAZR-X photoacoustic imaging). Mice were anesthetized with 1,5/2% isoflurane and placed on a heated pad (37°C) in prone position and ECG, respiration rate and body temperature were continuously monitored. Ultrasonic gel was applied on the shaved skin for an efficient transduction of ultrasound (US) and (photoacoustic) PA signal. PA and US imaging were performed with Vevo LAZR-X system (Fujifilm VisualSonics). Axial 3D scans of tumor masses were performed in B-Mode imaging by using a 55-MHz transducer. The volumes were subsequently measured delineating the region of interest (ROI) for every axial slide using Vevo LAB software.

**BrdU staining**

*In vivo* bromodeoxyuridine (BrdU) labeling was performed by intraperitoneal injection of 50 mg/kg BrdU (Sigma-Aldrich), 1 h prior to sacrifice. Tumor tissues were fixed overnight in 4% neutral buffered paraformaldehyde, paraffin embedded, and cut into 3-µm sections. Deparaffinized slides were treated with 2N HCl for 30 min at room temperature (RT) and neutralized with 0.1 M sodium borate (pH 8.5) for 15 min at RT. Slides were washed with PBS, incubated with 3% $H_2O_2$ for 15

min at RT and then with anti-BrdU antibodies (1:50 dilution) (Dako) was applied for 30 min. Slides were washed again and BrdU was detected using an immunohistochemistry kit (Dako REAL Detection system, peroxidase/DAB+) following the manufacturer's protocol. Five microscopic fields/number of cells were counted.

**Analysis of PGC-1α protein level in CCA tissue**

A total of 40 formalin-fixed, paraffin-embedded human liver tissue specimens were analyzed for the immunohistochemical expression of PGC-1α. All specimens were obtained after surgical resection and collected in the tissue bank at Humanitas Clinical Institute (Rozzano, Italy) in accordance with informed consent retrieved from patients and local ethics committee approval conforms to the ethical guidelines of the 1975 Declaration of Helsinki as reflected in a priori approval by the institution's human research committee.

The immunohistochemical expression of PGC-1α (Rabbit PGC1α Antibody (ab54481, Abcam)) was performed on the automated Leica Microsystems Bondmax® (Leica). Both cytoplasmic and nuclear staining was retained for scoring. Immunostaining was semiquantified using a three-tier scoring based on intensity of staining (0= negative; 1= weak; 3=moderate; 4= strong). Correlation analysis with clinicopathological CCA data were conducted as follows: continuous variables are presented as means and standard deviations, and categorical variables as number and percentages. Continuous variables were analyzed using a two-tailed, unpaired t-test, categorical variables were compared, categorical variables were analyzed using a chi-square or Fisher exact test for dichotomous data. A two-sided p value $<0.05$ was defined to be considered statistically significant. The OS was calculated from the date of surgery to the date of death or last follow-up visit. Kaplan-Meier estimator survival curves and log rank tests were used to evaluate and compare OS. All analyses were performed with SPSS ver. 25.0 (SPSS Inc).

**GSEA analysis**

Gene expression profiles for 104 tumors have been retrieved from GSE26566. Patients were stratified based on overall survival into a poor prognosis (OS<12 months) and a good prognosis (OS>12 months) group. Custom signatures for Krebs Cycle and complex I-IV were added as the text entry and associated with survival using gene set enrichment analysis (GSEA) [10] with signal2noise metric and otherwise default parameters. Time to recurrence (TTR) was used as a continuous trait and associated with signatures using Pearson's metric and otherwise default parameters.

**Correlation analysis**

An analysis between PGC-1α and other test genes was applied on a published microrarray-based study on cholangiocarcinoma tissue vs surrounding liver from 59 patients (GSE26566) [11]. Probe level normalized expression values were aggregated (median) at the gene level as in the GSEA analysis detailed above. The correlation analysis was based on Pearson's product moment correlation and p-values were corrected for multiple testing with the Benjamini-Hochberg procedure, both implemented in the stats package of the R statistical software.

**Library preparation and RNA-sequencing**

Total RNA was isolated from cells using the miRNeasy Mini Kit (Qiagen) according to the manufacturer's protocol. Total-RNA-sequencing (RNA-seq) library preparation was performed starting from 100 ng of total-RNA with the SMARTer Stranded Total RNA Sample Prep Kit - Low Input Mammalian (Clontech-Takara). The libraries obtained were qualitatively and qualitatively assessed by using TapeStation 4200 (Agilent) and quantified by Qubit Fluorimeter (ThermoFisher). Afterwards, they were multiplexed in an equimolar pool and sequenced on a NextSeq-500 Illumina Platform generating more than 60 million 75bp Paired End reads (bp-PE) per sample.

**Reads preprocessing**

Sequencing data was demultiplexed into separate, adapter free compressed fastq files using bcl2fastq v2.20.0.422 (Illumina, Inc.) and a reference sample sheet specifying for each sample the corresponding barcode. Reads were further processed using the fastp program [12] configured to use 20 threads for removing read pairs with at least 50% of bases with Q > 30, a minimal length of 70 bp, a complexity > 30%. No trimming was performed on reads.

**Reads alignment, abundance estimation and differential analysis**

Reads mapping was performed using the default options but specifying the --numGibbsSamples 500 and –validate Mappings options, on a reference transcriptome composed by the union of the human cDNA and ncDNA available from Ensembl (assembly GRCh38.p13) indexed with a kmer size of 23 by Salmon v0.14.1 [13]. Reads were imported into R using the tximport package [14] with the "Salmon" specific method. Gene level abundance was estimated from transcript level estimates using the summarizeToGene function of tximport working on a transcript to gene association table (further associating gene names for functional analysis, see below) obtained with Ensembl Biomart system [15] operating on Ensembl genes 98/GRCh38.p13 human genes.
Data matrices were eventually converted in DEseq2 objects using the ESeqDataSetFromTximport function, specifying the SPH vs MON phenotypes as the design contrast.

**Functional analysis**

For the functional analysis of the experiment the GSEA 4.0.2 software by BROAD Institute was used [10, 16], in the GSEAPreRanked mode using the t-statistic from the DESeq2 analysis as input metric for sorting. Gene lists were obtained from MSigDB 7.0 [17, 18] and gene names were converted into Ensembl gene IDs using a simple perl script reading the same table produced by

Biomart used for gene abundance estimation (see above). A selection of interesting gene sets from the different MSigDB collections (kegg, biocarta, gobp, hallmark, reactome) was obtained by a custom bash script that isolated those containing mitochondrial genes (GO:0005739:mitochondrion).

**Statistical Analysis**

GraphPad Prism v5 and SPSS v25.0 were used for data analysis. The error bars represent 1+/- SEM. The p value was calculated with Student's t test. In the *in vivo* experiments, group comparison was performed with the Mann-Whitney U-test. The statistical significance and p value are shown when relevant. In the humans sample experiments,group comparison was performed with the Fisher exact test.

**REFERENCES**

[1] Miyagiwa M, Ichida T, Tokiwa T, Sato J, Sasaki H. A new human cholangiocellular carcinoma cell line (HuCC-T1) producing carbohydrate antigen 19/9 in serum-free medium. In Vitro Cell Dev Biol 1989;25:503-510.
[2] Han C, Wu T. Cyclooxygenase-2-derived prostaglandin E2 promotes human cholangiocarcinoma cell growth and invasion through EP1 receptor-mediated activation of the epidermal growth factor receptor and Akt. J Biol Chem 2005;280:24053-24063.
[3] Shimizu Y, Demetris AJ, Gollin SM, Storto PD, Bedford HM, Altarac S, et al. Two new human cholangiocarcinoma cell lines and their cytogenetics and responses to growth factors, hormones, cytokines or immunologic effector cells. Int J Cancer 1992;52:252-260.
[4] Raggi C, Factor VM, Seo D, Holczbauer A, Gillen MC, Marquardt JU, et al. Epigenetic reprogramming modulates malignant properties of human liver cancer. Hepatology 2014;59:2251-2262.
[5] Raggi C, Correnti M, Sica A, Andersen JB, Cardinale V, Alvaro D, et al. Cholangiocarcinoma stem-like subset shapes tumor-initiating niche by educating associated macrophages. J Hepatol 2017;66:102-115.
[6] Bonacchi A, Romagnani P, Romanelli RG, Efsen E, Annunziato F, Lasagni L, et al. Signal transduction by the chemokine receptor CXCR3: activation of Ras/ERK, Src, and phosphatidylinositol 3-kinase/Akt controls cell migration and proliferation in human vascular pericytes. J Biol Chem 2001;276:9945-9954.
[7] Samudio I, Konopleva M, Hail N, Shi YX, McQueen T, Hsu T, et al. 2-Cyano-3,12-dioxooleana-1,9-dien-28-imidazolide (CDDO-Im) directly targets mitochondrial glutathione to induce apoptosis in pancreatic cancer. J Biol Chem 2005;280:36273-36282.
[8] Ye XQ, Li Q, Wang GH, Sun FF, Huang GJ, Bian XW, et al. Mitochondrial and energy metabolism-related properties as novel indicators of lung cancer stem cells. Int J Cancer 2011;129:820-831.
[9] Raggi C, Fiaccadori K, Pastore M, Correnti M, Piombanti B, Forti E, et al. Antitumor Activity of a Novel Fibroblast Growth Factor Receptor Inhibitor for Intrahepatic Cholangiocarcinoma. Am J Pathol 2019;189:2090-2101.
[10] Subramanian A, Tamayo P, Mootha VK, Mukherjee S, Ebert BL, Gillette MA, et al. Gene set enrichment analysis: a knowledge-based approach for interpreting genome-wide expression profiles. Proc Natl Acad Sci U S A 2005;102:15545-15550.
[11] Andersen JB, Spee B, Blechacz BR, Avital I, Komuta M, Barbour A, et al. Genomic and genetic characterization of cholangiocarcinoma identifies therapeutic targets for tyrosine kinase inhibitors. Gastroenterology 2012;142:1021-1031.e1015.
[12] Chen S, Zhou Y, Chen Y, Gu J. fastp: an ultra-fast all-in-one FASTQ preprocessor. Bioinformatics 2018;34:i884-i890.
[13] Patro R, Duggal G, Love MI, Irizarry RA, Kingsford C. Salmon provides fast and bias-aware quantification of transcript expression. Nat Methods 2017;14:417-419.
[14] Soneson C, Love MI, Robinson MD. Differential analyses for RNA-seq: transcript-level estimates improve gene-level inferences. F1000Res 2015;4:1521.
[15] Smedley D, Haider S, Ballester B, Holland R, London D, Thorisson G, et al. BioMart--biological queries made easy. BMC Genomics 2009;10:22.
[16] Mootha VK, Lindgren CM, Eriksson KF, Subramanian A, Sihag S, Lehar J, et al. PGC-1alpha-responsive genes involved in oxidative phosphorylation are coordinately downregulated in human diabetes. Nat Genet 2003;34:267-273.
[17] Liberzon A, Subramanian A, Pinchback R, Thorvaldsdóttir H, Tamayo P, Mesirov JP. Molecular signatures database (MSigDB) 3.0. Bioinformatics 2011;27:1739-1740.

[18] Liberzon A, Birger C, Thorvaldsdóttir H, Ghandi M, Mesirov JP, Tamayo P. The Molecular Signatures Database (MSigDB) hallmark gene set collection. Cell Syst 2015;1:417-425.

**Supplementary Figures**

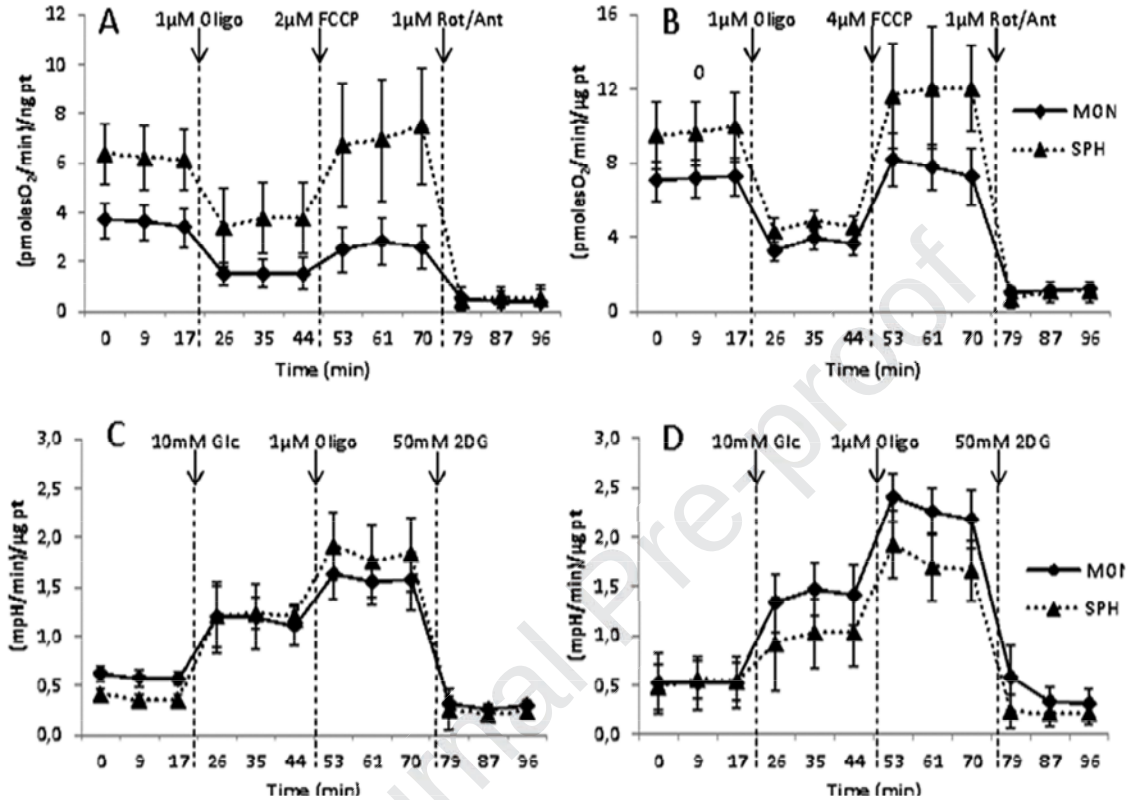


**Supplementary** Figure 1: Metabolic characteristics of CCA cells grown as monolayers (MON) or spheres (SPH). Seahorse XF assay profiles of HUCCT1 (A,C) and CCLP1 (B,D) cells grown under monolayer (♦ MON) or sphere (▲ SPH) condition exposed to metabolic stress in unbuffered medium (Mean and SEM). (A-B) Mitostress test profile: Oxygen Consumption rate was measured under sequential treatment with drugs perturbing mitochondrial performance, namely oligomycin A, FCCP and Rotenone/Antimycin A mixture at the doses reported in the graph. (C-D) Glycostress test profile: Extracellular acidification rate measured in unbuffered glucose-free medium under sequential treatment with drugs perturbing glycolysis, namely 10mM glucose, 1µM oligomycin and 50mM 2-DG. The analysis was performed with Seahorse XF24 analyzer (Agilent). OCR and ECAR were normalized on protein content measured by Bradford assay.

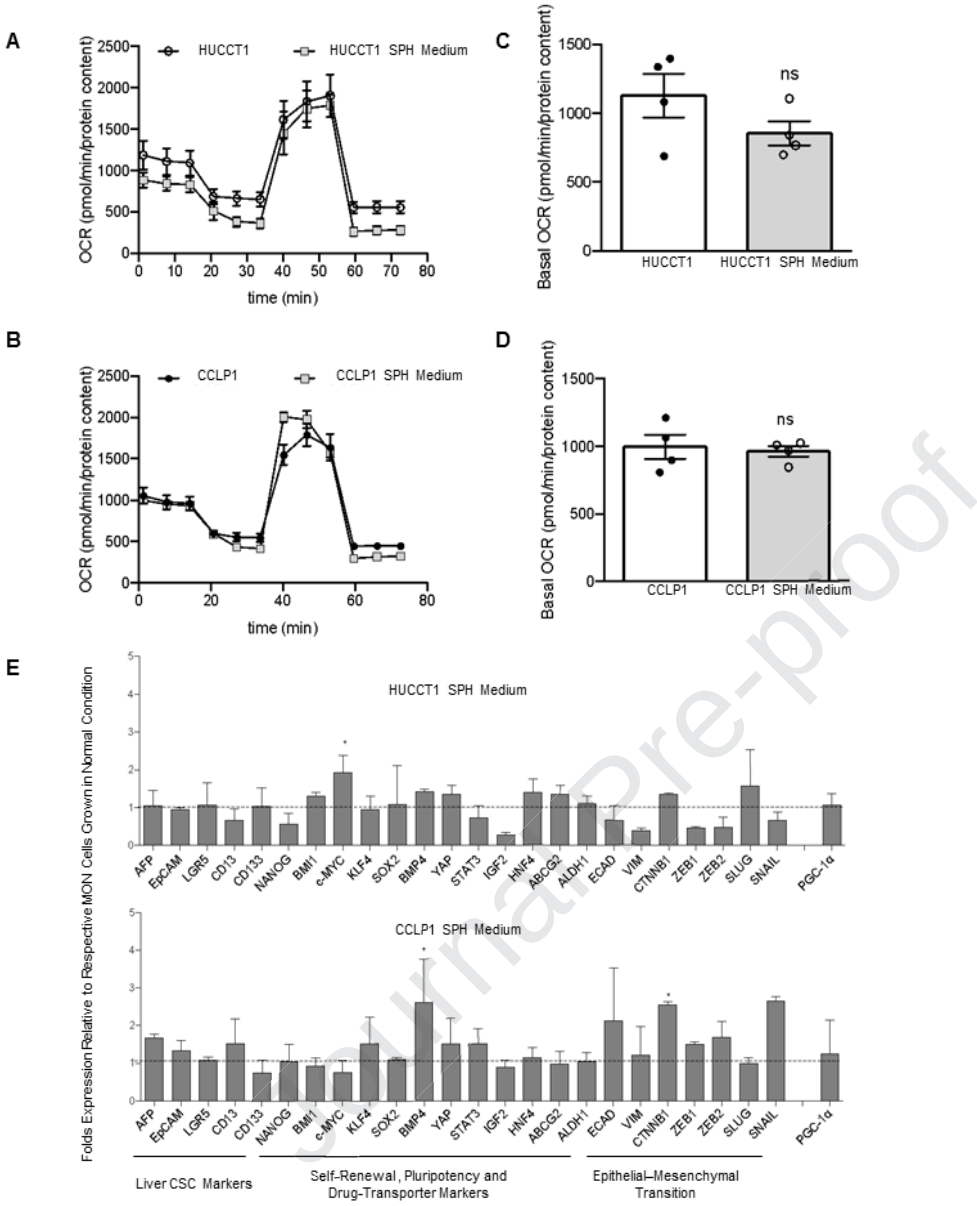


**Supplementary Figure 2: Metabolic features are independent of the culture medium**. (A-B) Representative Seahorse XF assay profiles of HUCCT1 and CCLP1 cells grown as monolayer condition exposed to SPH medium. Mitostress test profile: oxygen consumption rate (OCR) was measured under sequential treatment with drugs perturbing mitochondrial performance as reported above. (C,D) Basal OCR is represented for each cell line in the different medium condition. The analysis was performed with Seahorse XF24 analyzer (Agilent). OCR was normalized on protein content measured by Bradford assay. Data are mean ± SEM (n=3, p value versus control sample by Student t test, * $p \leq 0.05$). (E) qRT-PCR analysis of several stem-like related genes in MON and MON cells grown in SPH medium of CCLP1 and HUCCT1 cells. GAPDH was used as an internal

control. All mRNA levels are presented as fold changes normalized to 1 (mean expression of MON grown in normal condition). Data are mean ± SEM (n=3, *p≤0.05 vs. MON grown in normal condition).

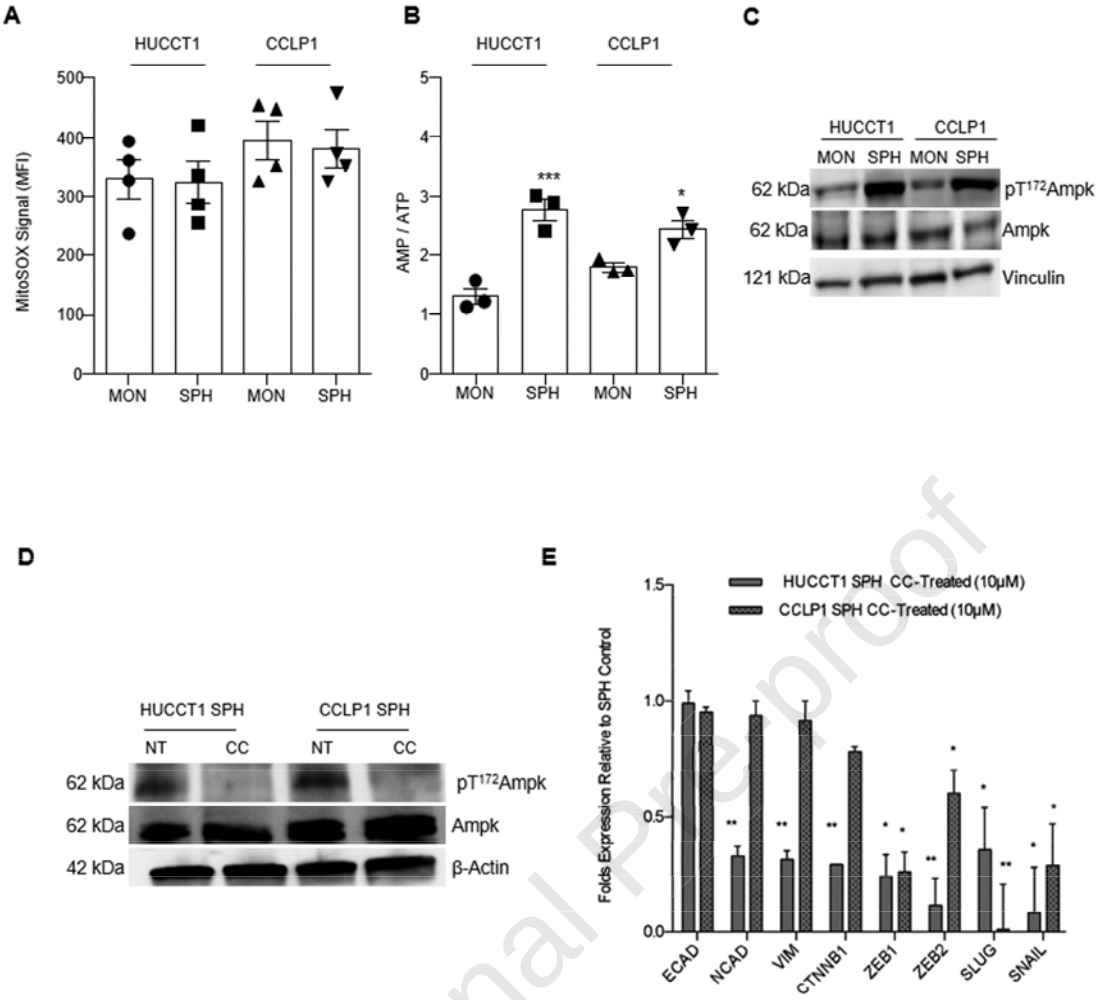


**Supplementary Figure 3: Role of AMPK in mediating activation of EMT genes.** (A) Evaluation of mitochondrial ROS production in MON and SPH cells by FACS, using MitoSOX. Histograms represent the Mean Fluorescence Intensity (MFI) of the MitoSOX probe. Data are mean ± SEM (n=3). (B) Measurement of AMP:ATP ratios in MON and SPH cells. The ratios of AMP:ATP derived from analysis of three independent samples for each condition. The results are shown as mean ± SEM (n=3, *p≤0.05, *** p≤0.001 vs. MON). (C) Immunoblot analysis of AMPK and Phospho-AMPK (Thr172) in monolayers (MON) or spheres (SPH) of CCLP1 and HUCCT1 cells. Vinculin immunoblot was performed to ensure equal loading. (D) Immunoblot analysis of AMPK and Phospho-AMPK (Thr172) in SPH after 24 hours treatment with 10μM compound C (CC). β-Actin immunoblot was performed to ensure equal loading. (E) qRT-PCR analysis of EMT-related genes in SPH and CC treated SPH cells. GAPDH was used as an internal control. All mRNA levels are presented as fold changes normalized to 1 (mean expression of SPH CTR cells). Data are mean±SEM (n=3, *p≤0.05 , **p≤0.01 vs. SPH CTR cells).

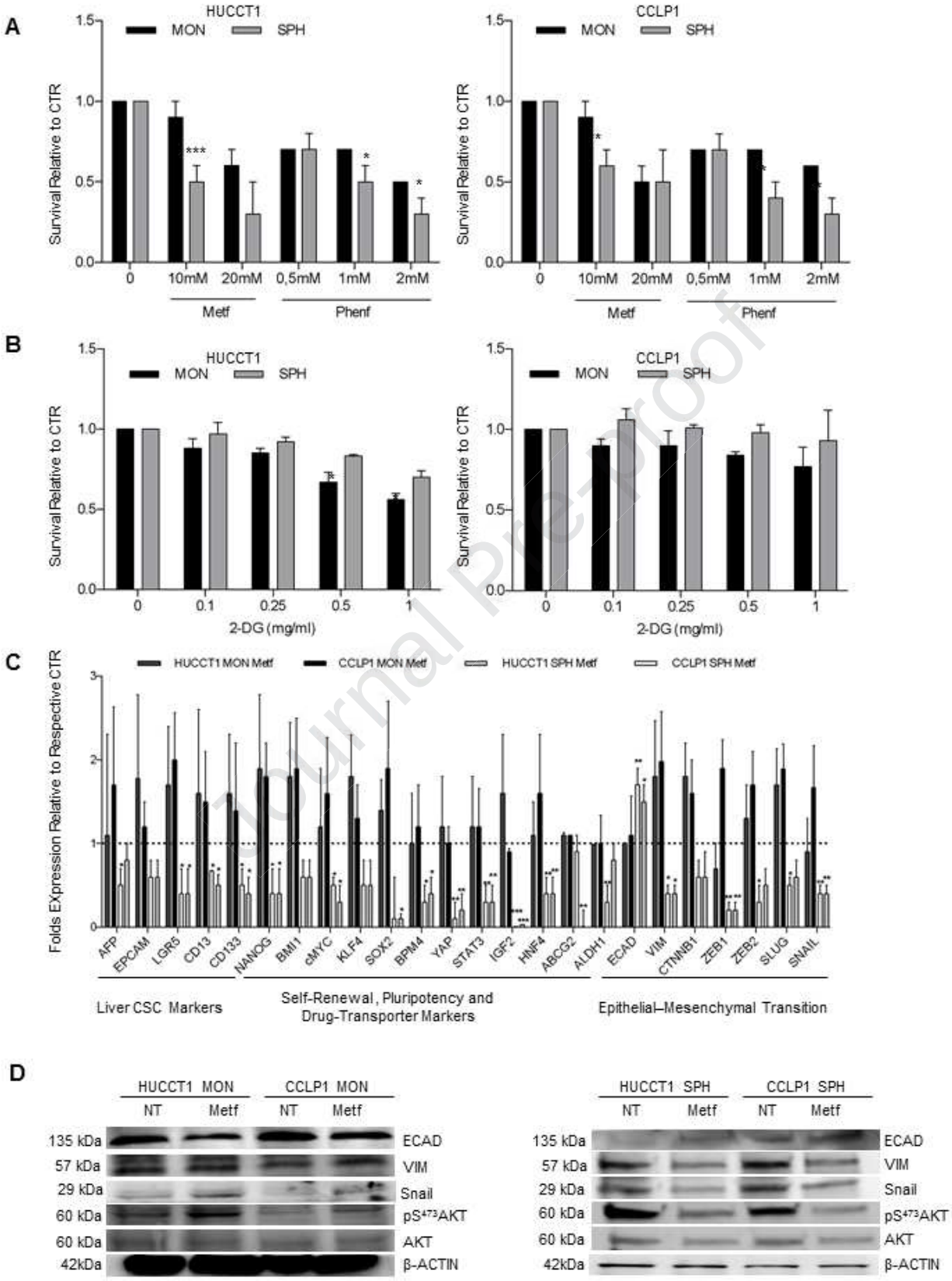
A
HUCCT1
MON
SPH
Survival Relative to CTR
0
10mM
20mM
0,5mM
1mM
2mM
Metf
Phenf
CCLP1
B
2-DG (mg/ml)
C
HUCCT1 MON Metf
CCLP1 MON Metf
HUCCT1 SPH Metf
CCLP1 SPH Metf
Folds EXpression Relative to Respective CTR
AFP
EPCAM
LGR5
CD13
CD133
NANOG
BMI1
cMYC
KLF4
SOX2
BPM4
YAP
STAT3
IGF2
HNF4
ABCG2
ALDH1
ECAD
VIM
CTNNB1
ZEB1
ZEB2
SLUG
SNAIL
Liver CSC Markers
Self-Renewal, Pluripotency and Drug-Transporter Markers
Epithelial–Mesenchymal Transition
D
HUCCT1 MON
CCLP1 MON
HUCCT1 SPH
CCLP1 SPH
NT
Metf
135 kDa
57 kDa
29 kDa
60 kDa
42kDa
ECAD
VIM
Snail
pS473AKT
AKT
β-ACTIN

**Supplementary Figure 4:** Effects of the OXPHOS inhibitors metformin (Metf) and phenformin (Phenf) in MON and SPH of HUCCT1 and CCLP1 cells. (A) Crystal Violet test was performed after 48 hours treatment. Results were normalized to control (CTR) samples. Data are mean ± SEM (n=3, * $p \leq 0.05$, ** $p \leq 0.01$, *** $p \leq 0.001$ vs. CTR). (B) HUCCT1 and CCLP1 MON show an increased sensitivity to the glycolysis inhibitor 2-Deoxyglucose (2-DG) compared to SPH cells. CV test was performed after 48 hours treatment. Results were normalized to control (CTR) sample. Data are mean ± SEM (n=3, p value versus CTR sample by Student t test, * $p \leq 0.05$). (C) Relative expression of transcripts encoding genes related to liver CSC, self-renewal, pluripotency and Epithelial-Mesenchymal Transition in HUCCT1 and CCLP1 SPH after 48 hours treatment with 10mM metformin. GAPDH was used as an internal control. All mRNA levels are presented as fold changes normalized to 1 (mean expression of CTR cells). Data are mean ± SEM (* $p \leq 0.05$, ** $p \leq 0.01$, *** $p \leq 0.001$ vs. NT). (D) Immunoblot analysis of EMT markers (ECAD, VIM, SNAIL), AKT and Phospho-AKT (Ser473) in MON and SPH of CCLP1 and HUCCT1 cells. β-Actin immunoblot was performed to ensure equal loading.

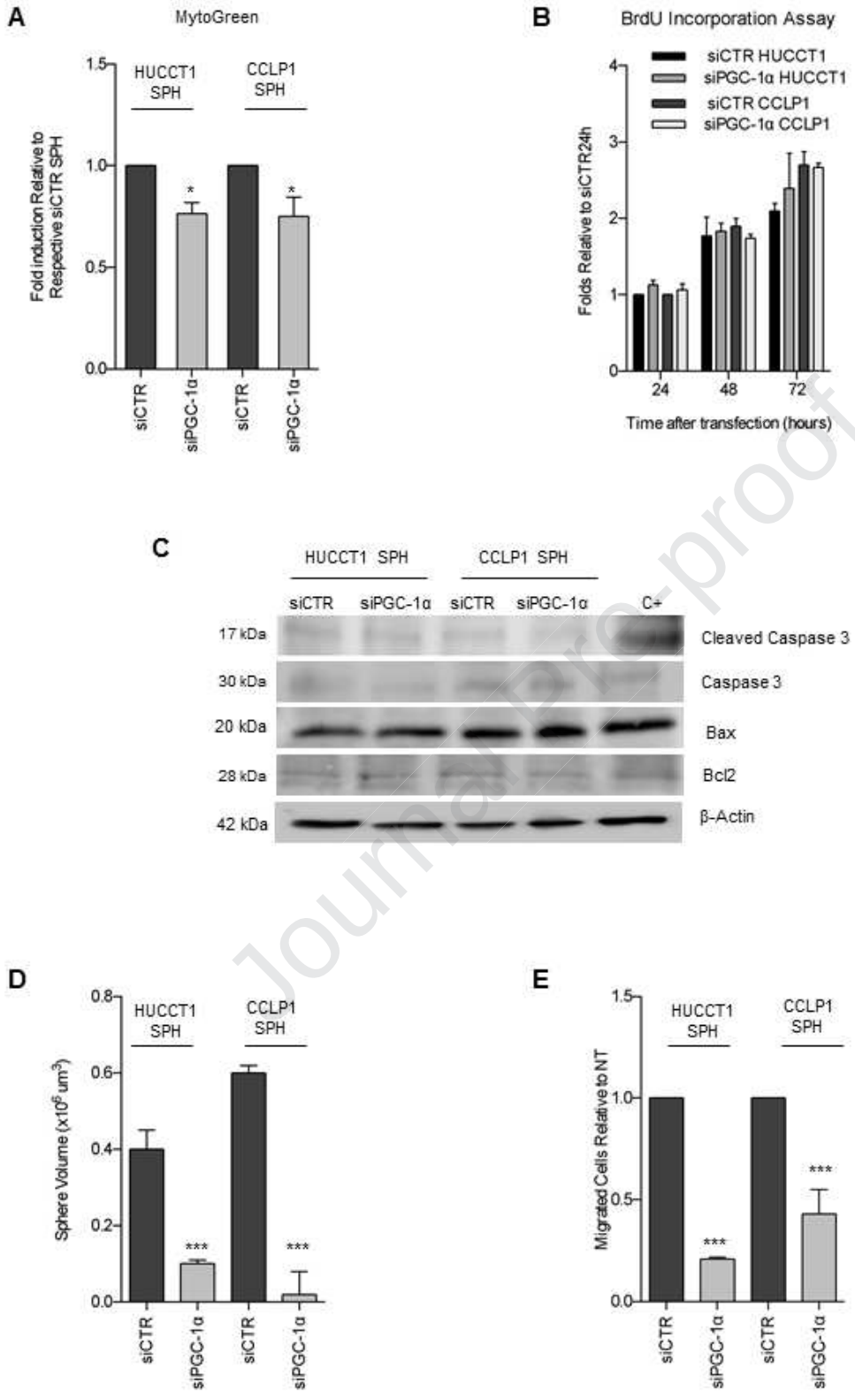

**Supplementary Figure 5: Effect of PGCα knockdown in CCA SPH.** (**A)** Mitochondrial mass, detected by FACS, using MitoTracker Green. Histograms represent the Mean Fluorescence Intensity (MFI) of the MitoTracker probe presented as fold induction normalized to 1 (mean MFI of siCTR). Data are mean ± SEM (n=3, p value versus siCTR by Student t test, * $p \leq 0.05$). (B) Effect of PGC-1α depletion on proliferation by BrdU incorporation at 24, 48 and 72 hours after silencing. Levels displayed as fold changes normalized to 1 (mean expression of siCTR at 24 hours) (n=3). Data are mean ± SEM. (C) Levels of Cleaved Caspase 3, Caspase 3, Bax and Bcl2 following PGC-1α silencing in HUCCT1 and CCLP1 SPH, as evaluated by Western blotting using β-Actin as a loading control. (D) Effect of siPGC1a depletion on CCA-SPH volume. Data are mean ± SEM (p value versus siCTR, *** $p \leq 0.001$). (D) Migration of PGC-1α-silenced CCLP1 and HUCCT cells was measured in Boyden chambers for 6 hours. Data are mean ± SEM (n=5, *** $p \leq 0.001$ vs. siCTR).

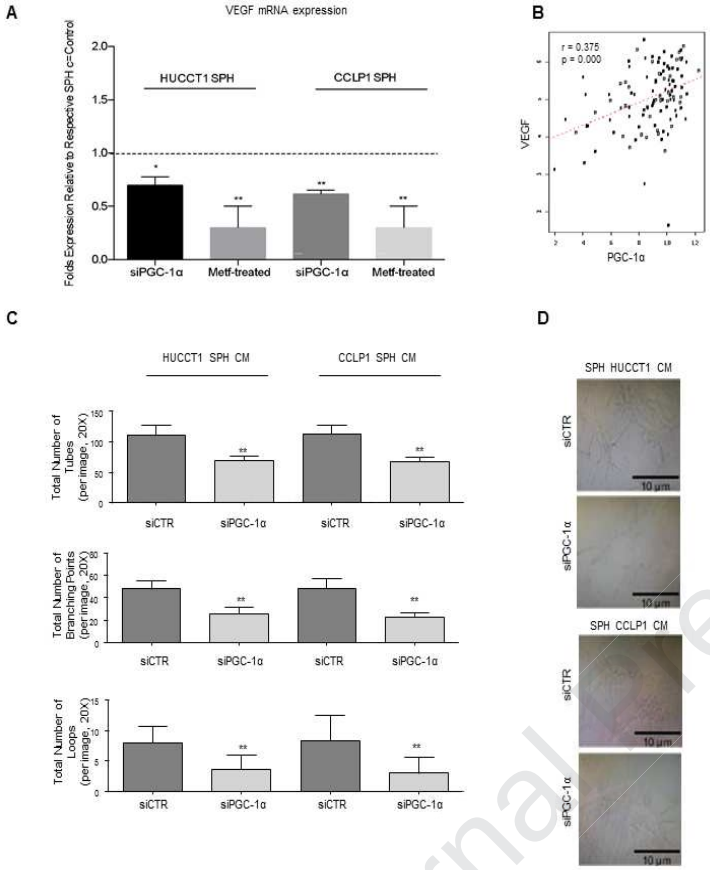


**Supplementary Figure 6: Effects of PGC-1α silencing on angiogenic pathways.** (A) VEGF mRNA levels in PGC-1α-silenced and metformin treated CCA SPH cells, expressed as fold changes normalized to 1 (mean expression of siCTR or control (CTR) sample). Data are mean ± SEM (n=3, * p≤0.05, ** p≤0.01 vs. siCTR/CTR). (B) Scatterplot representing the correlation between PGC-1α (x-axis) and VEGF (y-axis) expression in a published microrarray-based study comparing CCA vs surrounding liver in 59 patients (GSE26566 [22]). r: Pearson's correlation coefficient, n: number of samples. All adjusted (two tails) p values associated to correlation tests were < 1e-5. (C) Effects of conditioned medium from PGC-1α-silenced SPH (CM) on HUVEC tube formation. Data are presented as total numbers of tube/well, total number of branching points/well, total number of loops/well. Mean±SEM (n = 3, **p ≤0.01 vs. siCTR SPH CM). (D) Representative images of siCTR and siPGC-1α SPH CM effect on tube formation. Original magnification 40X.

A

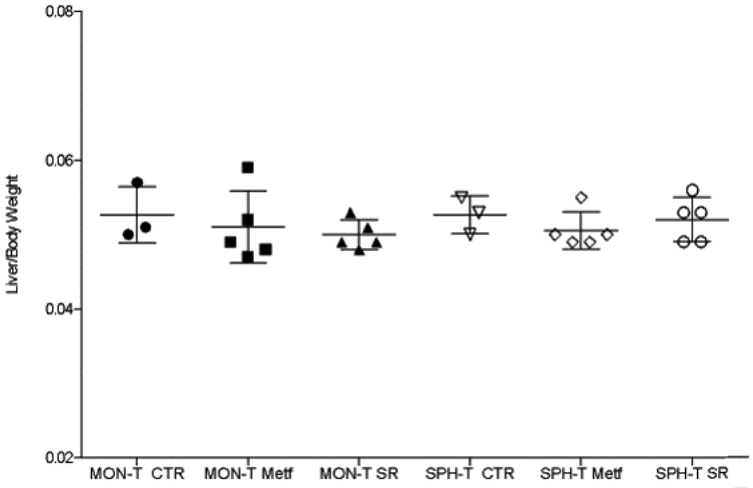


B

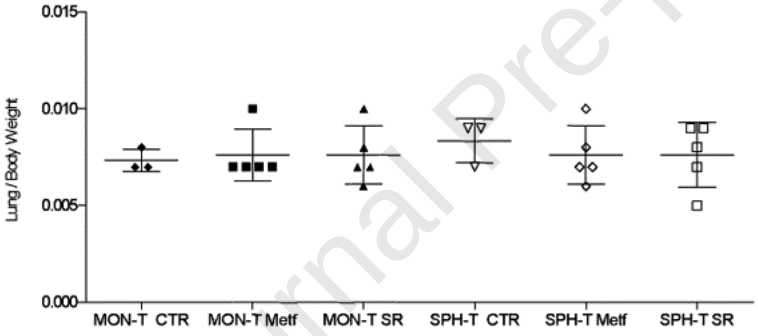




**Supplementary Figure 7: Liver/body weight ratio and lung/body weight ratio in mice with CCA tumor xenografts.** Tumors derived from HUCCT1 cells grown as MON (MON-T) or SPH (SPH-T) were obtained by subcutaneous injection of 1 x$10^6$ cells in NOD/SCID mice. After 7days, mice were treated five times a week with intraperitoneal injection of PBS (control, T-CTR) or 200 mg/kg metformin (T-Metf) or 45mg/kg SR-18292 (n=6 per group). Ratio of liver weight to body weight for each group. Data are mean ± SEM (n=6). (**B**) Ratio of lung weight to body weight for each group. Data are mean ± SEM (n=6).

**Supplementary Table 1. List of stem-like genes correlated with PGC-1α and Complex II**

| | Correlated genes | r | ADJ P-VALUE |
|---|---|---|---|
| **SDHA** | AFP | 0.3696648 | 0.0018 |
| | CD13 | 0.3046406 | 0.0327 |
| | ABCG2 | 0.5943840 | 0.0000 |
| | STAT3 | 0.2835567 | 0.0740 |
| | ALDH1a1 | 0.4821006 | 0.0000 |
| | PGC-1α | 0.4691994 | 0.0000 |
| **SDHB** | AFP | 0.5727547 | 0.0000 |
| | HNF4A | 0.5348040 | 0.0000 |
| | HNF4G | 0.3464601 | 0.0047 |
| | ALDH1a1 | 0.5193266 | 0.0000 |
| | PGC-1α | 0.4396749 | 0.0000 |
| **SDHC** | CD13 | 0.2968967 | 0.0530 |
| | ABCG2 | 0.3358473 | 0.0536 |
| | SOX2 | 0.3411690 | 0.0086 |
| **SDHD** | AFP | 0.6661503 | 0.0000 |
| | CD13 | 0.2921381 | 0.0404 |
| | ABCG2 | 0.5064105 | 0.0000 |
| | BMI1 | 0.3733502 | 0.0011 |
| | KLF4 | 0.2961764 | 0.0350 |
| | cMYC | 0.4372903 | 0.0000 |
| | IGF2 | 0.4436238 | 0.0000 |
| | HNF4A | 0.496548 | 0.0000 |
| | HNF4G | 0.5421162 | 0.0000 |
| | ALDH1a1 | 0.6601424 | 0.0000 |
| | PGC-1α | 0.4682400 | 0.0000 |
| **PGC-1α** | ABCG2 | 0.4262534 | 0.0010 |
| | IGF2 | 0.5625352 | 0.0000 |
| | HNF4A | 0.3560371 | 0.0080 |
| | AFP | 0.4934186 | 0.0000 |
| | CD13 | 0.4544777 | 0.0000 |
| | ALDH1a1 | 0.5954048 | 0.0000 |
| | VEGFA | 0.3753468 | 0.0007 |

**Journal of Hepatology**

**CTAT methods**

Tables for a "Complete, Transparent, Accurate and Timely account" (CTAT) are now mandatory for all revised submissions. The aim is to enhance the reproducibility of methods.

- Only include the parts relevant to your study
- Refer to the CTAT in the main text as 'Supplementary CTAT Table'
- Do not add subheadings
- Add as many rows as needed to include all information
- Only include one item per row

## 1.1 Antibodies

| Name | Citation | Supplier | Cat no. | Clone no. |
|---|---|---|---|---|
| Mouse CD31 mAb | | Cell Signaling Technology | #3528 | |
| Rabbit PKM2 mAb | | Cell Signaling Technology | #4053 | |
| Rabbit Hexokinase II mAb | | Cell Signaling Technology | #2867 | |
| Rabbit E-Cadherin mAb | | Cell Signaling Technology | #3195 | |
| Rabbit Vimentin mAb | | Cell Signaling Technology | #5741 | |
| Rabbit Phospho-Akt (Ser473) Antibody | | Cell Signaling Technology | #9271 | |
| Rabbit Akt Antibody | | Cell Signaling Technology | #9272 | |
| Rabbit Bax mAb | | Cell Signaling Technology | #5023 | |
| Rabbit Bcl-2 mAb | | Cell Signaling Technology | #4223 | |
| Rabbit Cleaved Caspase-3 Antibody | | Cell Signaling Technology | #9661 | |
| Rabbit Phospho-AMPKα (Thr172) mAb | | Cell Signaling Technology | #2535 | |

| | | | | |
|---|---|---|---|---|
| Rabbit AMPKα Antibody | | Cell Signaling Technology | #2532 | |
| Rabbit Caspase-3 Antibody | | Santa Cruz Biotechnology | #sc-7148 | |
| Rabbit Snail mAb | | Santa Cruz Biotechnology | #3879 | |
| Rabbit PGC-1α | | Abcam | #ab54481 | |
| Mouse BrdU | | DAKO | M0744 | |

**1.2 Cell lines**

| **Name** | **Citation** | **Supplier** | **Cat no.** | **Passage no.** | **Authentication test method** |
|---|---|---|---|---|---|
| HUCCT1 | | kind gift from Dr. A.J. Demetris | | | |
| CCLP1 | | kind gift from Dr. A.J. Demetris | | | |

**1.3 Organisms**

| **Name** | **Citation** | **Supplier** | **Strain** | **Sex** | **Age** | **Overall n number** |
|---|---|---|---|---|---|---|
| | | | | | | |

**1.4 Sequence based reagents**

| **Name** | **Sequence** | **Supplier** |
|---|---|---|
| | | |

**1.5 Biological samples**

| **Description** | **Source** | **Identifier** |
|---|---|---|
| | | |

### 1.6 Deposited data

| Name of repository | Identifier | Link |
|---|---|---|
| | | |

### 1.7 Software

| Software name | Manufacturer | Version |
|---|---|---|
| SPSS | SPSS Inc | ver. 25.0 |
| GraphPad Prism | GraphPad Software | ver.5 |

### 1.8 Other (e.g. drugs, proteins, vectors etc.)

| Name | Supplier | Cat.no |
|---|---|---|
| Metformin | Sigma | D150959 |
| SR-18292 | MedChemExpress. | HY-101491 |
| QuantiNova LNA PCR Focus Panels 384-well plates | Qiagen | #SBHS-133ZE |
| 2-Deoxy-D-glucose(2-DG) a glycolysis inhibitor | Sigma | |
| MitoTracker Red | ThermoFisher Scientific | M7512 |
| MitoTracker Green | ThermoFisher Scientific | M7514 |
| siPGC-1α SiRNA | Santa Cruz | sc-38884 |
| Lactate Assay Kit | Biovision | BVN-K607-100 |
| AMP colorimetric assay kit | Biovision | K229-100 |
| ATP colorimetric assay kit | Biovision | K354-100 |
| Seahorse XF Cell Mito Stress Test Kit | Agilent | 103015-100 |
| Seahorse XFe96FluxPak | Agilent | 102601-100 |
| MitoSOX Red Mitochondrial Superoxide Indicator | ThermoFisher Scientific | M36008 |
| 5-Bromo-2’-deoxyuridine | MERK | B5002 |

**1.9 Please provide the details of the corresponding methods author for the manuscript:**

Dr. Chiara Raggi, Dipartimento di Medicina Sperimentale e Clinica
Largo Brambilla 3
I50134 Florence, Italy
Tel: +39 0552758092
Fax: +39 055 2758099
Email: chiara.raggi@unifi.it

**2.0 Please confirm for randomised controlled trials all versions of the clinical protocol are included in the submission. These will be published online as supplementary information.**

**Highlights**

- The metabolic characteristics of cancer stem cells in cholangiocarcinoma are not known
- Cholangiocarcinoma stem-like cells preferentially use oxidative phosphorylation as a source of energy
- PGC-1α is a key molecule regulating the metabolic features of cholangiocarcinoma stem-like cells
- Interfering with oxidative phosphorylation or PGC-1α limits the development of tumors originating from stem-like cells *in vivo*
- Expression of PGC-1α or proteins of the mitochondrial respiratory complex correlate with clinical outcomes in patients with cholangiocarcinoma

# Mitochondrial oxidative metabolism contributes to maintain a cancer stem cell phenotype in cholangiocarcinoma

**Chiara Raggi[1], Maria Letizia Taddei[1], Elena Sacco[2,3], Nadia Navari[1], Margherita Correnti[4], Benedetta Piombanti[1], Mirella Pastore[1], Claudia Campani[1], Erica Pranzini[1], Jessica Iorio[1], Giulia Lori[1], Tiziano Lottini[1], Clelia Peano[5,6], Javier Cibella[5], Monika Lewinska[7], Jesper B Andersen[7], Luca di Tommaso[8,9], Luca Vigano[9,10], Giovanni Di Maira[1], Stefania Madiai[1], Matteo Ramazzotti[8], Ivan Orlandi[2,3], Annarosa Arcangeli[1], Paola Chiarugi[8,9], Fabio Marra[1,9,#]**



**Table of Contents**

**Supplementary Materials and Methods**

**Cell cultures and reagents**

HUCCT1 and CCLP1 cells, from intrahepatic bile duct cancer tissues, were a kind gift from Dr. A.J. Demetris. Cell lines were cultured as described [1-3]. SR-18292 was purchased by MedChemExpress.

**Sphere formation assay**

The cells were grown in anchoring-independent conditions into poly 2-hydroxyethyl methacrylate (poly-HEMA)-coated dishes (Sigma Aldrich) with selective serum-free DMEM/F12 medium supplemented with 1X B27 supplement without vitamin A (Life Technologies), 20 ng/mL EGF, and 20 ng/mL bFGF (R&D Systems). To prevent cell aggregation, 1% methylcellulose (R&D System) was added to the culture medium [4, 5].

To calculate sphere-forming efficiency, 500 CCA cells were grown in anchoring-independent conditions with selective serum-free medium. After 7 days, pictures were taken to measure the number and size of CCA-SPH using a Leica DMi1microscope (Leica). Average number of formed spheres microscopic field (20x) over five fields. CCA-SPH volume was calculated after measuring length 1 (L1) and the length 2 (L2) using the following formula: $V = (L1*L2*L2)/2$ .

**Bioenergetic profiling**

Bioenergetic parameters of HUCCT1 and CCLP1 cells grown for 10 days as monolayer or spheres were analyzed using Agilent Seahorse XF24 analyzer and a “Clark-type” oxygen electrode.
Bioenergetic parameters of HUCCT1 and CCLP1 cells grown for 10 days as monolayer or spheres were analyzed using Agilent Seahorse XF24 analyzer and a “Clark-type” oxygen electrode (Oxygraph System, Hansatech Instruments, Nortfolk, UK). Before the analysis, cells were collected by trypsinization and counted: (a) 4-5x$10^6$ cells were suspended in 2ml unbuffered medium (D5030

Sigma Aldrich w/o sodium bicarbonate, containing 142mM NaCl, 10mM glucose, 2 mM glutamine, pH 7.4), and promptly analyzed by Oxygraph at 37°C. Respiratory rates were determined from the slope of a plot of $O_2$ concentration against time, divided by the cellular concentration. (b) the remaining cells were suspended in exhaust medium at the concentration $5x10^5$ cells/ml, seeded in Seahorse XF24-well plates (100µl/well), and incubated for 5h or 20h at 37°C in a humidified atmosphere of 5% CO2- 95% air. Before XF analysis culture medium was replaced with unbuffered medium (w/o glucose for measurements of glycolytic parameters) and cell cultures were let equilibrate for 1h at 37°C in a no-$CO_2$ incubator. Seahorse XF analysis was performed at 37°C simultaneously measuring Oxygen consumption rate (OCR =pmoles$O_2$/min) and Extracellular acidification rate (ECAR = mpH/min) in all the 24 wells of the XF plate, 10 devoted to each condition, MON and SPH, per cell line, and 4 as no cells-wells control. At the end of XF analysis, medium was removed, cells were gently washed with PBS, suspended in JS lysis buffer and scraped after two freeze and thaw cycles. Protein content of cell lysates was measured by Bradford assay and used for normalizing respiratory and glycolytic parameters. Oxygen consumption rate was analyzed by both Seahorse XF analyzer and Oxygraph under basal condition and under treatments with an ATP synthase inhibitor (0,5-2 µM oligomycin A), a ETC accelerator ionophore (0,25-5 µM carbonilcyanide p-triflouromethoxyphenylhydrazone or FCCP) and a ETC inhibitors mixture (1µM rotenone and 1µM antimycin A). The addition of the minimum dose of oligomycin A, and FCCP which generates the maximal effect accounted for non-phosphorylating respiration, and uncoupled respiration, respectively. The addiction of the rotenone and antimycin A mixture accounted for non-mitochondrial oxygen consumption. XF analysis of respiratory parameters was performed according to seahorse mitostress test protocol, consisting of three sequential measurements in basal condition and after the injection of the optimal doses of oligomycin A, FCCP, and rotenone/antimycin A. Respiratory parameters were elaborated using the following formulas: basal mitochondrial respiration (Basal-MR) = OCRbasal-OCRrot/ant, non phosphorylating mitochondrial

respiration (oligo-NPMR) = OCRoligo-OCRrot/ant, FCCP-uncoupled mitochondrial respiration (FCCP-MR) = OCRFCCP-OCRrot/ant, spare respiratory capacity = [OCR(FCCP)-OCR(rot/ant)/OCR(basal)-OCR(rot/ant)]x100, coupling efficiency = [1-(OCR(oligo)-OCR(rot/ant)/OCR(basal)-OCR(rot/ant)]x100. XF analysis of glycolytic parameters was performed according to seahorse glycostress test protocol, consisting of three sequential measurements in no-glucose condition and after the injection of 10mM glucose, the optimal dose of oligomycin A, and 50mM 2-Deoxy-D-glucose(2-DG) a glycolysis inhibitor (Sigma). The addition of the minimum dose of oligomycin A, which generates the maximal effect accounted for glycolytic capacity. The addiction of 2-DG accounted for non-glycolytic extracellular acidification. Data were elaborated using the following formulas: Basal glycolysis = ECARglc-ECAR2-DG, Glycolytic capacity = ECARoligo-ECAR2-DG, Glycolytic reserve = ECARoligo-ECARglc.

**Western blot analysis**

Cells were lysed at 4°C with lysis buffer (1% Triton X-100, 50 mmol/L Tris–HCl, pH 7.4, 150 mmol/L NaCl, 1 mmol/L EDTA, 1 mmol/L sodium orthovanadate, 2 mmol/L PMSF, and 1 mmol/L each of leupeptin and pepstatin). After 30 minutes of lysis, cellular extracts were centrifuged for 10 min at 12000g, and the supernatant was used for Western blot experiments as detailed elsewhere [6]. Antibodies were used for Western blot analysis according to the manufacturer's recommendations. Immunoblots were incubated overnight at 4°C with primary antibody in 1% BSA in DPBS. Mouse CD31 mAb (#3528, Cell Signaling Technology), Rabbit PKM2 mAb (#4053, Cell Signaling Technology), Rabbit Hexokinase II mAb (#2867, Cell Signaling Technology), Rabbit PGC1α Antibody (ab54481, Abcam), Rabbit E-Cadherin mAb (#3195, Cell Signaling Technology), Rabbit Vimentin mAb (#5741, Cell Signaling Technology), Rabbit Snail mAb (#3879, Cell Signaling Technology), Rabbit Phospho-Akt (Ser473) Antibody (#9271, Cell Signaling Technology), Rabbit Akt Antibody (#9272, Cell Signaling Technology), Rabbit Bax mAb

(#5023, Cell Signaling Technology), Rabbit Bcl-2 mAb (#4223, Cell Signaling Technology), Rabbit Cleaved Caspase-3 Antibody (#9661, Cell Signaling Technology), Rabbit Caspase-3 Antibody (#sc-7148 Santa Cruz Biotechnology) Rabbit Phospho- AMPKα (Thr172) mAb (#2535 Cell Signaling Technology), Rabbit AMPKα Antibody (#2532, Cell Signaling Technology) antibodies were used. Immunoblots were then incubated with secondary antibody α-rabbit/mouse (1:4000) in 1% BSA in 1x DPBS for 1hour. Monoclonal anti-β-actin antibodies produced in mouse (A5441, Sigma) or monoclonal anti-vinculin antibodies produced in mouse (V9131, Sigma) were used as internal control (1:1000) in 1% BSA in 1x DPBS. Quantification of the signal was obtained by chemiluminescence detection on an Image Quant Las4000 (GE Healthcare Life Sciences) and subsequent analysis conducted with ImageJ software.

**Quantitative real-time polymerase chain reaction (RT-PCR)**

Total RNA was extracted with the RNeasy kit (Qiagen) according to the manufacturer's instructions. The RNA concentration and quality were measured using an optical NanoDrop ND1000 spectrophotometer (Thermo Fisher Scientific). Total RNA (500 ng) was transcribed with a High-Capacity cDNA Reverse Transcription Kit (Applied Biosystems). Changes in the mRNA expression level of target genes were detected using FAST SYBR-Green PCR Master Mix and the 7900HT Fast Real Time PCR System (Applied Biosystems). All amplifications were run on a 7500 Fast RealTime PCR System (Applied Biosystems). The primers for GLUT1 were 5'-CGGGCCAAGAGTGTGCTAAA-3' (forward), 5'-TGACGATACCGGAGCCAATG-3' (reverse). Data were normalized on β2 microglobulin. Data were reported as relative quantification with respect to the calibrator sample (MON) using the $2^{-\Delta\Delta Ct}$ method. The primers for stem-like genes, pluripotency and EMT were as described in [5]. The mRNA levels of glyceraldehyde 3-phosphate dehydrogenase (GAPDH) were used for normalization. Data are reported as relative quantification

with respect to the calibrator sample (SPH NT) using the $2^{-\Delta\Delta Ct}$ method. Results shown are the mean of three different experiments ± SD.

**List of Primers**

| **Gene** | **Sequence** |
|---|---|
| AFP-FW | AAGGCCAGGAACAGGAAGTC |
| AFP-REV | CACACCGAATGAAAGACTCG |
| EpCAM-FW | TGTGGTGATAGCAGTTGTTGC |
| EpCAM-REV | CTATGCATCTCACCCATCTCC |
| LGR5-FW | CTTCCAACCTCAGCGTCTTC |
| LGR5-REV | TTTCCCGCAAGACGTAACTC |
| CD13-FW | CAGTGACACGACGATTCTCC |
| CD13-REV | CCTGTTTCCTCGTTGTCCTT |
| CD133-FW | GCTTCAGGAGTTTCATGTTGG |
| CD133-REV | GGGGAATGCCTACATCTGG |
| NANOG-FW | GTCTCGTATTTGCTGCATCG |
| NANOG-REV | GAAACACTCGGTGAAATCAGG |
| BMI1-FW | TTGCTTTGGTCGAACTTGG |
| BMI1-REV | GTGCTTCTTTTGCAGACTGG |
| CMYC-FW | CGGAACTCTTGTGCGTAAGG |
| CMYC-REV | ACTCAGCCAAGGTTGTGAGG |
| KLF4-FW | AGACAGTCTGTTATGCACTGTGG |
| KLF4-REV | TGTTCTGCTTAAGGCATACTTGG |
| SOX-2-FW | ATGGGTTCGGTGGTCAAGT |
| SOX-2-REV | GGAGGAAGAGGTAACCACAGG |
| BMP4-FW | AGCGTAGCCCTAAGCATCAC |
| BMP4-REV | AGTCATTCCAGCCCACATCG |
| YAP-FW | ACCCTCGTTTTGCCATGAAC |
| YAP-REV | TTGTTTCAACCGCAGTCTCTC |

| | |
|---|---|
| STAT3-FW | GGCATTCGGGAAGTATTGTCG |
| STAT3-REV | GGTAGGCGCCTCAGTCGTATC |
| IGF2-FW | ACACCCTCCAGTTCGTCTGT |
| IGF2-REV | GGGGTATCTTGGGGAAGTTGT |
| HNF4-FW | CTCGTCGACATGGACATGGCCGACTAC |
| HNF4-REV | GGCTTGCTAGATAACTTCCTGCTTGGT |
| ABCG2 -FW | GGCTTTCTACCTGCACGAAAACCAGTTGAG |
| ABCG2 -REV | ATGGCGTTGAGACCAG |
| ALDH1a-FW | GCACGCCAGACTTACCTGTC |
| ALDH1a-REV | CCACTCACTGAATCATGCCA |
| ECAD-FW | AGGCCAAGCAGCAGTACATT |
| ECAD-REV | ATTCACATCCAGCACATCCA |
| VIM-FW | ACACCCTGCAATCTTTCAGACA |
| VIM-REV | GATTCCACTTTGCGTTCAAGGT |
| CTNNB1-FW | GCTGGGACCTTGCATAACCTT |
| CTNNB1-REV | ATTTTCACCAGGGCAGGAATG |
| ZEB1-FW | AAGAAAGTGTTACAGATGCAGCTG |
| ZEB1-REV | CCCTGGTAACACTGTCTGGTC |
| Zeb2-FW | AGGGACAGATCAGCACCAAA |
| Zeb2-REV | GTGCGAACTGTAGGAACCAG |
| SNAIL-FW | CCTCCCTGTCAGATGAGGAC |
| SNAIL-REV | CAAGGAATACCTCAGCCTGG |
| SLUG-FW | ACAGCGAACTGGACACACAT |
| SLUG-REV | GATGGGGCTGTATGCTCCT |
| VEGFa-FW | CACTGAGGAGTCCAACATCAC |
| VEGFa-REV | AGGAAGCTCATCTCTCCTATGT |
| PGC-1α-FW | TGCATGAGTGTGTGCTCTGT |
| PGC-1α-REV | GCACACTCGATGTCACTCCA |

| | |
|---|---|
| Glut1-FW | CGGGCCAAGAGTGTGCTAAA |
| Glut1-REV | TGACGATACCGGAGCCAATG |
| GAPDH-FW | GATCATCAGCAATGCCTCCT |
| GAPDH-REV | TGTGGTCATGAGTCCTCCCA |

**RT-PCR array**

Five µg of total RNA of in vivo tumors were reverse transcribed using the QuantiNova Reverse Transcription kit (Qiagen). qRT-PCR reaction was performed using the QuantiNova LNA PCR Focus Panels 384-well plates (#SBHS-133ZE, Qiagen). In each 384-well plates, 4 different tumor samples were tested for 84 genes specifically associated with liver cancer pathways. The expression values were calculated with the ΔCt method, using ACTB, GAPDH, RPLP0 and HPRT1 as housekeeping genes as reference. A cutoff of at least 1.5-fold increases and 0.5-fold decreases were considered significant.

**Glucose uptake**

Uptake of radioactive glucose was evaluated by treating $7x10^4$ CCLP1 or HUCCT1 cells seeded in 24-well plates with a buffered solution (140 mmol/L NaCl, 20 mmol/L Hepes/Na, 2.5 mmol/L MgSO4, 1 mmol/L CaCl2, and 5 mmol/L KCl, pH 7.4) containing 0.5 µCi/mL [U-$^{14}$C] glucose for 15 min at 37°C. Cells were subsequently washed with cold PBS and lysed with 0.1 mol/L NaOH. Incorporated radioactivity was assayed by liquid scintillation counting and normalized to protein content.

**Measurement of mitochondrial mass and mitochondrial membrane potential (ΔΨm)**

SPH and MON cells were harvested by trypsinization and washed. For measurement of mitochondrial mass and ΔΨm, cells were stained with 50 nM MitoTracker Green and 50nM MitoTracker Red (ThermoFisher Scientific), respectively. Cells were incubated at 37°C for 25 min,

washed twice and analyzed by flow cytometry with FACSCanto II (BD Biosciences). Dead cells were excluded using the Zombie Aqua™ Fixable Viability Kit (Biolegend). A fluorescence minus one (FMO) sample, containing all antibodies except the one of interest, was used as a negative control. Data analysis was performed with the FlowJo software (FlowJo, LLC) [7, 8].

**Lactate assay**

Lactate was measured in the cultured media with Lactate Assay kit (Biovision) according to the manufacturer's instruction.

**Quantification of AMP/ATP ratio**

AMP/ATP ratio was calculated after the absolute quantification of ATP and AMP measured in MON and SPH cells by using the ATP Colorimetric/Fluorometric Assay Kit (BioVision) and the AMP Colorimetric Assay Kit (BioVision) respectively according to the manufacturer's instruction.

**Determination of mitochondrial ROS**

Mitochondrial ROS was measured in SPH and MON cells with MitoSOX™ Red Mitochondrial Superoxide Indicator (Thermofisher) according to the manufacturer's instruction.

**Evaluation of spheres and Giemsa staining**

CCLP1 and HUCCT1 cells (750 cells/well) were seeded in poly-HEMA-coated 96-well plates and cultured for 96 hours. Cells silenced for PGC-1α, were harvested and cytospinned onto glass slides, fixed with methanol, stained with Giemsa, and photographed with an Olympus BX51 microscope with a 40x objective.

**Tube formation assay**

This assay was carried out as previously described [5], with slight modifications. In brief, 96-well plates were coated with 70µl of pre-thawed growth factor-reduced Matrigel (BD Biosciences). The plate was then kept at 37 °C for 1 hour to allow the matrix solution to gel. $1.8x10^4$ HUVEC cells were resuspended in the respective conditioned media, added to each well and incubated at 37°C for 6h. Images were acquired under an inverted microscope. Pro-angiogenic activity was quantified by measuring the number of tube structures formed between discrete endothelial cells in each well. Each experiment was performed in triplicate. Analysis of endothelial tube formation for total tube length and branching points was performed by Wimasis (2017) image analysis tool (WimTube: Tube Formation Assay Image Analysis Solution, Release 4.0; Onimagin Technologies, Cordoba, Spain). At least 3 images from each group were analyzed for endothelial tube formation assay.

**Cell transfection**

Control siRNA and siPGC-1α SiRNA (sc-38884) were from Santa Cruz. Cells were transfected as previously described using the Amaxa nucleofection technology (Amaxa) according to manufacturer's instructions.

**Cell proliferation assay**

Proliferation was evaluated by BrdU incorporation using a colorimetric immunoassay. SPH were dissociated and 7,5 $x10^3$ cells were seeded in a 96-well plate and allowed to grow overnight in SPH medium. The Cell Proliferation ELISA-BrdU (colorimetric) Kit (Roche) was used to detect the cell proliferation according to the manufacturer's protocols**.**

**Survival test by crystal violet staining**

CCA cells previously cultured as monolayer or sphere were seeded in 96-multiwell plates for 24 h before receiving Metformin or Phenformin or 2-deoxy-D-glucose or SR-12898 (at different doses as

indicated in the main text) for 48 h or 72h. Cellular growth was stopped by removing the medium and by the addition of a 0.5% crystal violet solution in 20% methanol. After 5 min of staining, the fixed cells were washed with phosphate-buffered saline (PBS) and solubilized with 200 µl/well of 0.1 M sodium citrate, pH 4.2. The absorbance at 595 nm was evaluated using a microplate reader.

**Chemoinvasion and migration assays**

48 hours after transfection, CCLP1 and HUCCT1 SPH cells were washed, trypsinized, and re-suspended in serum-free medium at a concentration of 1.5 x $10^5$ cells/ml. Chemoinvasion was measured in modified Boyden chamber equipped with 8 µm pore filters (Millipore Corp,) coated with Matrigel (150 µg/ml) (BD Biosciences) as described in detail elsewhere [9]. After incubation at 37 °C (24 h), the cells invaded to the underside of the filters were fixed, stained with Giemsa, mounted and counted at 40X magnification. Migration was measured in Boyden chamber equipped with 8 µm pore filters (Millipore Corp) coated with rat tail collagen (20 µg/ml) (Collaborative Biomedical Products, Bedford, UK), as described in detail elsewhere [6]. Cells were seeded in the upper chamber, while the (FBS 20%) was placed in the lower compartment. After six hours incubation at 37 °C, cells migrated to the underside of the filters were fixed, stained with Giemsa, mounted and counted at 40X magnification.

The values for both invasion and migration were expressed as the average number of invading cells per microscopic field (40X) over five fields. Each experiment was performed in triplicate.

***In vivo* experiments**

Animal experiments were performed in accordance with national guidelines and approved by the ethical committee of the Animal Welfare Office of Italian Health Ministry. All procedures conformed to the legal mandates and the Italian guidelines for the care and maintenance of laboratory animals. All animals received human care and study protocols comply with the

institution's guidelines. Studies involving animal experiments conform to the Animal Research: Reporting of In Vivo Experiments (ARRIVE) guidelines (http://www.nc3rs.org.uk/arrive-guidelines), developed by the National Centre for the Replacement, Refinement and Reduction of Animals in Research (NC3Rs) to improve standards and reporting of animal research.
Male NOD/SCID mice of six weeks (Charles River Laboratories International) were s.c. injected with $10^6$ HUCCT1 SPH cells. . After a week, mice were randomly allocated to receive repeated courses of intra-peritoneal vehicle solution (control mice) or 200 mg/kg of metformin or 45mg/kg SR-18292, five times a week. Animals (6 per group) were monitored daily.

**Ultrasound and photoacoustic imaging**

Tumor volumes were determined in vivo imaging system (Vevo LAZR-X photoacoustic imaging). Mice were anesthetized with 1,5/2% isoflurane and placed on a heated pad (37°C) in prone position and ECG, respiration rate and body temperature were continuously monitored. Ultrasonic gel was applied on the shaved skin for an efficient transduction of ultrasound (US) and (photoacoustic) PA signal. PA and US imaging were performed with Vevo LAZR-X system (Fujifilm VisualSonics). Axial 3D scans of tumor masses were performed in B-Mode imaging by using a 55-MHz transducer. The volumes were subsequently measured delineating the region of interest (ROI) for every axial slide using Vevo LAB software.

**BrdU staining**

*In vivo* bromodeoxyuridine (BrdU) labeling was performed by intraperitoneal injection of 50 mg/kg BrdU (Sigma-Aldrich), 1 h prior to sacrifice. Tumor tissues were fixed overnight in 4% neutral buffered paraformaldehyde, paraffin embedded, and cut into 3-µm sections. Deparaffinized slides were treated with 2N HCl for 30 min at room temperature (RT) and neutralized with 0.1 M sodium borate (pH 8.5) for 15 min at RT. Slides were washed with PBS, incubated with 3% $H_2O_2$ for 15

min at RT and then with anti-BrdU antibodies (1:50 dilution) (Dako) was applied for 30 min. Slides were washed again and BrdU was detected using an immunohistochemistry kit (Dako REAL Detection system, peroxidase/DAB+) following the manufacturer's protocol. Five microscopic fields/number of cells were counted.

**Analysis of PGC-1α protein level in CCA tissue**

A total of 40 formalin-fixed, paraffin-embedded human liver tissue specimens were analyzed for the immunohistochemical expression of PGC-1α. All specimens were obtained after surgical resection and collected in the tissue bank at Humanitas Clinical Institute (Rozzano, Italy) in accordance with informed consent retrieved from patients and local ethics committee approval conforms to the ethical guidelines of the 1975 Declaration of Helsinki as reflected in a priori approval by the institution's human research committee.

The immunohistochemical expression of PGC-1α (Rabbit PGC1α Antibody (ab54481, Abcam)) was performed on the automated Leica Microsystems Bondmax® (Leica). Both cytoplasmic and nuclear staining was retained for scoring. Immunostaining was semiquantified using a three-tier scoring based on intensity of staining (0= negative; 1= weak; 3=moderate; 4= strong). Correlation analysis with clinicopathological CCA data were conducted as follows: continuous variables are presented as means and standard deviations, and categorical variables as number and percentages. Continuous variables were analyzed using a two-tailed, unpaired t-test, categorical variables were compared, categorical variables were analyzed using a chi-square or Fisher exact test for dichotomous data. A two-sided p value $<0.05$ was defined to be considered statistically significant. The OS was calculated from the date of surgery to the date of death or last follow-up visit. Kaplan-Meier estimator survival curves and log rank tests were used to evaluate and compare OS. All analyses were performed with SPSS ver. 25.0 (SPSS Inc).

**GSEA analysis**

Gene expression profiles for 104 tumors have been retrieved from GSE26566. Patients were stratified based on overall survival into a poor prognosis (OS<12 months) and a good prognosis (OS>12 months) group. Custom signatures for Krebs Cycle and complex I-IV were added as the text entry and associated with survival using gene set enrichment analysis (GSEA) [10] with signal2noise metric and otherwise default parameters. Time to recurrence (TTR) was used as a continuous trait and associated with signatures using Pearson's metric and otherwise default parameters.

**Correlation analysis**

An analysis between PGC-1α and other test genes was applied on a published microrarray-based study on cholangiocarcinoma tissue vs surrounding liver from 59 patients (GSE26566) [11]. Probe level normalized expression values were aggregated (median) at the gene level as in the GSEA analysis detailed above. The correlation analysis was based on Pearson's product moment correlation and p-values were corrected for multiple testing with the Benjamini-Hochberg procedure, both implemented in the stats package of the R statistical software.

**Library preparation and RNA-sequencing**

Total RNA was isolated from cells using the miRNeasy Mini Kit (Qiagen) according to the manufacturer's protocol. Total-RNA-sequencing (RNA-seq) library preparation was performed starting from 100 ng of total-RNA with the SMARTer Stranded Total RNA Sample Prep Kit - Low Input Mammalian (Clontech-Takara). The libraries obtained were qualitatively and qualitatively assessed by using TapeStation 4200 (Agilent) and quantified by Qubit Fluorimeter (ThermoFisher). Afterwards, they were multiplexed in an equimolar pool and sequenced on a NextSeq-500 Illumina Platform generating more than 60 million 75bp Paired End reads (bp-PE) per sample.

**Reads preprocessing**

Sequencing data was demultiplexed into separate, adapter free compressed fastq files using bcl2fastq v2.20.0.422 (Illumina, Inc.) and a reference sample sheet specifying for each sample the corresponding barcode. Reads were further processed using the fastp program [12] configured to use 20 threads for removing read pairs with at least 50% of bases with Q > 30, a minimal length of 70 bp, a complexity > 30%. No trimming was performed on reads.

**Reads alignment, abundance estimation and differential analysis**

Reads mapping was performed using the default options but specifying the --numGibbsSamples 500 and –validate Mappings options, on a reference transcriptome composed by the union of the human cDNA and ncDNA available from Ensembl (assembly GRCh38.p13) indexed with a kmer size of 23 by Salmon v0.14.1 [13]. Reads were imported into R using the tximport package [14] with the "Salmon" specific method. Gene level abundance was estimated from transcript level estimates using the summarizeToGene function of tximport working on a transcript to gene association table (further associating gene names for functional analysis, see below) obtained with Ensembl Biomart system [15] operating on Ensembl genes 98/GRCh38.p13 human genes.
Data matrices were eventually converted in DEseq2 objects using the ESeqDataSetFromTximport function, specifying the SPH vs MON phenotypes as the design contrast.

**Functional analysis**

For the functional analysis of the experiment the GSEA 4.0.2 software by BROAD Institute was used [10, 16], in the GSEAPreRanked mode using the t-statistic from the DESeq2 analysis as input metric for sorting. Gene lists were obtained from MSigDB 7.0 [17, 18] and gene names were converted into Ensembl gene IDs using a simple perl script reading the same table produced by

Biomart used for gene abundance estimation (see above). A selection of interesting gene sets from the different MSigDB collections (kegg, biocarta, gobp, hallmark, reactome) was obtained by a custom bash script that isolated those containing mitochondrial genes (GO:0005739:mitochondrion).

**Statistical Analysis**

GraphPad Prism v5 and SPSS v25.0 were used for data analysis. The error bars represent 1+/- SEM. The p value was calculated with Student's t test. In the *in vivo* experiments, group comparison was performed with the Mann-Whitney U-test. The statistical significance and p value are shown when relevant. In the humans sample experiments,group comparison was performed with the Fisher exact test.

**REFERENCES**

[1] Miyagiwa M, Ichida T, Tokiwa T, Sato J, Sasaki H. A new human cholangiocellular carcinoma cell line (HuCC-T1) producing carbohydrate antigen 19/9 in serum-free medium. In Vitro Cell Dev Biol 1989;25:503-510.
[2] Han C, Wu T. Cyclooxygenase-2-derived prostaglandin E2 promotes human cholangiocarcinoma cell growth and invasion through EP1 receptor-mediated activation of the epidermal growth factor receptor and Akt. J Biol Chem 2005;280:24053-24063.
[3] Shimizu Y, Demetris AJ, Gollin SM, Storto PD, Bedford HM, Altarac S, et al. Two new human cholangiocarcinoma cell lines and their cytogenetics and responses to growth factors, hormones, cytokines or immunologic effector cells. Int J Cancer 1992;52:252-260.
[4] Raggi C, Factor VM, Seo D, Holczbauer A, Gillen MC, Marquardt JU, et al. Epigenetic reprogramming modulates malignant properties of human liver cancer. Hepatology 2014;59:2251-2262.
[5] Raggi C, Correnti M, Sica A, Andersen JB, Cardinale V, Alvaro D, et al. Cholangiocarcinoma stem-like subset shapes tumor-initiating niche by educating associated macrophages. J Hepatol 2017;66:102-115.
[6] Bonacchi A, Romagnani P, Romanelli RG, Efsen E, Annunziato F, Lasagni L, et al. Signal transduction by the chemokine receptor CXCR3: activation of Ras/ERK, Src, and phosphatidylinositol 3-kinase/Akt controls cell migration and proliferation in human vascular pericytes. J Biol Chem 2001;276:9945-9954.
[7] Samudio I, Konopleva M, Hail N, Shi YX, McQueen T, Hsu T, et al. 2-Cyano-3,12-dioxooleana-1,9-dien-28-imidazolide (CDDO-Im) directly targets mitochondrial glutathione to induce apoptosis in pancreatic cancer. J Biol Chem 2005;280:36273-36282.
[8] Ye XQ, Li Q, Wang GH, Sun FF, Huang GJ, Bian XW, et al. Mitochondrial and energy metabolism-related properties as novel indicators of lung cancer stem cells. Int J Cancer 2011;129:820-831.
[9] Raggi C, Fiaccadori K, Pastore M, Correnti M, Piombanti B, Forti E, et al. Antitumor Activity of a Novel Fibroblast Growth Factor Receptor Inhibitor for Intrahepatic Cholangiocarcinoma. Am J Pathol 2019;189:2090-2101.
[10] Subramanian A, Tamayo P, Mootha VK, Mukherjee S, Ebert BL, Gillette MA, et al. Gene set enrichment analysis: a knowledge-based approach for interpreting genome-wide expression profiles. Proc Natl Acad Sci U S A 2005;102:15545-15550.
[11] Andersen JB, Spee B, Blechacz BR, Avital I, Komuta M, Barbour A, et al. Genomic and genetic characterization of cholangiocarcinoma identifies therapeutic targets for tyrosine kinase inhibitors. Gastroenterology 2012;142:1021-1031.e1015.
[12] Chen S, Zhou Y, Chen Y, Gu J. fastp: an ultra-fast all-in-one FASTQ preprocessor. Bioinformatics 2018;34:i884-i890.
[13] Patro R, Duggal G, Love MI, Irizarry RA, Kingsford C. Salmon provides fast and bias-aware quantification of transcript expression. Nat Methods 2017;14:417-419.
[14] Soneson C, Love MI, Robinson MD. Differential analyses for RNA-seq: transcript-level estimates improve gene-level inferences. F1000Res 2015;4:1521.
[15] Smedley D, Haider S, Ballester B, Holland R, London D, Thorisson G, et al. BioMart--biological queries made easy. BMC Genomics 2009;10:22.
[16] Mootha VK, Lindgren CM, Eriksson KF, Subramanian A, Sihag S, Lehar J, et al. PGC-1alpha-responsive genes involved in oxidative phosphorylation are coordinately downregulated in human diabetes. Nat Genet 2003;34:267-273.
[17] Liberzon A, Subramanian A, Pinchback R, Thorvaldsdóttir H, Tamayo P, Mesirov JP. Molecular signatures database (MSigDB) 3.0. Bioinformatics 2011;27:1739-1740.

[18] Liberzon A, Birger C, Thorvaldsdóttir H, Ghandi M, Mesirov JP, Tamayo P. The Molecular Signatures Database (MSigDB) hallmark gene set collection. Cell Syst 2015;1:417-425.

**Supplementary Figures**

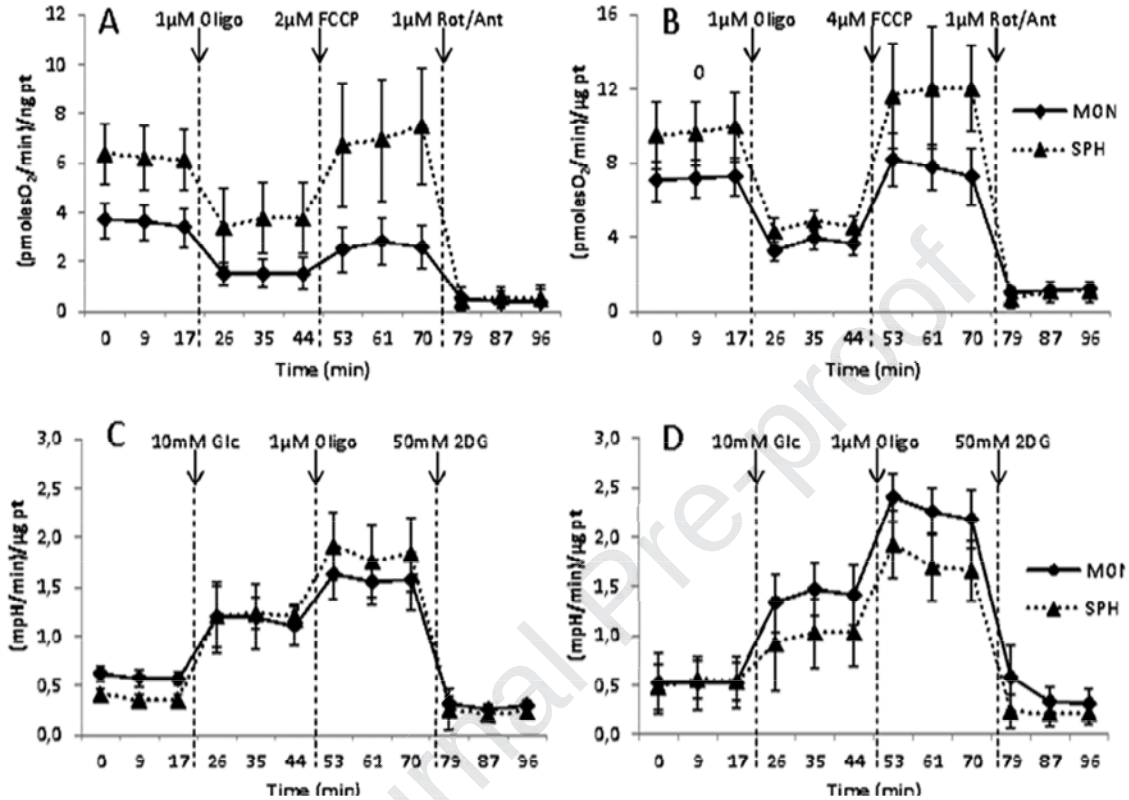


**Supplementary** Figure 1: Metabolic characteristics of CCA cells grown as monolayers (MON) or spheres (SPH). Seahorse XF assay profiles of HUCCT1 (A,C) and CCLP1 (B,D) cells grown under monolayer (♦ MON) or sphere (▲ SPH) condition exposed to metabolic stress in unbuffered medium (Mean and SEM). (A-B) Mitostress test profile: Oxygen Consumption rate was measured under sequential treatment with drugs perturbing mitochondrial performance, namely oligomycin A, FCCP and Rotenone/Antimycin A mixture at the doses reported in the graph. (C-D) Glycostress test profile: Extracellular acidification rate measured in unbuffered glucose-free medium under sequential treatment with drugs perturbing glycolysis, namely 10mM glucose, 1µM oligomycin and 50mM 2-DG. The analysis was performed with Seahorse XF24 analyzer (Agilent). OCR and ECAR were normalized on protein content measured by Bradford assay.

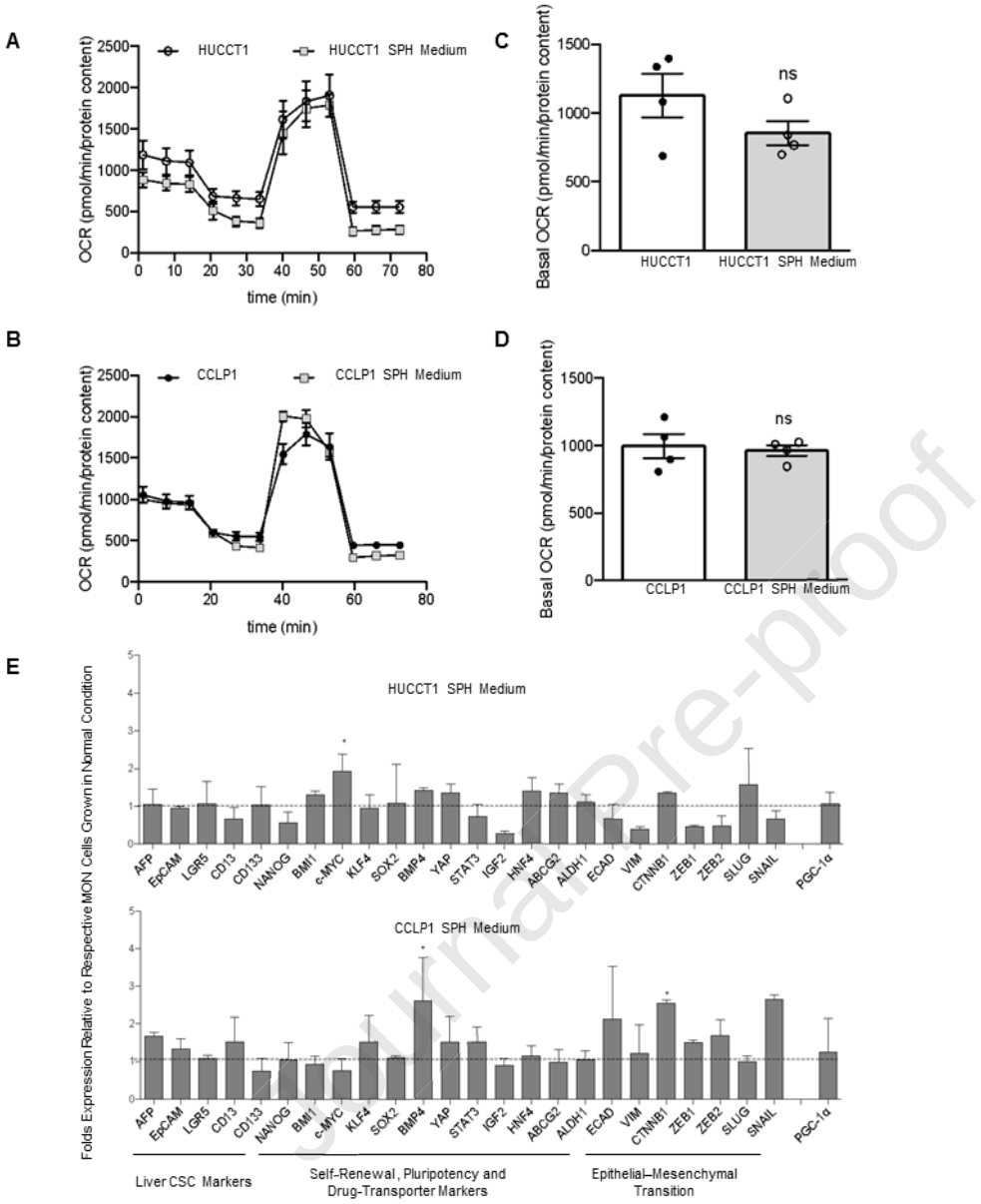


**Supplementary Figure 2: Metabolic features are independent of the culture medium**. (A-B) Representative Seahorse XF assay profiles of HUCCT1 and CCLP1 cells grown as monolayer condition exposed to SPH medium. Mitostress test profile: oxygen consumption rate (OCR) was measured under sequential treatment with drugs perturbing mitochondrial performance as reported above. (C,D) Basal OCR is represented for each cell line in the different medium condition. The analysis was performed with Seahorse XF24 analyzer (Agilent). OCR was normalized on protein content measured by Bradford assay. Data are mean ± SEM (n=3, p value versus control sample by Student t test, * $p \leq 0.05$). (E) qRT-PCR analysis of several stem-like related genes in MON and MON cells grown in SPH medium of CCLP1 and HUCCT1 cells. GAPDH was used as an internal

control. All mRNA levels are presented as fold changes normalized to 1 (mean expression of MON grown in normal condition). Data are mean ± SEM (n=3, *p≤0.05 vs. MON grown in normal condition).

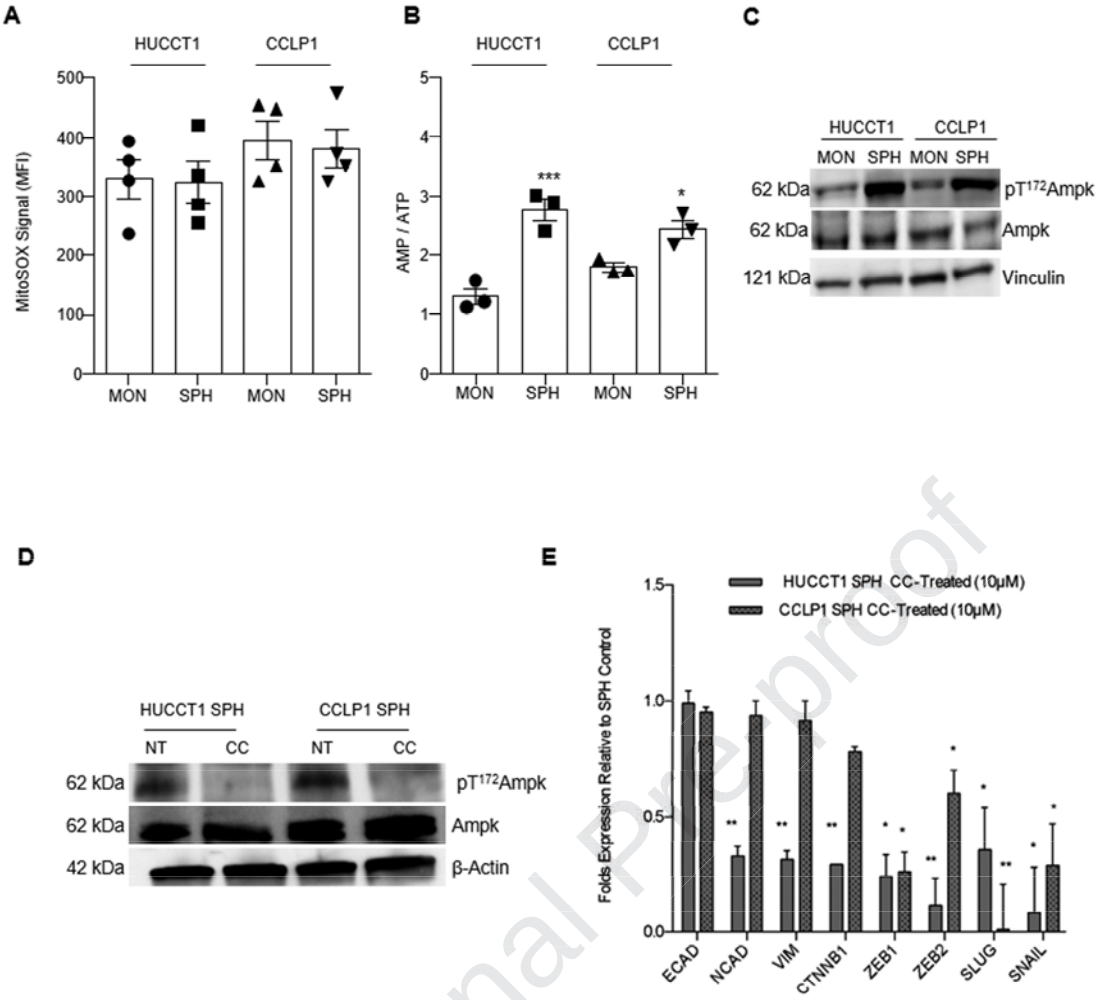


**Supplementary Figure 3: Role of AMPK in mediating activation of EMT genes.** (A) Evaluation of mitochondrial ROS production in MON and SPH cells by FACS, using MitoSOX. Histograms represent the Mean Fluorescence Intensity (MFI) of the MitoSOX probe. Data are mean ± SEM (n=3). (B) Measurement of AMP:ATP ratios in MON and SPH cells. The ratios of AMP:ATP derived from analysis of three independent samples for each condition. The results are shown as mean ± SEM (n=3, *p≤0.05, *** p≤0.001 vs. MON). (C) Immunoblot analysis of AMPK and Phospho-AMPK (Thr172) in monolayers (MON) or spheres (SPH) of CCLP1 and HUCCT1 cells. Vinculin immunoblot was performed to ensure equal loading. (D) Immunoblot analysis of AMPK and Phospho-AMPK (Thr172) in SPH after 24 hours treatment with 10μM compound C (CC). β-Actin immunoblot was performed to ensure equal loading. (E) qRT-PCR analysis of EMT-related genes in SPH and CC treated SPH cells. GAPDH was used as an internal control. All mRNA levels are presented as fold changes normalized to 1 (mean expression of SPH CTR cells). Data are mean±SEM (n=3, *p≤0.05 , **p≤0.01 vs. SPH CTR cells).

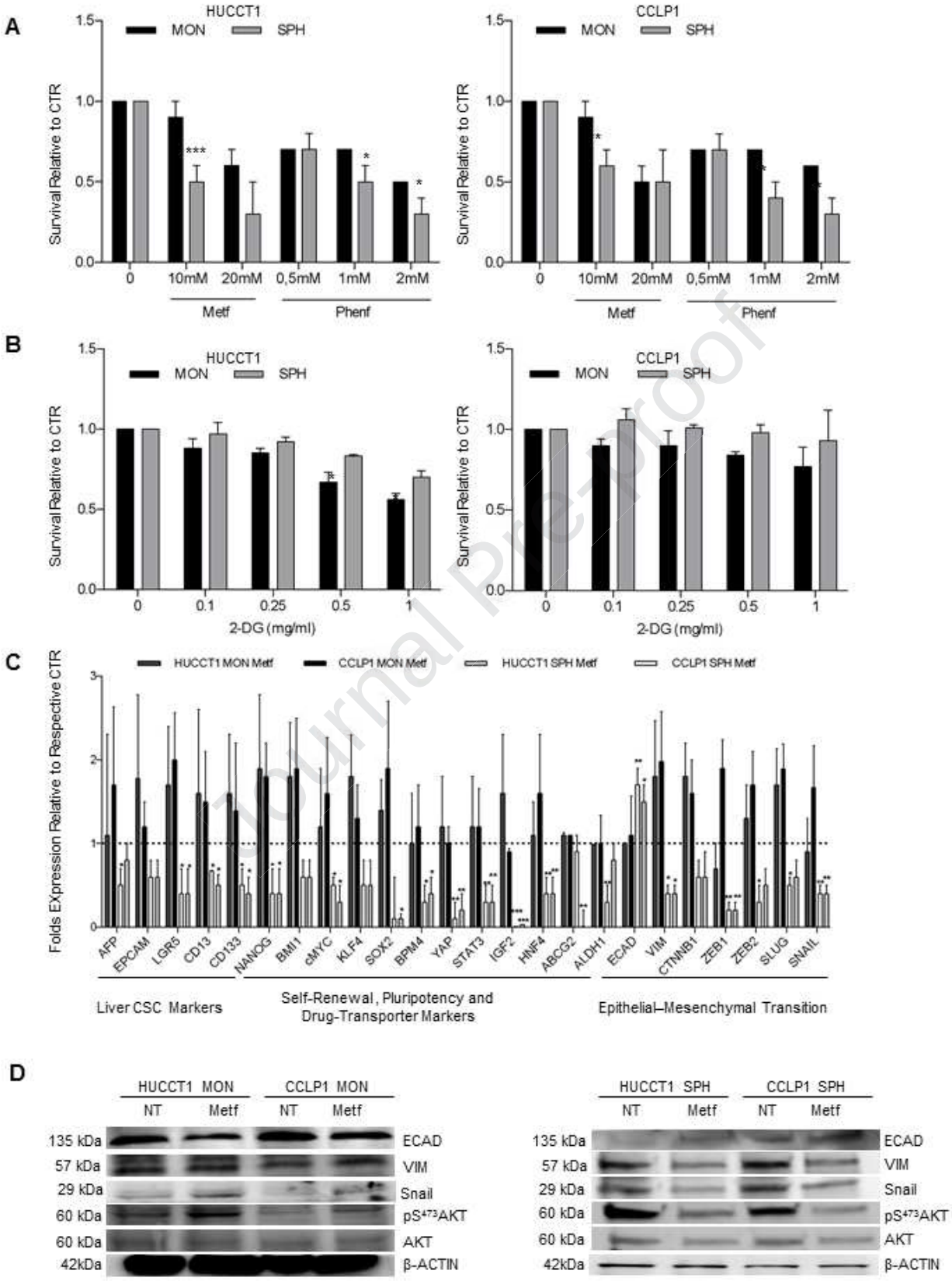
A
HUCCT1
MON
SPH
Survival Relative to CTR
0
10mM
20mM
0,5mM
1mM
2mM
Metf
Phenf
CCLP1
B
2-DG (mg/ml)
C
HUCCT1 MON Metf
CCLP1 MON Metf
HUCCT1 SPH Metf
CCLP1 SPH Metf
Folds EXpression Relative to Respective CTR
AFP
EPCAM
LGR5
CD13
CD133
NANOG
BMI1
cMYC
KLF4
SOX2
BPM4
YAP
STAT3
IGF2
HNF4
ABCG2
ALDH1
ECAD
VIM
CTNNB1
ZEB1
ZEB2
SLUG
SNAIL
Liver CSC Markers
Self-Renewal, Pluripotency and Drug-Transporter Markers
Epithelial–Mesenchymal Transition
D
HUCCT1 MON
CCLP1 MON
HUCCT1 SPH
CCLP1 SPH
NT
Metf
135 kDa
57 kDa
29 kDa
60 kDa
42kDa
ECAD
VIM
Snail
pS473AKT
AKT
β-ACTIN

**Supplementary Figure 4:** Effects of the OXPHOS inhibitors metformin (Metf) and phenformin (Phenf) in MON and SPH of HUCCT1 and CCLP1 cells. (A) Crystal Violet test was performed after 48 hours treatment. Results were normalized to control (CTR) samples. Data are mean ± SEM (n=3, * $p \leq 0.05$, ** $p \leq 0.01$, *** $p \leq 0.001$ vs. CTR). (B) HUCCT1 and CCLP1 MON show an increased sensitivity to the glycolysis inhibitor 2-Deoxyglucose (2-DG) compared to SPH cells. CV test was performed after 48 hours treatment. Results were normalized to control (CTR) sample. Data are mean ± SEM (n=3, p value versus CTR sample by Student t test, * $p \leq 0.05$). (C) Relative expression of transcripts encoding genes related to liver CSC, self-renewal, pluripotency and Epithelial-Mesenchymal Transition in HUCCT1 and CCLP1 SPH after 48 hours treatment with 10mM metformin. GAPDH was used as an internal control. All mRNA levels are presented as fold changes normalized to 1 (mean expression of CTR cells). Data are mean ± SEM (* $p \leq 0.05$, ** $p \leq 0.01$, *** $p \leq 0.001$ vs. NT). (D) Immunoblot analysis of EMT markers (ECAD, VIM, SNAIL), AKT and Phospho-AKT (Ser473) in MON and SPH of CCLP1 and HUCCT1 cells. β-Actin immunoblot was performed to ensure equal loading.

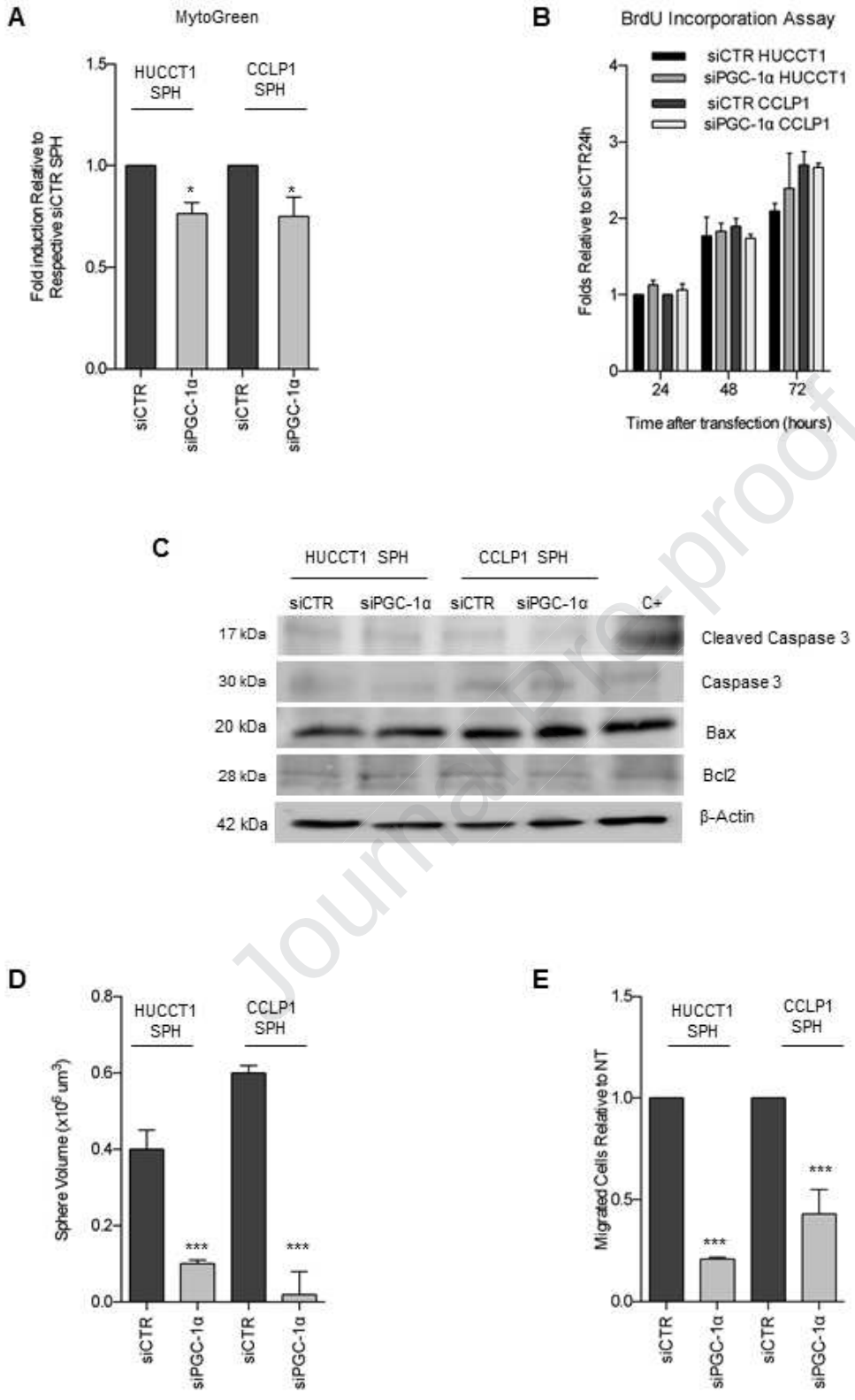

**Supplementary Figure 5: Effect of PGCα knockdown in CCA SPH.** (**A)** Mitochondrial mass, detected by FACS, using MitoTracker Green. Histograms represent the Mean Fluorescence Intensity (MFI) of the MitoTracker probe presented as fold induction normalized to 1 (mean MFI of siCTR). Data are mean ± SEM (n=3, p value versus siCTR by Student t test, * $p \leq 0.05$). (B) Effect of PGC-1α depletion on proliferation by BrdU incorporation at 24, 48 and 72 hours after silencing. Levels displayed as fold changes normalized to 1 (mean expression of siCTR at 24 hours) (n=3). Data are mean ± SEM. (C) Levels of Cleaved Caspase 3, Caspase 3, Bax and Bcl2 following PGC-1α silencing in HUCCT1 and CCLP1 SPH, as evaluated by Western blotting using β-Actin as a loading control. (D) Effect of siPGC1a depletion on CCA-SPH volume. Data are mean ± SEM (p value versus siCTR, *** $p \leq 0.001$). (D) Migration of PGC-1α-silenced CCLP1 and HUCCT cells was measured in Boyden chambers for 6 hours. Data are mean ± SEM (n=5, *** $p \leq 0.001$ vs. siCTR).

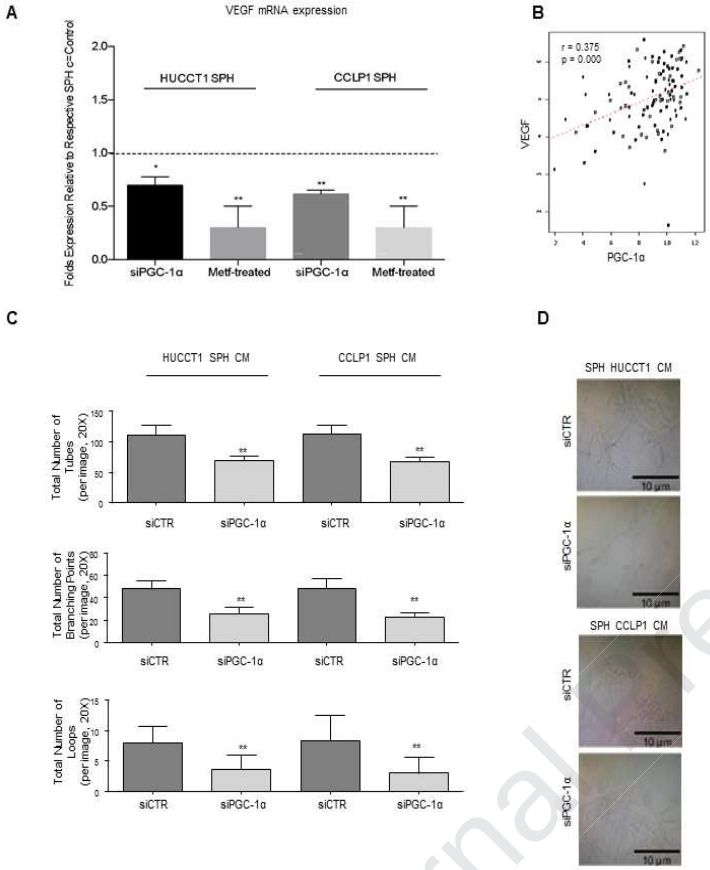


**Supplementary Figure 6: Effects of PGC-1α silencing on angiogenic pathways.** (A) VEGF mRNA levels in PGC-1α-silenced and metformin treated CCA SPH cells, expressed as fold changes normalized to 1 (mean expression of siCTR or control (CTR) sample). Data are mean ± SEM (n=3, * p≤0.05, ** p≤0.01 vs. siCTR/CTR). (B) Scatterplot representing the correlation between PGC-1α (x-axis) and VEGF (y-axis) expression in a published microrarray-based study comparing CCA vs surrounding liver in 59 patients (GSE26566 [22]). r: Pearson's correlation coefficient, n: number of samples. All adjusted (two tails) p values associated to correlation tests were < 1e-5. (C) Effects of conditioned medium from PGC-1α-silenced SPH (CM) on HUVEC tube formation. Data are presented as total numbers of tube/well, total number of branching points/well, total number of loops/well. Mean±SEM (n = 3, **p ≤0.01 vs. siCTR SPH CM). (D) Representative images of siCTR and siPGC-1α SPH CM effect on tube formation. Original magnification 40X.

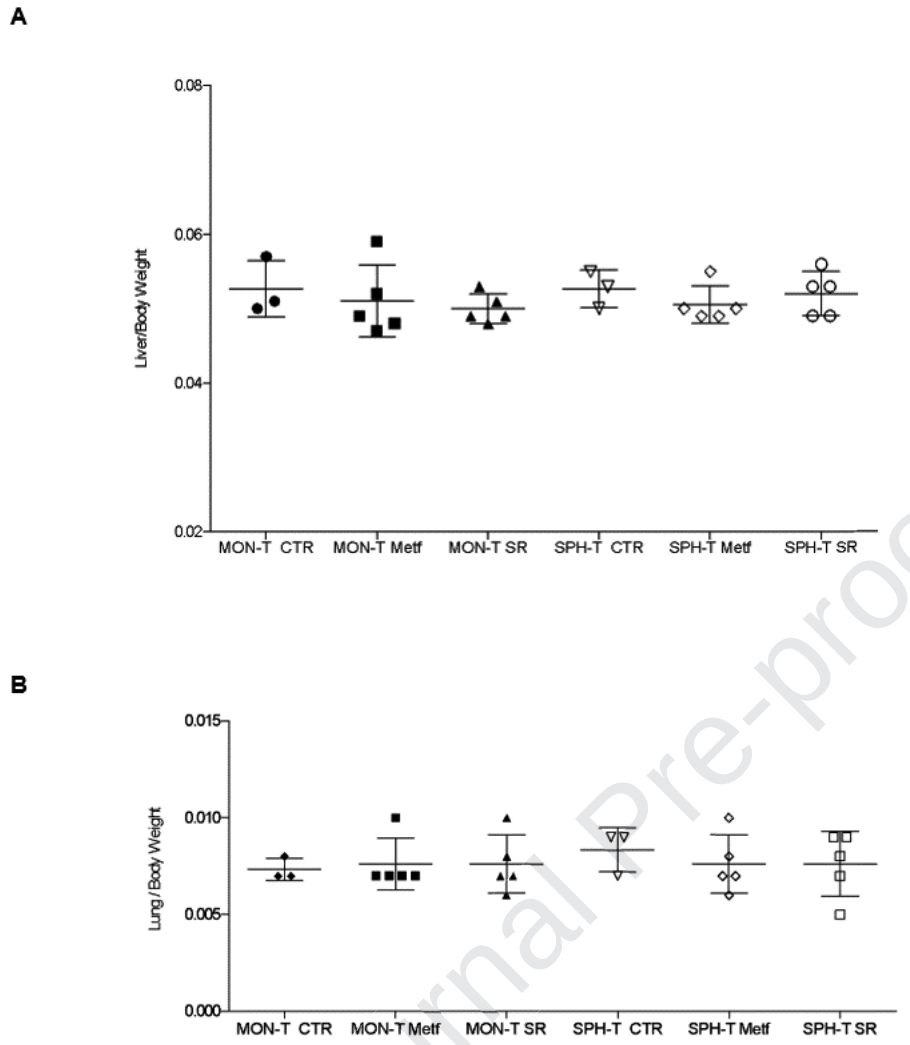




**Supplementary Figure 7: Liver/body weight ratio and lung/body weight ratio in mice with CCA tumor xenografts.** Tumors derived from HUCCT1 cells grown as MON (MON-T) or SPH (SPH-T) were obtained by subcutaneous injection of 1 x$10^6$ cells in NOD/SCID mice. After 7days, mice were treated five times a week with intraperitoneal injection of PBS (control, T-CTR) or 200 mg/kg metformin (T-Metf) or 45mg/kg SR-18292 (n=6 per group). Ratio of liver weight to body weight for each group. Data are mean ± SEM (n=6). (**B**) Ratio of lung weight to body weight for each group. Data are mean ± SEM (n=6).

**Supplementary Table 1. List of stem-like genes correlated with PGC-1α and Complex II**

| | Correlated genes | r | ADJ P-VALUE |
|---|---|---|---|
| **SDHA** | AFP | 0.3696648 | 0.0018 |
| | CD13 | 0.3046406 | 0.0327 |
| | ABCG2 | 0.5943840 | 0.0000 |
| | STAT3 | 0.2835567 | 0.0740 |
| | ALDH1a1 | 0.4821006 | 0.0000 |
| | PGC-1α | 0.4691994 | 0.0000 |
| **SDHB** | AFP | 0.5727547 | 0.0000 |
| | HNF4A | 0.5348040 | 0.0000 |
| | HNF4G | 0.3464601 | 0.0047 |
| | ALDH1a1 | 0.5193266 | 0.0000 |
| | PGC-1α | 0.4396749 | 0.0000 |
| **SDHC** | CD13 | 0.2968967 | 0.0530 |
| | ABCG2 | 0.3358473 | 0.0536 |
| | SOX2 | 0.3411690 | 0.0086 |
| **SDHD** | AFP | 0.6661503 | 0.0000 |
| | CD13 | 0.2921381 | 0.0404 |
| | ABCG2 | 0.5064105 | 0.0000 |
| | BMI1 | 0.3733502 | 0.0011 |
| | KLF4 | 0.2961764 | 0.0350 |
| | cMYC | 0.4372903 | 0.0000 |
| | IGF2 | 0.4436238 | 0.0000 |
| | HNF4A | 0.496548 | 0.0000 |
| | HNF4G | 0.5421162 | 0.0000 |
| | ALDH1a1 | 0.6601424 | 0.0000 |
| | PGC-1α | 0.4682400 | 0.0000 |
| **PGC-1α** | ABCG2 | 0.4262534 | 0.0010 |
| | IGF2 | 0.5625352 | 0.0000 |
| | HNF4A | 0.3560371 | 0.0080 |
| | AFP | 0.4934186 | 0.0000 |
| | CD13 | 0.4544777 | 0.0000 |
| | ALDH1a1 | 0.5954048 | 0.0000 |
| | VEGFA | 0.3753468 | 0.0007 |

**Journal of Hepatology**

**CTAT methods**

Tables for a "Complete, Transparent, Accurate and Timely account" (CTAT) are now mandatory for all revised submissions. The aim is to enhance the reproducibility of methods.

- Only include the parts relevant to your study
- Refer to the CTAT in the main text as 'Supplementary CTAT Table'
- Do not add subheadings
- Add as many rows as needed to include all information
- Only include one item per row

## 1.1 Antibodies

| Name | Citation | Supplier | Cat no. | Clone no. |
|---|---|---|---|---|
| Mouse CD31 mAb | | Cell Signaling Technology | #3528 | |
| Rabbit PKM2 mAb | | Cell Signaling Technology | #4053 | |
| Rabbit Hexokinase II mAb | | Cell Signaling Technology | #2867 | |
| Rabbit E-Cadherin mAb | | Cell Signaling Technology | #3195 | |
| Rabbit Vimentin mAb | | Cell Signaling Technology | #5741 | |
| Rabbit Phospho-Akt (Ser473) Antibody | | Cell Signaling Technology | #9271 | |
| Rabbit Akt Antibody | | Cell Signaling Technology | #9272 | |
| Rabbit Bax mAb | | Cell Signaling Technology | #5023 | |
| Rabbit Bcl-2 mAb | | Cell Signaling Technology | #4223 | |
| Rabbit Cleaved Caspase-3 Antibody | | Cell Signaling Technology | #9661 | |
| Rabbit Phospho-AMPKα (Thr172) mAb | | Cell Signaling Technology | #2535 | |

| | | | | |
|---|---|---|---|---|
| Rabbit AMPKα Antibody | | Cell Signaling Technology | #2532 | |
| Rabbit Caspase-3 Antibody | | Santa Cruz Biotechnology | #sc-7148 | |
| Rabbit Snail mAb | | Santa Cruz Biotechnology | #3879 | |
| Rabbit PGC-1α | | Abcam | #ab54481 | |
| Mouse BrdU | | DAKO | M0744 | |

**1.2 Cell lines**

| **Name** | **Citation** | **Supplier** | **Cat no.** | **Passage no.** | **Authentication test method** |
|---|---|---|---|---|---|
| HUCCT1 | | kind gift from Dr. A.J. Demetris | | | |
| CCLP1 | | kind gift from Dr. A.J. Demetris | | | |

**1.3 Organisms**

| **Name** | **Citation** | **Supplier** | **Strain** | **Sex** | **Age** | **Overall n number** |
|---|---|---|---|---|---|---|
| | | | | | | |

**1.4 Sequence based reagents**

| **Name** | **Sequence** | **Supplier** |
|---|---|---|
| | | |

**1.5 Biological samples**

| **Description** | **Source** | **Identifier** |
|---|---|---|
| | | |

### 1.6 Deposited data

| Name of repository | Identifier | Link |
|---|---|---|
| | | |

### 1.7 Software

| Software name | Manufacturer | Version |
|---|---|---|
| SPSS | SPSS Inc | ver. 25.0 |
| GraphPad Prism | GraphPad Software | ver.5 |

### 1.8 Other (e.g. drugs, proteins, vectors etc.)

| Name | Supplier | Cat.no |
|---|---|---|
| Metformin | Sigma | D150959 |
| SR-18292 | MedChemExpress. | HY-101491 |
| QuantiNova LNA PCR Focus Panels 384-well plates | Qiagen | #SBHS-133ZE |
| 2-Deoxy-D-glucose(2-DG) a glycolysis inhibitor | Sigma | |
| MitoTracker Red | ThermoFisher Scientific | M7512 |
| MitoTracker Green | ThermoFisher Scientific | M7514 |
| siPGC-1α SiRNA | Santa Cruz | sc-38884 |
| Lactate Assay Kit | Biovision | BVN-K607-100 |
| AMP colorimetric assay kit | Biovision | K229-100 |
| ATP colorimetric assay kit | Biovision | K354-100 |
| Seahorse XF Cell Mito Stress Test Kit | Agilent | 103015-100 |
| Seahorse XFe96FluxPak | Agilent | 102601-100 |
| MitoSOX Red Mitochondrial Superoxide Indicator | ThermoFisher Scientific | M36008 |
| 5-Bromo-2’-deoxyuridine | MERK | B5002 |

**1.9 Please provide the details of the corresponding methods author for the manuscript:**

Dr. Chiara Raggi, Dipartimento di Medicina Sperimentale e Clinica
Largo Brambilla 3
I50134 Florence, Italy
Tel: +39 0552758092
Fax: +39 055 2758099
Email: chiara.raggi@unifi.it

**2.0 Please confirm for randomised controlled trials all versions of the clinical protocol are included in the submission. These will be published online as supplementary information.**